INVESTIGATIONS OF ZNO MICROVARISTOR FOR STRESS CONTROL ON POLYMERIC OUTDOOR INSULATORS

A thesis submitted to Cardiff University
in candidature for the degree of
Doctor of Philosophy

By

RAHISHAM ABD RAHMAN
M.Eng (Hons)

School of Engineering, Cardiff University

August 2012

DECLARATION

This work has not previously been accepted in substance for any degree and is not concurrently submitted in candidature for any degree.

Signed : ……………………....... (Rahisham Abd Rahman) Date: 20 Aug 2012

STATEMENT 1

This thesis is being submitted in partial fulfilment of the requirements for the degree of PhD

Signed : ……………………....... (Rahisham Abd Rahman) Date: 20 Aug 2012

STATEMENT 2

This thesis is the result of my own work/investigation, except where otherwise stated. Other sources are acknowledged by explicit references.

Signed : ……………………....... (Rahisham Abd Rahman) Date: 20 Aug 2012

STATEMENT 3

I hereby give consent for my thesis, if accepted, to be available for photocopying and for inter-library loan, and for the title and summary to be made available to outside organisations.

Signed : ……………………....... (Rahisham Abd Rahman) Date: 20 Aug 2012

SUMMARY

This thesis is concerned with the investigation of the efficacy of Zinc Oxide microvaristor compound for stress control on polymeric outdoor insulators. The preliminary work has involved a comprehensive literature survey, followed by extensive computational modelling and simulation studies as well as laboratory works covering experimental investigations and fabrication of insulator prototypes.

The literature survey reviewed stress-induced degradations as the cause of ageing and insulation failures, the determination of electric field distributions, considerations for outdoor insulator modelling, and field-optimisation techniques for achieving stress relief.

An 11 kV polymeric insulator has been modelled and simulated under dry-clean and wet-polluted surface conditions in order to obtain electric field distribution along the insulator creepage path. The critical high field regions on polymeric surfaces were identified. In addition, clean fog solid layer tests were carried out to experimentally examine dry band formation and electric discharges. Experimental investigations confirmed the results previously achieved from theoretical simulations.

A non-linear pollution model has been developed for simulating polluted outdoor insulators. The field-dependent conductivity was derived from layer conductance measurements in a non-standard low voltage test. The proposed model was used to simulate insulators under fog and light rain conditions which respectively represent a uniform and non-uniform wetting action in practice. It was demonstrated that the non-linear pollution model yields a more detailed and realistic field distribution compared with results obtained with models using constant/linear conductivity.

Short-length microvaristor coating, having a cone-shaped structure, was introduced at both insulator ends for controlling high field, particularly near the high voltage and ground terminals. The performance of field grading was evaluated through a number of simulation scenarios. The introduction of microvaristor material with an appropriate switching characteristic has led to a substantial improvement in the electric field and heat distributions along the insulator profile.

The prototype of an 11kV insulator with microvaristor grading material was fabricated in-house for preliminary tests. Lightning impulse (1.2/50 μs) flashover tests were carried out using the ‘up and down’ method, and the flashover voltage was estimated by the 50% probability breakdown, U_{50}. The results of the lightning impulse test have indicated a considerable increase in the flashover voltage up to 21% when using microvaristor-graded insulator. Favourable field distributions obtained in the simulation study have indicated a strong correlation with the experimental results.

All praise is due to Allah, the most gracious, the most merciful.
Peace and blessings be upon our Prophet Muhammad
and upon his family and companions

***

To my parents and beloved wife, Farah Dayana
for their unconditional love, support
and encouragement

ACKNOWLEDGEMENTS

I would like to express my appreciation and sincere gratitude to my academic supervisors Professor A. Haddad and Dr. N. Harid for all their invaluable guidance and encouragement throughout the duration of this work. I have greatly benefited from their recognised extensive knowledge and expertise in this research field. I would like to extend my thanks to Prof. R. T. Waters for his advice and encouragement.

I am grateful to all members of staff and technicians within the department, particularly to Dr. Partha, Chris and Dr. Dong Sheng for their assistance in the laboratory. A special thanks my friends in the group: Abdel-Baset, Panos, Shuaib, Saufi, Alex, Fabian, Ahmed, Mohamed, Fahmi, Stephen, David and Haziah, for their friendship, inspiration and fruitful discussions.

I am thankful to my sponsors, Universiti Tun Hussein Onn Malaysia (UTHM) and the Ministry of Higher Education of Malaysia for providing financial support, which enabled me to complete my PhD study at Cardiff University.

I am eternally indebted to my wife, Dr. Farah Dayana, my parents, Mr. Abd Rahman, Mrs. Rodiah, Mr. Yusof and Mrs. Noraini, for their selfless patience and endless support especially during the difficult days.

Lastly, I thank everyone who has contributed directly or indirectly to this work that is now being presented here.

PUBLICATIONS

Journal:

i) **Abd-Rahman R.**, Haddad A., Harid N., Griffiths H., 'Stress control on polymeric outdoor insulators using zinc oxide microvaristor composites', *IEEE Transactions on Dielectrics and Electrical Insulation* , Vol.19 Issue. 2 (2012) pp. 705-713, ISSN 1070-9878, 2012.

Conference Proceedings:

i) **Abd Rahman R.**, Haddad A., Harid N., 'Dynamic Non-linear Model for Polluted Outdoor Insulators', Proceedings of Seventeenth International Symposium on High Voltage Engineering - ISH 2011, 22-26 August 2011, Hannover Germany, 2011.

ii) **Abd-Rahman R.**, Haddad A., Harid N., 'Performance Of Non-linear Grading Coating On Polymeric Outdoor Insulators Under Lightning Impulse Voltages', Proceedings of Twenty first International Conference and Exhibition on Electricity Distribution - CIRED 2011, No. 1276, 6-9 June 2011, Frankfurt Germany, 2011.

iii) **Abd-Rahman R.**, Haddad A., Harid N., 'Stress Control on Polymeric Outdoor Insulators', Proceedings of Forty fifth International Universities' Power Engineering Conference - UPEC 2010, 31 Aug-3 Sept 2010, Cardiff UK , ISBN 978-1-4244-7667-1, 2010.

iv) **Abd-Rahman R.**, Haddad A., Harid N., Field Control on Polymeric Outdoor Insulators, Thirteen Universities High Voltage Network - UHVNet 2010, Colloquium on Technologies for Future High Voltage Infrastructure, 19-20 Jan 2010, Manchester, 2010.

INVESTIGATIONS OF ZNO MICROVARISTOR FOR STRESS CONTROL ON POLYMERIC OUTDOOR INSULATORS

CHAPTER 1: INTRODUCTION

CHAPTER 2: DESIGN AND PERFORMANCE OF POLYMERIC OUTDOOR INSULATORS: A REVIEW

CHAPTER 3: INVESTIGATIONS OF ELECTRIC FIELD DISTRIBUTION OVER THE SURFACE OF POLYMERIC INSULATORS

CHAPTER 4: A NEW DYNAMIC SIMULATION MODEL FOR POLLUTED INSULATOR

CHAPTER 5: PROPOSAL FOR STRESS CONTROL ON INSULATOR SURFACE USING ZNO MICROVARISTOR COMPOUNDS

CHAPTER 6: DEVELOPMENT OF A MICROVARISTOR-GRADED INSULATOR PROTOTYPE AND LABORATORY CHARACTERISATION UNDER IMPULSE CONDITIONS

CHAPTER 7: General Conclusions And Future Works

References

LIST OF FIGURES

LIST OF TABLES

LIST OF ABBREVIATIONS

AC	Alternating current
ATH	Alumina trihydrate
BEM	Boundary element method
CAD	Computer aided design
DC	Direct current
DSO	Digital storage oscilloscope
EPDM	Ethylene-propylene-diene-monomer
ESDD	Equivalent salt deposit density
FEM	Finite element method
FRP	Fibre reinforced plastic
HV	High voltage
LMW	Low molecular weight
NaCl	Sodium chloride
PDE	Partial differential equation
SEM	Scanning electron microscope
SiR	Silicone rubber
UHV	Ultra high voltage
UV	Ultra violet
ZnO	Zinc oxide
2D/3D	Two/three dimensional

LIST OF SYMBOLS

ε	Permittivity
σ	Conductivity
ρ	Resistivity
A	Surface area
E	Electric field
J	Current density
P	Dissipated power
G	Layer conductance
I	Current
R	Resistance
V	Voltage
F	Form factor of insulator profile
d	Leakage distance
ΔG	Change in conductance
$R_{\Delta G}$	Rate of change in conductance
t	Thickness of pollution layer
S	Pollution section area
r	Radius with respect to insulation surface
d	Separation distance of electrodes
U_k	Impulse magnitude
U_{50}	50% probability of flashover
Ω	Ohm

$^{\circ}$	Degree (angle)
$^{\circ}C$	Degree Celsius
τ	Constant that defines field switching threshold
α	Constant that defines conduction threshold of microvaristor

CHAPTER 1:

INTRODUCTION

1.1. BACKGROUND

Developments of the modern world depend significantly upon a continuous electric power supply. With growing demand, utilities must provide secure and reliable power delivery while maximising the performance of the power distribution system from both technical and economic standpoints. Interruptions or failures within the power systems may result not only in damage to valuable high-voltage equipment, but can also lead to considerable loss of revenue, particularly for industrial consumers.

Outdoor insulators are among the key components in the electric power transmission network, essentially required for two primary purposes: i) to isolate the transmission tower from the high-voltage source, and ii) to provide a load-bearing platform capable of supporting heavy overhead conductors well above the ground [1]. While in use, line insulators must withstand a wide range of voltage magnitude under normal operating conditions, as well as surge transients imposed by lightning strikes and switching operations.

Ceramic insulation systems, such as glass and porcelain insulators, have been in use for more than 100 years [2]. They have undergone substantial modifications and refinement to guarantee the present satisfactory performance from the disc string design currently used worldwide. Ceramic insulators have demonstrated a proven track record in various aspects of the insulation performance, particularly ageing and lifespan. In addition to high mechanical strength, they provide excellent resistance to material degradation cause by electrical stress and discharge activities [3]. Nevertheless, their electrical performance is greatly affected by pollution and humidity [4]. The insulator surface exhibits hydrophilic properties, which means that water can easily form a continuous conductive film along the creepage path. Flow of high-magnitude leakage current under adverse weather conditions could lead to complete flashover and power outage.

In recent decades, composite polymeric insulators have started to gain wide acceptance among power utilities worldwide as replacements for the traditional ceramic insulators [5], [6]. Composite polymeric insulators offer many advantages such as: light weight, ease of handling, low operation and maintenance costs, improved mechanical strength, anti-vandalism properties, and more importantly, excellent electrical performance under moderately to heavily polluted environments [7], [8]. Polymeric material, such as silicone rubber, demonstrates a strong hydrophobic (water-repellent) property by which water on the polymeric surface tends to form discrete droplets, which have small contact areas on the insulator surface. This unique property helps to minimise the leakage current and the probability of dry band formation.

1.2. EFFECTS OF POLLUTION AND FIELD STRESS

In practice, outdoor insulators are constantly exposed to various environmental contaminants, including natural and agricultural substances and industrial emissions, during their period of service. Insulators near coastal regions, for example, encounter sea salts whereas those in urban areas are subjected to ash, dust, and chemical particles. These airborne particles tend to deposit and accumulate on the insulator surface, although the open profile of polymeric insulation housing normally allows for natural cleaning by rain and wind flow. The contaminants form a layer that may become conductive when exposed to wet atmospheric conditions such as fog, mist and drizzle. The presence of pollutants covering the insulator surface could also reduce the hydrophobicity of the polymeric material, thereby promoting the formation of a continuous conductive film. The resulting leakage current under system voltage generates resistive heating that evaporates water from the wet surfaces, risking the formation of dry bands [9]. In addition, the general shape of polymeric insulators causes non-uniform current density that promotes uneven surface drying, establishing dry patches on the insulator surface. Potential gradients across the electrode-like filament, coupled with the high electric field, trigger electrical discharges. In favourable conditions, the discharges may elongate over many dry bands and, consequently, may lead to complete flashover [10].

One of the main factors contributing to the development of discharges on insulator surfaces is the electric field distribution on the insulator surface, which in turn controls the current density. The usually non-uniform field profile along the surface has peak regions in which dry bands are formed. Of great concern to many researchers is the electrical stress in the region near the high voltage and the ground terminals. High electric fields trigger corona and discharge activities that contribute considerably to premature degradation through surface tracking and erosion. Under extreme conditions, intense electric arcs could puncture the polymeric housing and, more seriously, cause insulation failure from severe deterioration [11], [12].

In addition to the primary problems of pollution flashover and material degradation, corona and electric discharges can also result in secondary problems such as audible noise and electromagnetic interferences. Electric discharges produce constant buzzing sounds, and the established high-frequency wave could cause disturbances in radio and television, as well as in other communication signals [13].

1.3. CONTROL OF ELECTRIC FIELD

Considering the above-mentioned problems, electric field control is highly desirable to alleviate the effect of electrical discharges on polymeric outdoor insulators. Several grading techniques have been introduced to regulate the high field over the insulator surface. The grading ring is the most common device used for high-voltage insulators to control excessive stress near the high-voltage and ground terminals [14], [15]. The presence of the ring structure redistributes the concentrated field lines over wider regions, reducing high field strength at both insulator ends. Field optimisation can also be achieved through an appropriate end-fitting design and the shape of insulation housing. Smooth and rounded edges prevent field enhancement on critical regions along the creepage path.

The use of field grading compound is another popular method for controlling high electric field on polymeric insulation systems. This can be realised by using a material that has a high dielectric constant for capacitive grading or a compound with conductive fillers for resistive grading. In recent years, the potential for non-linear grading compounds to achieve stress relief for polymeric insulators has been explored.

Preliminary research results from both simulation [16] and experimental [17] studies have offered promising results, creating interest in further investigations.

1.4. DIRECTION OF RESEARCH AND OBJECTIVES

The focus of the present research is to contribute an alternative approach to the existing technique for optimising field distribution on polymeric outdoor insulators. Non-linear compounds composed of semi-conductive microvaristor particles have been introduced as a field grading material to control high electric fields at both insulator ends. The non-linear electrical properties of the grading compound are expected to provide a better and more uniform field distribution along the polymeric surface, thereby minimising the probability of dry band formation and the risk of surface discharges.

Determination of electric field over the insulator surface is important for predicting high stress regions on the insulator surface. Field distribution was computed through numerical simulation based on the finite element method. A polluted insulator with non-linear, field-dependent conductivity was modelled and simulated to provide better insight into realistic electric distributions. The specific objectives of this research are outlined below:

i) To review current knowledge related to the study undertaken, which includes stress-ageing phenomena, determination of electric field, insulator modelling, and field optimisation techniques.

ii) To evaluate field distribution along the leakage path and observe the consequent electric discharge on the surface of polymeric insulation housing.

iii) To propose a new pollution model with dynamic non-linear electrical properties for more realistic and accurate field modelling.

iv) To investigate the potential use of non-linear grading compound for controlling high field at the end fitting regions.

v) To examine the effectiveness of field grading material under impulse and transient overvoltage conditions in the high voltage laboratory.

1.5. CONTRIBUTION OF THE PRESENT WORK

The major achievements and contributions of this research investigation can be summarised as follows:

i) Electric stress on polymeric insulators was investigated by means of computer simulations and experiments. Good correlation was achieved between simulated field distributions and practical observations on discharge activities. Small discrepancies due to test arrangement and conditions were addressed and explained.

ii) The reduction in pollution conductivity due to surface heating and evaporation was quantified through experimental measurements. This led to the derivation of a new non-linear pollution model, which was used in the finite element simulations of polluted insulators. A more detailed and realistic field distribution obtained from the proposed model will result in a better dry band prediction.

iii) The potential was explored for the use of non-linear grading materials as a stress control solution for polymeric outdoor insulators. Comparative field studies have demonstrated that microvaristors, with an appropriate geometrical design and switching property, could effectively minimise field stress on the critical region near metal electrodes.

iv) Results from preliminary tests with lightning impulse voltage on the prototype of an 11kV insulator equipped with microvaristor grading material were encouraging. The effectiveness of the non-linear grading scheme was confirmed with a considerable increase in the breakdown threshold. Field simulations provide better understanding of the response under impulse energisation that leads to such improvement.

1.6. ORGANISATION OF THESIS

This thesis is divided into seven chapters:

CHAPTER 2 provides an extensive review of published literature pertaining to the study undertaken. General insights into polymeric insulators including key advantages, structural design, and factors contributing to the ageing process are presented. Practical measurements and a simulation approach for determining accurate field distribution around the insulator are discussed. The present techniques for controlling high electric field on insulator surfaces are reviewed, and the possibilities of different field grading material are considered.

CHAPTER 3 presents the investigation of electric stress on polymeric insulators by means of computer simulations and laboratory test programmes. A commercial finite element package is employed for insulator modelling to determine electric potential and field distribution along the creepage path under dry-clean and wet-polluted surface conditions. The simulation results are discussed in this chapter. To examine visually the effect of high electric field, an artificial pollution test based on the solid layer method is carried out on a practical insulator. Observations of discharge activities through video and thermal recording are analysed and correlated with the results from simulation studies.

CHAPTER 4 proposes the use of a non-linear pollution model, characterised by field-dependent conductivity, to achieve a better and more realistic field simulation. The field-conductance relationship is developed from experimental measurements in a non-standard low-voltage layer conductance test. Laboratory test procedures and the derivation of the non-linear electrical property are described. The proposed pollution model is simulated under two wet atmospheric conditions: fog and a light rain, which respectively represent uniform and non-uniform wetting action. The simulation results are evaluated and discussed in this chapter.

CHAPTER 5 presents an approach to achieving stress relief in the high field region near terminals through the use of non-linear microvaristor coating. The principle of a field-controlled solution that leads to near-uniform field distributions is described in this chapter. A case study is carried out for a typical 11 kV polymeric insulator to highlight the merits and effectiveness of the non-linear grading scheme. Analysis of field distribution is quantified under dry-clean and wet-polluted conditions for both standard non-graded and microvaristor-graded insulators. In addition, dissipated power is computed to examine surface heating and losses in the grading regions and for the complete insulator.

CHAPTER 6 evaluates the performance of polymeric insulators equipped with microvaristor grading material under impulse conditions through experimental work and computational modelling. A commercial microvaristor compound is tested to determine its non-linear electrical properties. A graded insulator prototype is designed and moulded using in-house vacuum-casting facilities, which is then subjected to U_{50} breakdown test procedures. The experimental results for both graded and non-graded insulators are compared and discussed in this chapter. For a better understanding, numerical simulations are performed to facilitate the interpretation of field response under impulse energisation.

CHAPTER 7 presents general conclusions based on the findings in this study, and outlines some recommendations for future investigation.

CHAPTER 2:

DESIGN AND PERFORMANCE OF POLYMERIC OUTDOOR INSULATORS: A REVIEW

2.1. INTRODUCTION

Polymeric insulators for outdoor applications have been commercially produced for more than four decades, and the demand is increasing rapidly due to their encouraging performance under diverse conditions. Massive deployment of polymeric insulators throughout the power industries has resulted in large-scale research investigations aimed at enhancing in-service operation that could last for at least thirty to forty years, just as was the case of their ceramic counterparts.

This chapter presents a comprehensive review of the studies related to the research programme concerning electric stress control on polymeric outdoor insulators. Factors contributing to polymeric ageing and associated problems are discussed to understand better the need for an improved stress grading scheme. Equally important is the determination of electric field, which needs to consider various modelling criteria for realistic computer simulations. This is particularly important in predicting high field regions that are susceptible to dry band formation and electric discharges. As an approach to field control, the possible use of field grading material, especially non-linear composite, is emphasised in addition to the present field optimisation techniques which are also reviewed in this chapter.

2.2. POLYMERIC OUTDOOR INSULATORS

The chronology and development of composite insulators from the time when these were first introduced for indoor application in the 1940s is briefly presented in [18] and [19]. Polymeric insulators for commercial use on the transmission network were available only from the 1970s, after undergoing a process of evolution and refinement. In the early stages of their introduction, the practical performance of these insulators was far less than satisfactory, with a number of problems and failures. However, with continuous advancement in both material formulation and fabrication technology, the reliability of polymeric insulators has improved considerably [20], [21].

2.2.1. Benefits and Limitations of Polymeric Insulators

Polymeric outdoor insulators made of polymeric material, especially silicone rubber, exhibit excellent electrical performances under moderate to heavily polluted environments [22], [23]. In a wet atmosphere, water tends to bead up on the polymeric surface, thus reducing the leakage current and the probability of dry band formation, which consequently results in reduced flashover voltages. The strong water-repellent property is attributed to the diffusion of low molecular weight (LMW) silicone chains from the bulk material to the surface, forming a lattice type thin layer consisting of methyl groups (CH_3) [24]. Interestingly, this property can also be transferred to an overlying pollution layer [25] enabling improved pollution performance for insulation systems in highly contaminated regions such as coastal and industrial areas. Even though silicone housing can temporarily lose its hydrophobicity under severe conditions, the materials have been reported [26], [27] to be able to regain hydrophobicity after a sufficient resting period with the absence of discharge activity.

Polymeric insulators offer significant weight reduction compared to the corresponding ceramic insulation systems [28]. There is less need for strong heavy support and cranes for installation, which results in easier handling and substantial savings in overall installation, operation and maintenance costs. In addition, voltage up-rating and compact transmission tower design for Ultra-High Voltage (UHV) distribution networks can be practically realised with polymeric insulators. Considering these benefits, it is not surprising that being ‘lightweight’ was among the main reasons for power utilities to switch to polymeric insulators, according to a survey conducted by Non-Ceramic Insulators Technical Committee, Japan [6].

Polymeric insulators have a high mechanical strength to weight ratio that allows for longer spans and less expensive tower structures. They provide improved mechanical strength under bending, deflection and compression stress. It has been reported [29] that polymeric insulators passed mechanical tests under extreme conditions without any permanent damage. Insulation housing with elastic properties also helps to prevent the risk of breakage during transportation or vandalism from gunshots that could lead to cascading failure as was experienced with ceramic insulators. In addition, complex weather shed designs are feasible and easily moulded using polymeric composite material.

Despite the abovementioned advantages, polymeric outdoor insulators however suffer from a problem of material deterioration, known as ageing. This is primarily due to concurrent stresses; environmental, electrical and mechanical stresses encountered in diverse range of service conditions. Polymeric materials which are organic in nature have weaker bonds, and hence susceptible to chemical change and compound degradations. Ageing of weathersheds housing will reduce insulation performance and cause other fatal consequences such as flashover and power outage.

Other than the ageing problem, fabrication of polymeric insulation housing for outdoor applications often required complex material formulations and design optimisation to suit specific environmental conditions. Appropriate amount and type of additives and weathersheds profiles need to be considered to inhibit degradation and ageing process, hence assuring good insulation performance throughout years of service. As the polymeric insulators have shorter service experience compared with the traditional glass porcelain system, long term ageing and outdoor performance remain unclear. As for now, accelerated weathering test is the best alternative to predict and evaluate the insulation performance over a longer period of time.

2.2.2. Design and Structural Shape

General construction design of polymeric insulators comprises three essential components: i) end-fitting terminals made of forged steel to support heavy load conductors on transmission towers, ii) fibre-reinforced core to provide essential mechanical strength and insulation between the two terminals, and iii) polymeric weather shed housing to protect the fibre core from various environmental impacts while providing sufficient leakage distance under wet surface conditions. Figure 2.1 shows the assembly of these three components where flanges are crimped to a fibre reinforced rod encapsulated within weather shed polymeric housing.

The insulation housing in modern design is moulded as one piece to avoid failure from multiple interfaces gluing between the polymeric sheath and the sheds, as experienced by early generation models [18]. Typical weather shed design with an aerodynamic and open profile encourages natural cleaning of deposited pollutants by wind or rain, which is particularly useful for resisting the accumulation of pollution on the insulator surface.

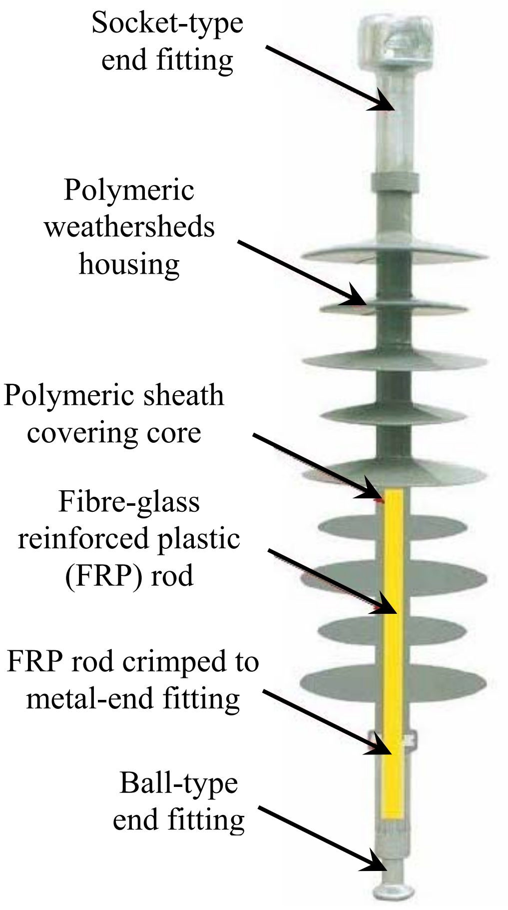

Figure 2.1: Typical polymeric insulator components [30]

The selection of outdoor insulators is essentially governed by the minimum specific creepage distance, taking into account two important aspects: i) system requirements, and ii) environmental conditions, as recommended in IEC 60815 Standard [31]. In addition, Young et al. [32] have suggested two other criteria: i) the resistance index, and ii) the distribution of current density, particularly for polymeric insulators that are subjected to variations in shape and weather shed design. Realising the importance of selecting appropriate outdoor insulators, CIGRE, through task force 33.04.01 [33], has outlined a structured approach, shown in Figure 2.2, which can be a guide in determining suitable insulator characteristics to be used in a given area.

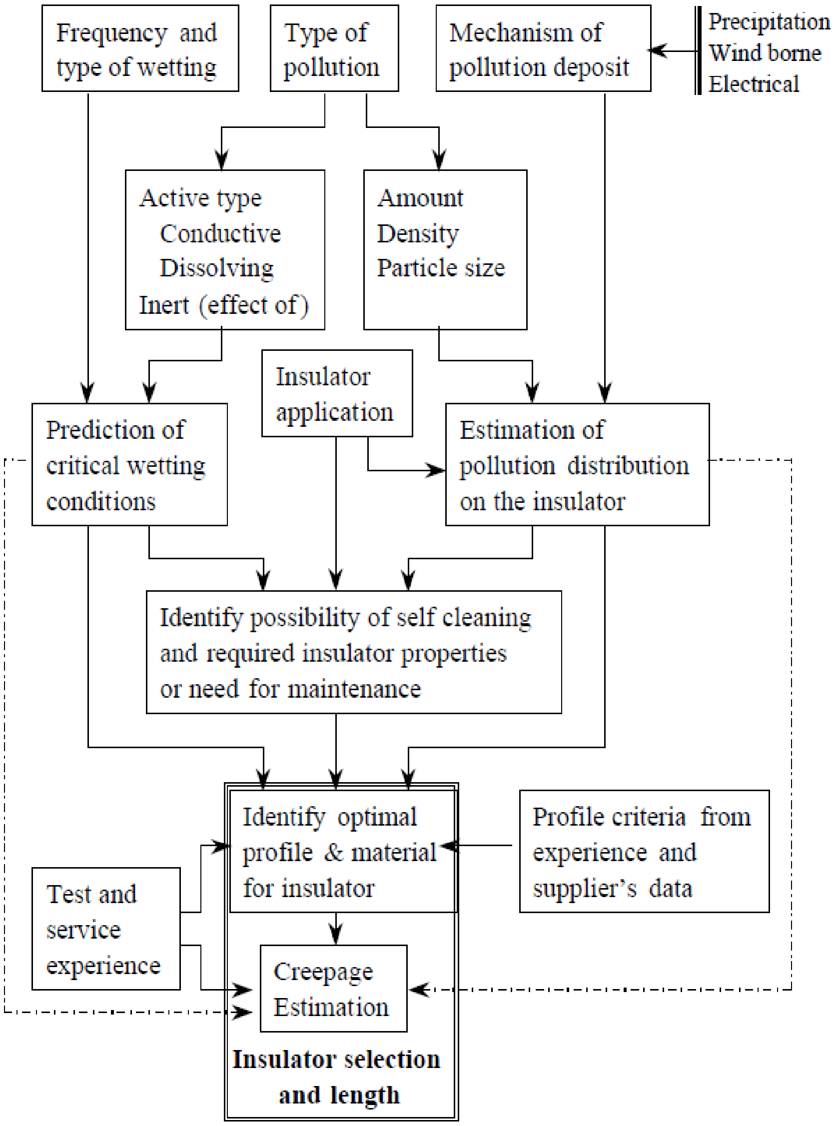

Figure 2.2: An approach to the design and selection of insulator profiles [33]

2.2.3. Polymeric Insulation Housing

Ethylene-propylene-diene-monomer (EPDM) and silicone rubber (SiR) are the two most common polymeric compounds used for outdoor high voltage insulation system. Both materials have their characteristic strengths with regard to in-service performance. Polymeric housing made of EPDM materials offers good mechanical properties and high resistance to arc-induced degradation. Experimental findings published in [34] evidently indicate that EPDM composite has suffered the least impact in surface erosion test when compared with other polymeric compounds, including silicone rubber. On the other hand, silicone compound is generally preferred because of its excellent electrical performance in various polluted environments. This is attributed to the strong hydrophobic surface properties, contrasted with EPDM which starts to show hydrophilic effects on exposure to prolonged wetting and electrical activity [35]. In an attempt to overcome the shortfall in both materials, EPDM and silicone rubber have been blended together to take advantage of their mechanical and electrical properties. Experimental evidence in [36] shows substantial improvement in the overall performance when using the mixed compounds, i.e. EPDM + SiR.

Polymeric materials used for outdoor insulation housing are usually formulated with other elements called fillers, which help to minimise the stress effects and to establish protection schemes against damaging electrical activities. Fillers are categorised into two main classes based on their functionality: i) reinforcing fillers for mechanical strength, and ii) extending fillers for some desirable properties such as surface degradation [37]. Silica and carbon black are examples of reinforcing fillers that enhance physical, tensile and tear strength through molecular bonding with the silicone polymer. Extending fillers such as Alumina Trihydrate (ATH) and quartz impart tracking and erosion resistance, especially when the polymeric surface has poor hydrophobic recovery [38]. The presence of both silica and ATH in compounds also improves thermal conductivity, which helps to remove heat from the intense dry band area. Barium Titanate, ($BaTiO_3$), on account of its excellent piezoelectric property, is the most popular element for increasing relative permittivity of insulator compounds [39]. In addition, the use of antimony (Sb) with doped tin oxide (SnO) fillers will increase the electrical conductivity of composite polymers, which is beneficial in reducing field stresses, thereby minimizing the effects of arcing and erosion damage. Table 2.1 provides a summary of the most commonly used fillers and their roles in protecting the insulation housing.

Table 2.1: Summary of common fillers in high voltage insulation material [39]

Filler	Property change	Contribution
• $Al_2O_3.3H_2O$ • SiO_2	Thermal conductivity	• Resistance to dry band arcing, partial discharge and Corona
• $BaTiO_2$ • $BaTiO_3$ + Al • SiC	Relative permittivity	• Electric field grading
• Varistor (ZnO) • Sb_2O_3 + SnO	Electrical conductivity	• Pollution performance • Electric field grading

It has been reported in [40], [41] and [42] that the effectiveness of fillers depends on the particle size and shape, as well as the volume concentration. For example, polymeric materials filled with fumed silica exhibit improved mechanical properties when compared to those with precipitated silica [40] . Thus, the selection of fillers with appropriate properties is a key component in formulating the weather shed insulation housing for optimum in-service performance.

2.3. STRESS INDUCED DEGRADATIONS

Polymeric insulators used for outdoor applications encounter a range of concurrent stresses while in service. These stresses can be grouped into three main categories, namely, electrical, mechanical and environmental stress [43]. The polymeric materials, due to their weak organic bonds, are vulnerable to chemical change on exposure to these stresses, which consequently lead to degradation and ageing of the polymeric insulator [44].

2.3.1. Electrical Stress

Electrical performance of high voltage insulators is governed by the distribution of electric fields around the insulator profile. Non-uniform and high fields could lead to electric discharges in the form of corona, dry band arcing and flashover.

2.3.1.1. Corona

Electric field distribution on polymeric insulators is generally more non-linear than the distribution on the equivalent disc string ceramic insulators. The magnitude of the electric field near the end fittings could be several times higher than the field in the middle. Traditional glass and porcelain systems have the advantage of a natural grading effect from their large capacitance [45] and also the intermediate metal parts along the string [46], which is not the case for polymeric insulators. The assembly and physical structure of polymeric insulators with low permittivity materials causes large potential gradients to occur at the high voltage and ground terminals. Such conditions develop a high field that places a constant stress on the polymeric surface in the nearby regions. The stress is considerably more for longer insulator strings with higher operating voltages.

It is now well known that the electric field is normally highest at regions near terminal fittings [47], [48]. Under dry surface conditions, when the electric field in these regions is sufficiently high to reach the air ionisation threshold, metallic induced corona is triggered. The corona normally exists as faint streamer discharges anchored at the metal electrodes. Two common by-products from corona activities are ozone and nitrogen oxide, which are converted into nitrous and nitric acid in the presence of moisture.[49] The acid attacks the insulation surface by destroying crosslinks in the polymeric compound, and the combined effect of chemical and thermal stress consequently results in the degradation of the insulation material and is believed to cause brittle damage to the core-conductor interface. However, Moreno et al. [50], through their experimental investigations, have rejected the possibility of thermal heating that leads to material degradation. The highest surface temperature recorded during the corona test was far less than the threshold level of 200-300˚C required to initiate degradation.

2.3.1.2. Droplet Induced Discharge

Water droplets on the insulator surface, due to their high permittivity, cause local field enhancement around their extremities at the triple-point interface – water-air-dielectric [51], [52]. Figure 2.3 provides examples of equipotentials and field distribution profile indicating the high field region. If sufficiently high, field intensification could initiate random partial discharges over the insulator surface. It has been reported [53] that the corona onset level for water droplets ranges from 4 to 10 kV/cm, depending on various parameters such as droplet shape and volume, hydrophobicity and atmospheric conditions.

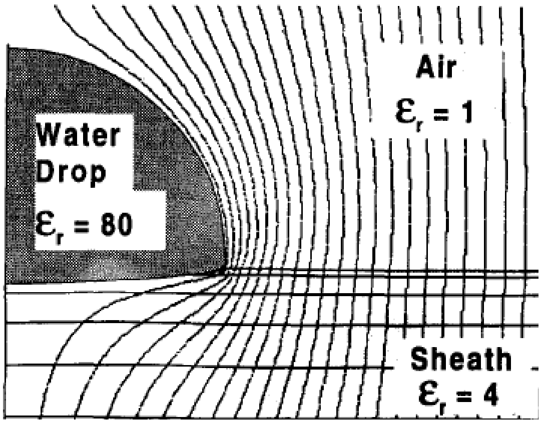

(a) Equipotential lines

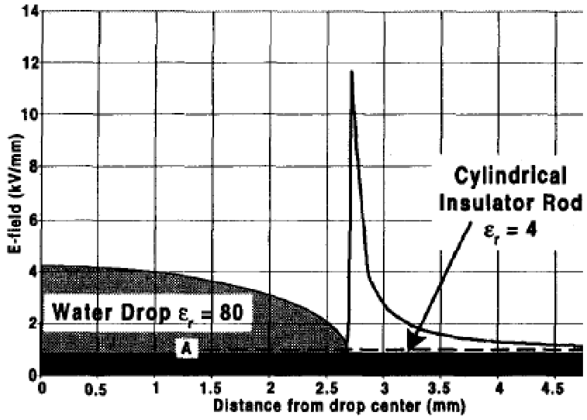

(b) Electric field profile

Figure 2.3: Field enhancement at the triple junction of water droplet [53]

Intense and continuous discharge activities can destroy hydrophobicity and gradually consume the insulation surface through tracking and erosion, as shown in Figure 2.4. In small scale experiments reported in [50], early signs of material degradations due to electric discharges were manifested as surface crazing (< 5 μm depth), cracking (> 50 μm depth) and discoloration. In some cases, the insulator may show the appearance of chalky white traces, attributed to the ATH fillers that diffused to the surface.

Figure 2.4: Degradation trace on polymeric insulator surface [54]

2.3.1.3. Dry Band Discharge

Despite the advantages of hydrophobicity, continuous conductive film on the insulator surface can still occur in several ways:

i) Corona and random surface discharges, as described in the previous section, could result in the loss of hydrophobicity, creating an increase in surface wettability, hence allowing the spread of water on hydrophilic regions.

ii) When the polymeric insulator is coated with pollution, deposited soluble elements such as salt and chemical fertilizer may dissolve in water to form an electrolyte layer covering the insulator surface. In other cases, water may diffuse through the LMW lattice to establish a conductive path beneath the pollution surface [55].

iii) Water droplets are subjected to deformation under voltage energisation [56]. Induced charges within the droplet experience a strong electromagnetic force that causes the hemispherical shaped droplet to flatten and extend in the direction of the electric field, thus covering a wider surface area. Such deformation is more vigorous under A.C. energisation where droplets are subjected to vibration due to the change of voltage polarity, as observed in experimental investigation by Katada et al. [57] depicted in Figure 2.5.

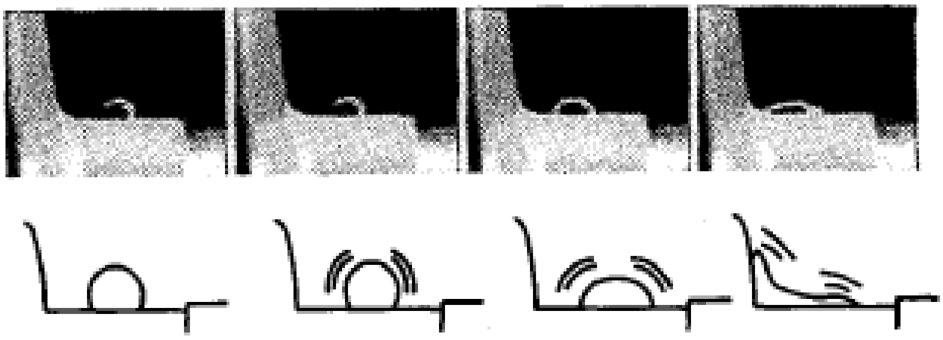

0 kV **5kV** **15 kV** **20 kV**

Figure 2.5: Behaviour of water droplet under different A.C. energisation [57]

Dry band discharges normally occur when water has the opportunity to wet the polymeric surface, thus allowing the flow of leakage current along the conductive path. The resulting resistive heating leads to surface water evaporation and drying of the wet insulator surface. Dry bands are likely to appear on the smallest circumferential region where the current density and dissipated power are greatest [58]. Large potential difference sustained between the electrode-like filaments combined with the highly non-uniform electric field can result in intense electric discharges to bridge the dry region.

2.3.1.4. Insulator Flashover

Active discharge activities from corona, water droplets and dry band arcing generate considerable thermal heating to cause further drying on the insulator surface. Electric discharges that are short at the beginning gradually elongate as the dry regions widen. Under favourable conditions, successive discharges may extend over multiple dry bands and join with other electric discharges that can eventually lead to a complete flashover [55]. Figure 2.6 illustrates the development of flashover on the polymeric surface.

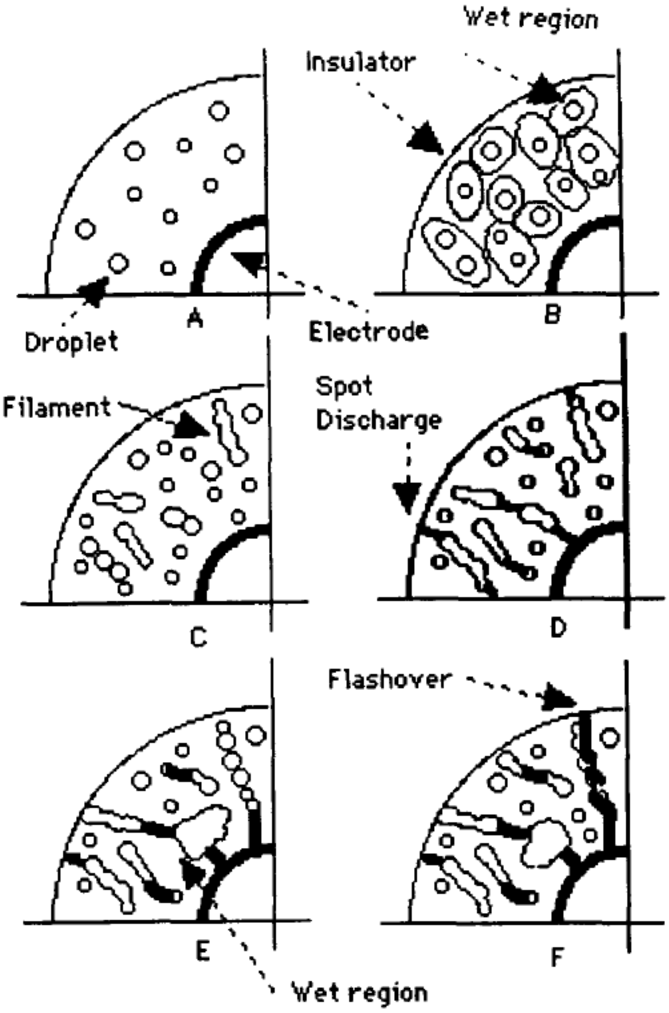

Figure 2.6: Illustration of flashover mechanism on polymeric insulator [55]

In the event of prolonged wetting and heavy rain, polymeric weather sheds can be bridged by the water stream [59]. The role of the creepage path along the insulator surface in limiting leakage current in this case is not effective. Water cascading promotes inter-shed arcing, and can easily lead to insulator flashover even at lower pollution severity. In addition, the flashover can occur at much lower voltage levels than the rated value. Polymeric insulators with an alternating shed design can be a good practice to minimise the probability of water bridging the weather sheds.

2.3.2. Environmental Stress

2.3.2.1. Pollutions

Environmental pollution is one of the major threats to polymeric outdoor insulation systems. Depending on the location and the surrounding area, insulators encounter different types of pollutants: sand and soil elements in desert and mining areas, metallic and chemical substances in industrial and agricultural lands, and salt particles in coastal regions. Deposits of these airborne particles gradually form a solid pollution layer on the insulator surface, which has a significant effect on both short and long-term performance of the insulation system. Electric field distribution is highly distorted by a non-uniform pollution layer on the insulator surface [60]. This contributes to localised field enhancement which could trigger corona and random partial discharges over the polymeric surface. In the presence of moisture, soluble contaminants dissolve in water establishing a conductive pollution film that allows the flow of leakage current along the creepage distance, increasing the risk of damaging dry band discharges.

In some cases, the insulator may also be subject to conductive moisture sources such as salt water, industrial acid fog, chemical mist and fertilizers, crop spraying and acid rain. These electrolyte-type pollutants can cause instantaneous leakage current and trigger flashover voltage even without the accumulation of pollution on the insulator surface [61].

2.3.2.2. Ultra-violet Radiation

Polymeric insulators installed for outdoor applications are open to ultra violet (UV) radiation from sunlight. The surfaces are attacked by UV photons that release substantial energy to break crosslink chains or individual molecules within the base matrix [62], [63]. Polymeric compounds for high voltage insulation housing contain impurities such as vulcanising agents, catalysts and fillers that are vulnerable to UV radiation due to their weak molecular bond. The presence of these additives weakens the strong carbon-based polymer i.e. C-C, C-H and Si-O bonds, thereby reducing the resistance of polymeric weather sheds housing to UV exposure. Thermal and photo-oxidation cause chain scissions that destroy hydrophobicity and lead to surface cracking and degradation of the polymeric material [64], [65]. The condition is exacerbated in high temperature regions such as deserts. From service experience reported in [66] and [67], polymeric surfaces that faced the sun appeared to be less hydrophobic and showed chalking and discoloration compared to those on the shaded side.

2.3.3. Mechanical Stress

An important function of the line insulator is to transfer mechanical support from the transmission tower to hold the heavy overhead conductor well in the air. Line insulators experience vertical load (tensile and compression stress) or cantilever/transverse load (bending stress) depending on system configuration and tower structure. Suspension insulators, when first installed on transmission towers, for example, encounter constant axial stress by the loading of bundle cables in which the weight could reach up to several tonnes for UHV transmission systems [1]. Over time, continuous strain could gradually deteriorate and weaken the joint between the core and the terminal, which will eventually result in the mechanical failure of the polymeric insulators.

Extra mechanical stress may also develop when strong winds move the line, causing oscillation. The consequent vibrations can cause the formation of fissures at the joint interface between the core and the metal flanges. In some cold-climate countries, ice accretion on both the conductor and weather sheds housing could generate additional loading stress on the polymeric insulator. In hot desert regions, the average temperature can easily reach 40˚C during the day, and drop below 10˚C at night. This considerable change in ambient temperature results in a cyclic process of thermal expansion and shrinkage that can loosen the connection at the core-end fitting interface, affecting the mechanical strength of the polymeric insulators.

2.4. DETERMINATION OF ELECTRIC FIELD DISTRIBUTION

Results from many accelerated ageing tests have indicated that electrical stress plays a significant role in material degradation and ageing of polymeric insulators. Non-uniform and high electric field, combined with other stresses, triggers damaging discharge activities on the insulator surface. Determination of the electric field provides a better understanding of the phenomena associated with surface discharges, and is particularly important for insulator design and optimisation in order to avoid such undesirable consequences. The electric field around the polymeric insulator can be obtained through two approaches: i) experimental measurements, and ii) numerical computations.

2.4.1. Experimental Measurements

Typical experimental setups for measuring the electric field around full-scaled practical insulators include electrostatic probes, spherical dipoles and electro-optic sensors.

2.4.1.1. Electrostatic Probe

The electrostatic probe is one of the most popular techniques used in the laboratory to measure the electric field around the insulator. The experimental setup and procedures involved are simple and cost-effective. The system employs an indirect method in which the electric field is obtained from the measurement of potential distribution. Figure 2.7 provides an example of the electrostatic probe arrangement, using phosphor bronze wire as a detector [68].

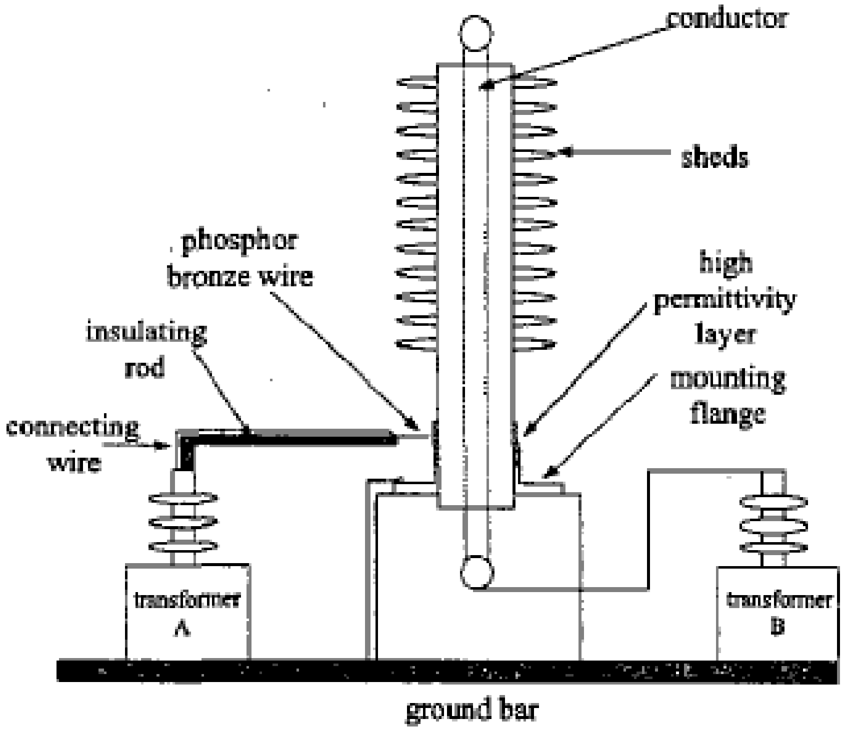

Figure 2.7: Experimental setup for electrostatic probe [68]

The wire probe is connected to a voltage regulator and phase shifter, and placed within millimetres of the insulator surface. The wire detector will deflect or vibrate when the potential and phase angle of the probe are different from those at the desired reference point. The potential measurement is obtained when the wire detector is in a static condition, and it is measured point by point along the creepage distance to determine field distribution over the insulator surface. However, measurement using this technique is subject to a slight error. The presence of the metallic probe usually distorts the original equipotential and field distributions around the insulator, thus giving an inaccurate field measurement. Furthermore, this method may not be suitable for metallic surfaces.

2.4.1.2. Spherical Dipole

The use of spherical dipoles is a long-established approach for determining the electric field distribution around an insulator [69]. This method is normally used on ceramic insulators that have intermediate metal parts along the disc string. The arrangement of this measurement technique is shown in Figure 2.8 [70].

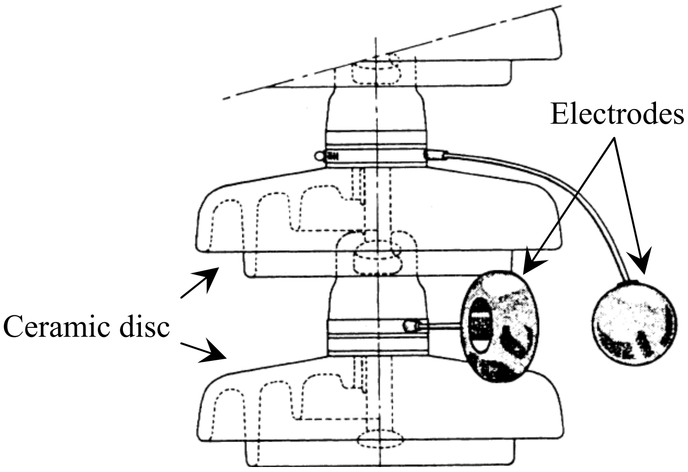

Figure 2.8: Arrangement of spherical dipole on ceramic disc insulator [70]

Two equal diameter sphere electrodes, spaced at a fixed distance, are connected across a ceramic disc. The applied voltage across the insulator string is gradually increased until the sphere gap produces an electric spark. The voltage drop across the sphere gap is used to compute the corresponding electric field. Similar to the electrostatic probe, this method does not provide accurate results as the spherical metallic electrodes cause distortion to the actual electric field distribution. Moreover, this measurement technique is not suitable for polymeric insulator designs.

2.4.1.3. Optical Sensors

With increasing demand for an accurate measurement tool, researchers have developed a more advanced and reliable probe using optical sensors to obtain voltage and field distribution at higher precision [71], [72]. Passive measurement based on Pockels effect offers many advantages which include i) direct electric field measurement, ii) wide range in frequency up to GHz, iii) less distortion, and iv) fully dielectric sensor [73]. Figure 2.9 shows a general block diagram for the principle of electric field measurement in Pockels optical system.

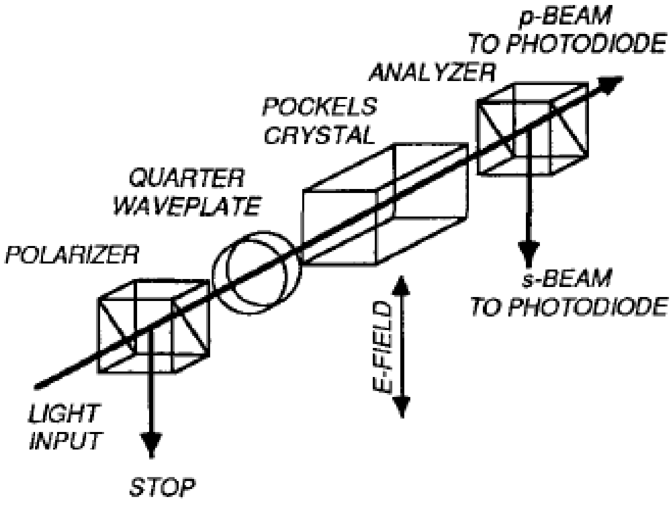

Figure 2.9: General principle of electro-optic effect using Pockels sensor [72]

A standard system consists of a Pockels crystal sensor, collimation and polarization optics, fibre optics, a monochromatic light source, and a photo-detection device. The system normally requires a proper laboratory setup, giving less flexibility for field measurements. However, in recent investigation, Zeng et. al. [74] have successfully developed an integrated electro-optic sensor featuring a small and compact portable design which makes on-site measurements more feasible.

2.4.2. Numerical Computation

Numerical approaches have always been a useful technique for solving many high voltage insulation problems. These approaches become more important when practical measurements are difficult or impossible to implement, highly risky and expensive with sophisticated laboratory setup and equipment [75], [76]. Numerical computations through analytical expression [77], [78], [79] or circuit representations [80] can be a good alternative, but these methods are rather complex and not applicable for diverse practical problems. For these reasons, numerical techniques using computer modelling and simulation are preferred among researchers. Field simulation packages offer faster and cost effective methods to obtain desirable results with substantial accuracy. This method is particularly useful in the design optimisation and development of many high voltage and power systems.

There are a number of packages that can be used to perform electric field analysis on outdoor insulation systems. Most of the available software is based on two numerical methods, namely, Finite Element Method (FEM) and Boundary Element Method (BEM). In this work, modelling and field simulations have been carried out using finite element analysis in COMSOL Multiphysics. The software offers non-linear electric field analysis in electroquasistatics module, which hardly found in any other commercial packages. This feature gives an opportunity for a better and reliable field computation especially when dealing with ZnO microvaristors that has non-linear material properties.

2.4.2.1. Finite Element Method

Finite element method (FEM) is a numerical approach to solve the partial differential equation (PDE) that represents a physical system. In FEM, the entire domain problem is discretised into a number of smaller non-overlapping subdivisions called elements, which normally have a triangular shape for 2D models, and are tetrahedral for 3D geometry. Each individual element is assigned with a simpler mathematical approximation, which is then solved to obtain the global solution for the physical system. The finite element solution is suitable for small domain problems with limited and closed boundary conditions. However, it is less effective when solving a large problem with an open boundary condition. A large number of mesh elements are generated to occupy the extended space, which could significantly affect the processing time. In addition, the wide range in the geometrical sizes of the physical problem, from several millimetres (e.g. curvature radius) up to 50 m (e.g. tower structure), could increase computation time and lead to numerical errors. Nevertheless, the shortfalls can be overcome by using sub-modelling methods [75]. In this case, the large physical problem is initially solved with coarse meshes. The solutions near the region of interest are used as global reference for boundaries of the reduced sub-model, which is then solved independently using finer meshing. For a larger physical system, parallel FEM computations [81] can be useful to enhance further the efficiency of field computations.

2.4.2.2. Boundary Element Method

Boundary element method (BEM) is a numerical approach based on boundary integral equations. Unlike the FEM, discretisation for BEM is applied only to the boundaries of system geometry, instead of the entire space domain [82]. The solution is obtained by solving the assigned integral equations for the discretised boundaries. For this reason, the computation and processing time in BEM is not greatly affected by the size of the physical system. The method can execute a large or unbounded problem for no extra effort, without serious numerical errors. However, the presence of populated matrices and integral equations for non-linear or inhomogeneous problems could reduce computation performance [83].

2.5. MODELLING OF POLYMERIC OUTDOOR INSULATOR

Distributions of electric field around outdoor insulators are greatly influenced by a range of parameters which include insulator design, tower configuration, conductors, and hardware attachments such as corona rings. These parameters need to be considered when modelling outdoor insulators in order to obtain a more realistic and accurate field distribution [84]. In addition, increased concerns among researchers with problems under hostile surface conditions have resulted in numerous studies investigating environmental aspects such as pollution and water droplets on the insulator surface.

2.5.1. General Consideration

2.5.1.1. 2D vs. 3D Insulator Model

Modelling of outdoor insulators can be implemented either in 2D or 3D geometrical representations. Researchers tend to employ 3D modelling when dealing with non-symmetrical problems, where practical configurations such as adjacent tower structures and hardware fittings need to be accounted for in the study [46], [85] . This presents the opportunity to obtain a more realistic and accurate field distribution around insulators. Developing a 3D model with complex structures, however, can be a great challenge, and often requires advanced drawing skills. In addition, 3D simulation encounters the common issue of intense and slow numerical computations, especially when dealing with large problems. To resolve this issue, some researchers have used modelling simplifications which help to improve the computation and processing time. For example, authors in [86] have considered only a 10˚ to 15˚ portion of the full 360˚ cylindrical shape, while in another investigation [87], only the first two sheds near the insulator terminals are considered in the simulation study. These simplifications, however, can be applied only within the individual case study, so as not to affect the accuracy of the desired simulation results.

In the case of an ideal symmetrical condition, 2D representation is always the first option and preferred primarily due to its simplicity and fast processing time [88], [89]. Field distributions can be computed with minimal effort by both human and machine to give a comparable result with those obtained from 3D modelling. Moreover, the perfect cylindrical property allows the insulator to be represented by only half of its symmetrical structure, which makes the numerical computation even more efficient [90].

Depending on the aspect of research investigations, the selection of drawing dimensions, using either a 3D or a 2D model, is essential for an effective and accurate field analysis. It is important to assess the given parameters and determine the most suitable geometrical representation for each situation.

2.5.1.2. Regions of Interest

Practical experience and laboratory observations have indicated that corona and electric discharges, due to the high electric field, can severely deteriorate the insulation material. A lot of research, therefore, has focused on the determination of the electric field distribution along the creepage path of the polymeric insulator [75]. These fields, especially the tangential component, drive the flow of leakage current on the insulator surface, which in turn promotes dry band formations and consequent damaging discharges. Particular attention has been given to the sheath region near terminal fittings, where the electric field is normally the highest [91]. Some researchers also studied the electric field on the insulator electrodes and the attached grading ring. This can be useful in developing a better end fitting design to minimise the effect of field stress in the vicinity area.

2.5.2. Hardware Structure and Arrangement

Electric field distribution along the creepage path of an ideal polymeric insulator without hardware fittings is symmetrical, with a general ‘U’ shaped profile [92]. It is high at both the high voltage and ground terminals, and gradually decreases towards the middle of the insulator. In practice, the presence of hardware structures such as the transmission tower, cable and other hardware attachments cause a redistribution of field profile. The electric field is generally higher at the high voltage terminal compared to that at the ground end. It has been reported [46] that the insulator with dead end configuration experiences greater field stress at the high voltage electrode (as high as 30% for a 500 kV system) than the suspension insulator, as shown in Figure 2.10.

The grading ring (also known as the corona ring) is a common protection device installed on insulation systems greater than 300 kV. At present, there is no proper standard to be used as guidance for grading ring design and installation. Inappropriate dimensions or placement of the corona ring could result in corona and premature failure of the insulator. Therefore, many authors [87], [89], [93], [94] have investigated the effect of grading ring parameters such as diameter, cross-section radius and distance from metal electrodes to achieve the best possible field performance. It has been agreed that the optimal dimensions and location of the grading ring structure vary depending on specific insulator applications and arrangements.

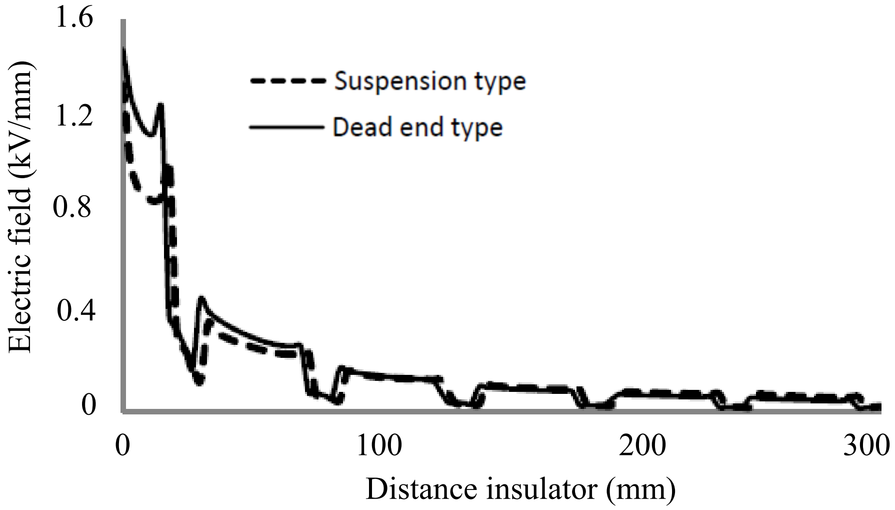

Figure 2.10: Field distribution for different types of polymeric insulators [46]

In a recent publication, Doshi et al. [46] have studied the effect of bundled conductors and multiple insulator units that are normally used for transmission systems with operating voltage greater than 500 kV. It was found that the increase in the number of conductors for each bundle can reduce peaks on the insulator surface. In addition, the use of multiple insulators for each suspension string provides an improved field distribution around the insulator compared with the arrangements using a single insulator unit.

2.5.3. Hostile Surface Conditions

2.5.3.1. Pollution Layer

Modelling of a polymeric insulator covered with a pollution layer is useful in representing realistic outdoor insulators which are subjected to various inland and sea contaminants with different severity. It is found that naturally aged insulators have shown a near-uniform deposition of pollutants over the insulator surface [95], [96]. Many researchers have, therefore, created a pollution layer with a uniform thickness when modelling polluted outdoor insulator [90], [97]. Electrical properties such as permittivity and conductivity of the pollution were normally assigned with constant values, obtained from simplified assumptions and sometimes from experimental measurements.

In an attempt to provide a better and more realistic outdoor insulator model, some researchers have considered various practical conditions for representing/ characterising the pollution layer on the insulator surface. For example, El-Hag et al. [98] have modelled polluted insulators based on wetting action. The uniform pollution layer on the insulator surface was classified into three main regions, which were specified with different conductivity values obtained from equivalent salt deposit density (ESDD) measurement. In another investigation, Yong et al. [99] have modelled a non-uniform pollution distribution where the cylindrical insulator was divided axially into four equal regions, which were assigned with different resistivity to represent heavy, moderate and no pollution on the insulator surface. They also studied asymmetric top and bottom surface contamination. In recent publications, Zhou et al. [92] and Jianyuan et al. [97] have investigated field performance around polymeric insulators with the presence of pollution dry bands. Electric field computations obtained from these pollution models have improved understanding of field behaviours under different insulator surface conditions that are commonly found in practice.

2.5.3.2. Water Droplet

Water on the polymeric surface tends to remain as droplets due to the strong hydrophobicity properties of the surface. In many publications [46], [100] and [101], water drops have been typically modelled with a hemispherical shape having a 90˚ contact angle and a diameter ranging between 6 and 10 mm. Field enhancement on the insulator surface due to water droplets could reach as high as 50%, as reported in [46]. Other authors [101] have used water droplets for modelling insulator under rain and fog conditions. For the rain model, the droplets were created only on the upper shed while the other regions were assumed dry. The same model was adopted for the fog condition with the bottom shed surface being covered by a thin continuous water film.

A hemispherical shape with 90° contact angle can be too ideal to represent a water droplet on a practical insulator. Therefore, Weigue et al. [102] have introduced a more realistic droplet model, based on photographs captured during the wetting of a polymeric insulator in a fog chamber, shown in Figure 2.11. The droplets were categorised according to the hydrophobicity classification (HC) recommended by the Swedish Transmission Research Institute (STRI) [103]. From the simulation results, it was demonstrated that the field enhancement factor varies depending upon the shape and distribution of water droplets on the polymeric surface.

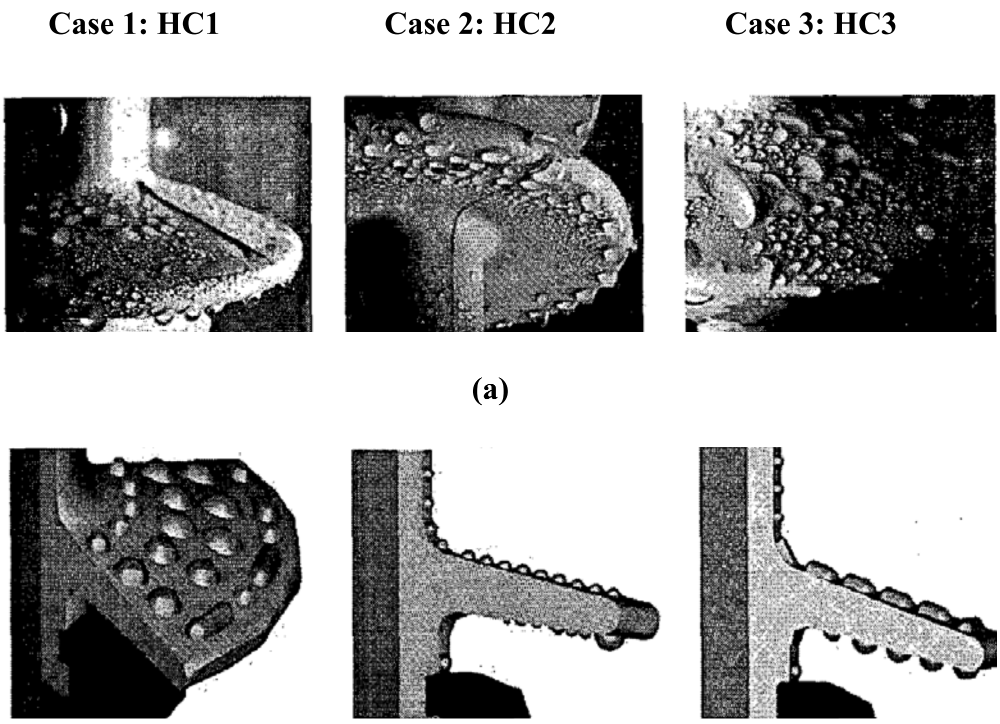

(a)

(b)

Figure 2.11: (a) Photographs of water droplets on the insulator surface, and (b) the corresponding droplet models used in the numerical simulations [102]

2.6. FIELD OPTIMISATION TECHNIQUES

It is well understood that high electric fields lead to corona and surface discharge activity, which may contribute to premature degradation of the insulation material. Control of high electric fields on polymeric insulators, particularly near both insulator terminals, is extremely important to minimise such undesirable effects, ensuring satisfactory performance during the period of service.

2.6.1. Grading Ring

The grading ring is a common device used to control field stress at the high voltage and ground terminals. Installation on practical insulators can effectively reduce high fields at critical areas on the insulation surface and metal hardware. The ring structure, with smooth rounded edges, grades the concentrated field near the electrode, hence lowering the field magnitude below the corona inception threshold, and minimises the possibility of breakdown with the highest voltage drop. In addition, the presence of the grading ring could also relocate the high field at a short distance away from the vulnerable area around the triple junction, metal-dielectric-air. The plot in Figure 2.12 clearly indicates significant field reductions for a range of operating voltages when using the grading ring [46]. It has been suggested in [14] that one corona ring on the high voltage end is sufficient for a power system at 220 kV. However, additional rings at both insulator ends are required for systems that operate at 400 kV or higher [24].

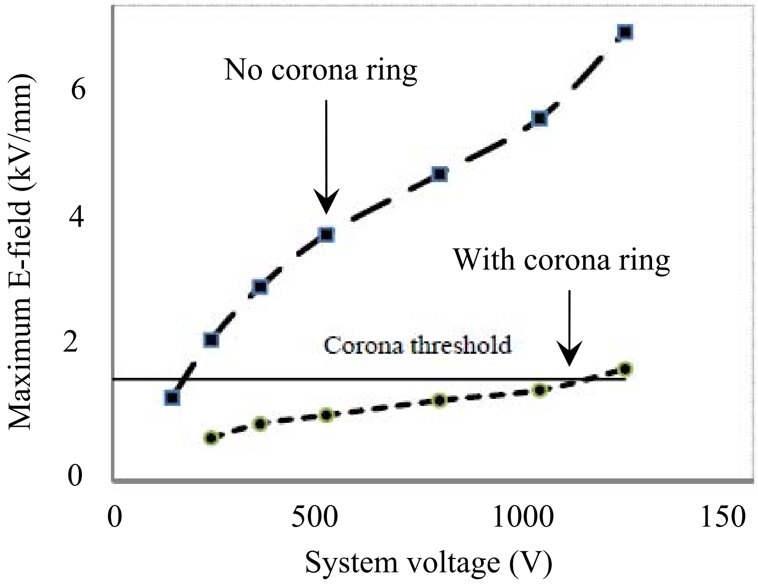

Figure 2.12: Comparison of maximum electric field for system with and without corona ring at high voltage end [46]

Potential and electric field distributions on the insulator surface especially near the terminals can be regulated by varying ring design parameters such as the cross-section diameter, ring radius, and the distance from the end fittings. Computational results in published works [14], [104], [105] showed that a large cross-sectional tube contributes to the reduction of electric field at the triple junction area. The increase in ring diameter and the distance from end fittings also result in field improvements to some extent in these high field regions. As the electric field is greatly influenced by hardware assemblies, optimisations of the grading ring have usually been performed based on specific system configurations, taking into account voltage rating and the orientation in actual applications [94].

2.6.2. End-fitting Design

An appropriate end-fitting design can provide an effective self-grading mechanism which is capable of minimising the high field around the metal electrodes. Smooth and rounded edges on the terminal help to grade the concentrated field, similar to the grading effect from the corona ring. Figure 2.13 shows examples of end-fitting design with the bulge shapes near the insulation housing that are commonly used in practice [93]. It has been demonstrated [90] that a larger electrode radius results in a reduction of the maximum electric field on the insulator surface.

2.6.3. Weather Shed Insulation Profile

Other than the end fitting design, the geometrical shape of polymeric weather shed housing is equally important in controlling field distribution on the insulation surface. The electric field along the axial length of the insulation housing is usually magnified at the intersecting point between the sheath and shed surfaces where there are sharp edges in the curvature. The regions that are close to the metal electrode encounter

(1) (2) (3) (4)

- **Design 1**- Rounded end fitting close to the last shed
- **Design 2** - Rounded end fitting at a short distance away from the last shed
- **Design 3** - Rounded end fitting completely covered by silicone rubber
- **Design 4** - Rounded end fitting partly covered by silicone rubber

Figure 2.13: Typical end fitting designs for polymeric insulators [93]

the greatest impact from this field intensification. Reduction of the impact at these critical junctions can be achieved through the use of polymeric housing with a large arc radius. This results in the redistribution of equipotential lines over a wider surface area, thereby reducing peaks and field stress. If the radius is sufficiently large, the arcs between two sheds will merge to form a rounded surface on the shank regions. This design has been implemented on insulators with a stacked sheds profile at the high voltage and ground electrode, with the intention of protecting the shank region from damaging discharge activities. Results from simulation studies by Weigue et al. [87], shown in Figure 2.14, have clearly indicated a considerable improvement in field distribution when introducing the stacked sheds design. The number of peaks is reduced by half, and they appear smoother than those for a standard insulator profile.

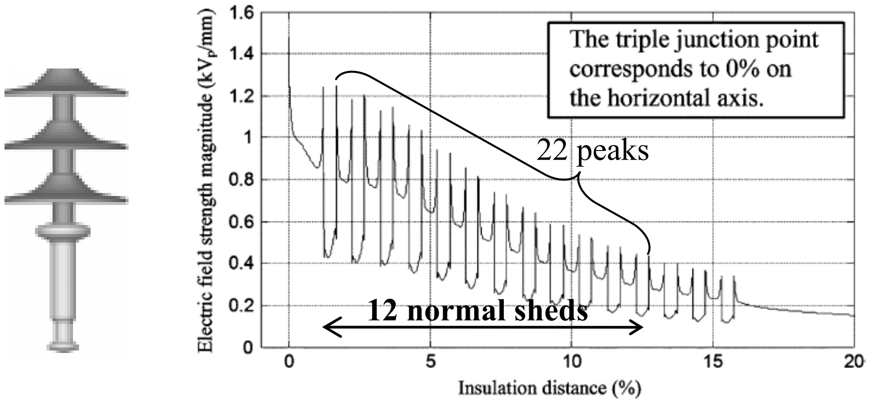

(a) Standard insulator profile

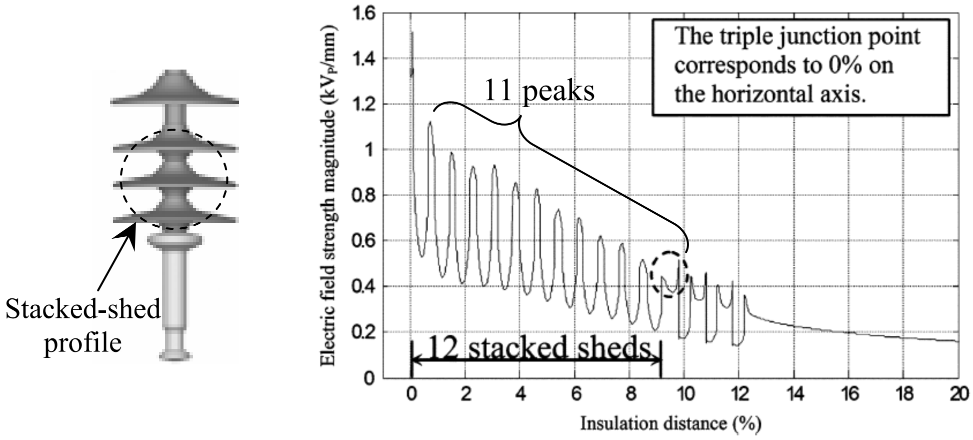

(b) Stacked-shed insulator design

Figure 2.14: Electric field distribution on polymeric surface near the high voltage terminal [87]

Chakravorti et al. [90] have performed extensive parametric studies to investigate the effect of insulator design parameters such as shed slope angle and diameter, core radius, axial length and arc radius. The results from numerical computations showed the effect of stress relief when increasing the insulator axial length as well as the shed and arc radius. However, the increase in core radius causes a slight field enhancement on the insulator surface. El-Hag et al. [98] have reported a significant field reduction, from 1260 V/mm down to 390 V/mm when increasing the distance of the first shed from the electrodes from 10 mm to 35 mm. This optimised distance will, however, vary depending on the insulator profile and configuration in practice.

2.6.4. Combined Insulator Assembly

In recent publications [106] and [107], a new optimisation technique has been proposed for controlling high fields around the insulator terminals. The method utilises ceramic discs which are connected to the live end terminal where electrical stress is the greatest, as illustrated in Figure 2.15. The ceramic discs have excellent self-capacitive grading which can regulate high fields in these hazardous regions. Moreover, ceramic insulators that are less susceptible to corona and discharge activities could avoid the problem of premature degradation near terminals as experienced by the polymeric material. It has been demonstrated that the maximum electric field improves by nearly 40% when using the proposed combined assembly design [107].

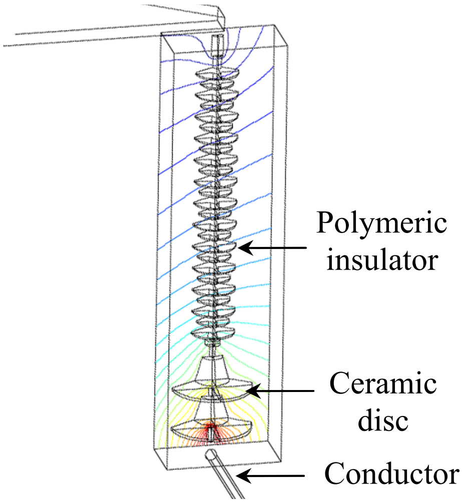

Figure 2.15: Field control at live end using combined insulator assembly [106]

2.6.5. Insulation Jacket for Line Conductor

Mei et al. [108] have introduced an attractive method to minimise field stress at the live end terminal. In this approach, insulation material made of silicone rubber was installed on the bare conductor close to the region where the polymeric insulator is attached. This implementation can be clearly seen from the pictures provided in Figure 2.16. The results from simulation studies [108] have indicated field reductions on the polymeric surface, particularly near the high voltage terminal, when using appropriate length and thickness of the insulation coating. For optimum stress relief, it was suggested that 2 m of silicone coating at thickness of 6 mm should be used on 220 kV systems. An appropriate insulation jacket design with additional grading ring attachments could effectively minimise corona and surface discharge activities, hence improving ageing and in-service outdoor insulator performance.

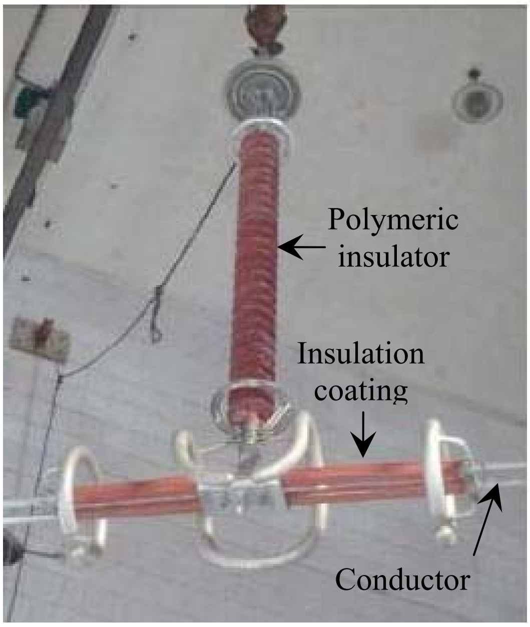

Figure 2.16: High field control using insulation coating for live conductor [108]

2.7. FIELD GRADING MATERIAL

Field grading materials have been successfully used for many years to control electrical stress on many high voltage applications such as cable terminations and machine windings. They can be grouped into two main categories; capacitive and resistive grading, which are classified based on the nature of current displacement within the material. In this technique, the grading action occurs within the materials, which results in the redistribution of equipotential on the surrounding regions such as on insulation surfaces.

2.7.1. Capacitive Grading

In capacitive grading, the electric field is regulated by a material that has a high dielectric constant and, hence, the displacement current is predominantly capacitive. Equipotentials are redistributed when passing through different dielectric materials having different permittivity values. The lines become farther apart and this reshapes field distributions along the insulation surface. In addition, high permittivity materials result in lower surface impedance, which could further reduce field stress [109]. Ying Shen et al. [68] have investigated the effects of high permittivity layers on composite insulation systems. $BaTiO_3$ and aluminium particles were added to liquid silicone rubber to produce a high permittivity compound. The layer which was varied in thickness, length and permittivity was coated at the mounting end where the electric field is the highest. It has been observed that the use of silicone coating with optimised layer thickness and permittivity value reduces the high field by more than 50% compared with values obtained from standard uncoated systems, as shown in Figure 2.17.

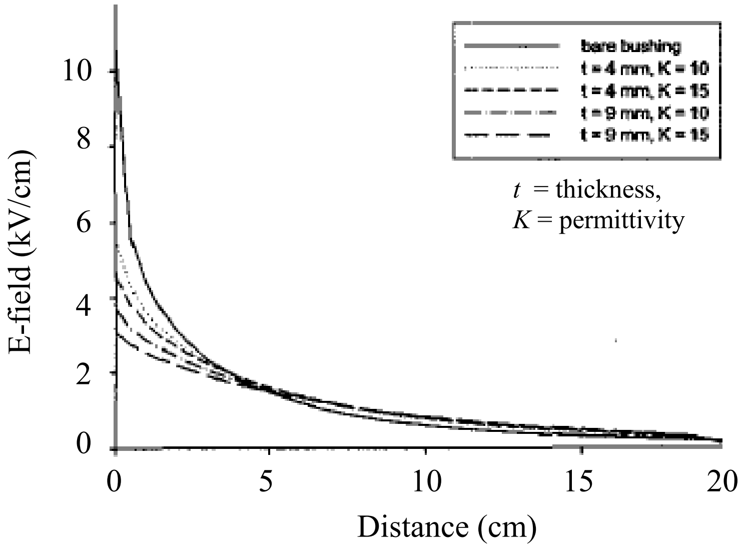

Figure 2.17: Effect of permittivity coating on polymeric surface [68]

Capacitive grading techniques can also be realised by using appropriate geometrical shapes of conducting or high permittivity material to alleviate field stress. Most of the field optimisation methods as described in Section 2.6 can be regarded as capacitive grading approaches For example, the use of rounded edges for end fitting design improves field distribution on the polymeric surface, and the integration of the corona ring structure made of conductive material helps to grade concentrated equipotentials at the high voltage and ground terminals. In cable applications, this capacitive controlled principle can be applied by introducing a cone-shaped dielectric material, intended to provide a smooth and gentle interruption at the splice and high voltage screened cable, as illustrated in Figure 2.18 [109]. In this way, equipotential lines will be spread out over a larger region, thus minimising field concentration and stress in the high-risk areas.

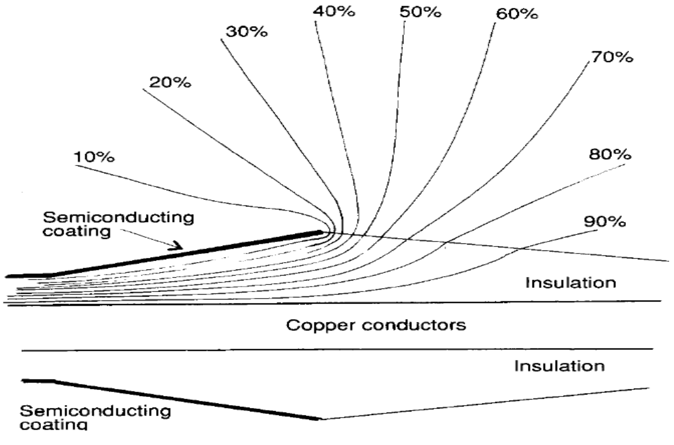

Figure 2.18: Cone-shaped stress grading in cable application [109]

2.7.2. Resistive Grading

Resistive grading material controls field distribution by means of the bulk conductivity of the material, and the current is predominantly resistive. Sufficient amounts of conductive elements such as carbon black filler are added into the polymer matrix to establish a path for current conduction within the material. Wei et al. [110] have studied the effectiveness of thin resistive layers in controlling peaks and high fields on the insulation surface. The grading layer was prepared by mixing semi-conductive particles, mainly antimony-doped tin oxide with liquid silicone rubber. The slurry was then sprayed onto the polymeric insulation surface forming a thin resistive coating at thickness 0.2 to 0.5 mm. The laboratory measurements were encouraging. With a 100 MΩ layer, high electric fields at critical areas on the polymeric surface were successfully relieved. However, there was a slight reduction in the improvement when increasing the resistivity from 100 MΩ to 1000 MΩ. This suggests that the selection of resistive coating with the appropriate amount of conductive fillers is important to obtain a compound with the desired electrical properties for specific applications. Comparison of equipotential plots, provided in Figure 2.19, indicates field improvement due to the effect of resistive coating.

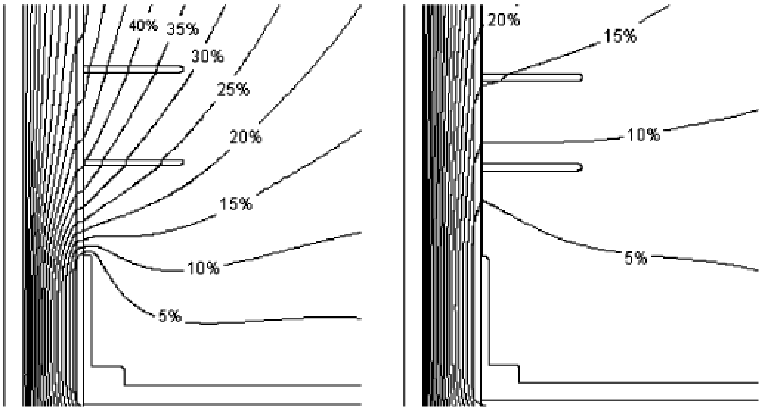

(a) **(b)**

Figure 2.19: Equipotential lines around high field region: (a) with no stress grading, and (b) with a resistive silicone rubber coating [110]

The material that exhibits non-linear electrical properties is another example of resistive grading. Electroceramic particles such as ZnO microvaristors [111] and Silica Carbide [112] can be used as functional fillers in polymeric compounds to impart non-linear current-voltage dependency to the grading compound. Figure 2.20 shows examples of electrical characteristics of ZnO microvaristors with different field switching thresholds, E_{th} at approximately 200 V/mm and 700 V/mm. In the linear region where the current density is low, the grading material operates as an insulator. An increase in the electric field causes minimal change in current density. As soon as the electric field exceeds the threshold levels, the material enters a high conduction regime and hence its grading benefits can be exploited. In this work, such properties have been utilised to propose a new field distribution control on outdoor polymeric insulators.

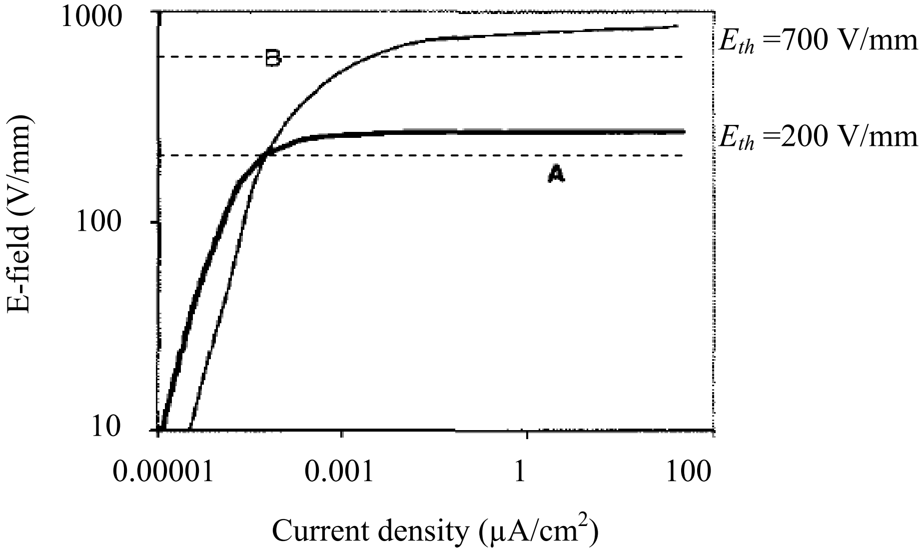

Figure 2.20: Electrical characteristic of microvaristors with different switching filled composite as a function of electric field [113]

2.8. ZINC OXIDE MICROVARISTORS

The superior performance of zinc oxide surge arresters compared with that of previous overvoltage protection devices is mainly due to their highly non-linear voltage-current characteristics and their energy absorption capability [114]. Recent developments in ZnO microvaristor manufacturing, coupled with subsequent compounding with silicone-based materials, offer a unique opportunity to control field distribution on polymeric insulation surfaces [115].

2.8.1. Fabrication of Microvaristor Filled Elastomers

Production of microvaristor compounds is rather complex, requiring advanced equipment and processing techniques [116]. A detailed manufacturing procedure for producing microvaristor compounds that have non-linear characteristics is revealed in a patent document [117]. In general, water-based slurry that contains zinc oxide and other dopants such as bismuth, antimony, manganese and cobalt, is first spray-dried to produce varistor granules. The agglomerates are then transformed into micro-scaled varistor particles, shown in Figure 2.21, through a sintering process at high temperatures around 900-1300ºC. After this, the microvaristors are sieved to particle size, ranging from 3 μm to 300 μm in diameter. Finally, appropriate amounts of microvaristor powder are blended in insulating elastomers using a high-speed disperse machine before being moulded into various shapes depending on the application. The electrical properties of microvaristors can always be tailored to suit specific requirements by adjusting the sintering conditions, i.e. temperature and doping elements [115].

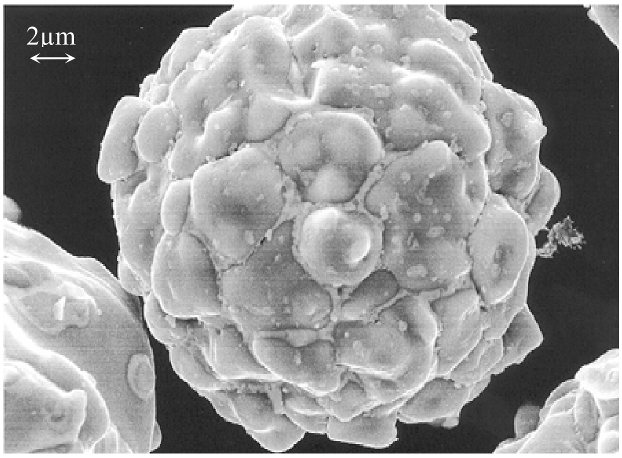

Figure 2.21: Microvaristor particle viewed using SEM [118]

2.8.2. ZnO Microvaristors for Outdoor Polymeric Insulators

Although there is very limited research work [119] in this area, encouraging results related to field control using non-linear grading material have already been reported, [118], [120], [121]. There are also patent documents [122], [123], [124] unveiling new inventions that adopt such control principle on high voltage equipments such as bushing and cable terminations. The application on polymeric outdoor insulators, however, receives little attentions and hence, will be explored in this study.

In recent publications [125], [126] a composite insulator having a core fully coated with a thin microvaristor layer was modelled using the finite element method, and the results indicated suppression of discharge activities. The electric field distribution along the insulator surface was notably improved. In another investigation [17], full insulators were fabricated for laboratory testing using microvaristor-filled elastomers as an insulation housing, replacing conventional composite materials. In the artificial rain test, the insulator prototypes have shown an excellent performance compared with the conventional composite insulator. Electric discharges on the surface were rarely seen, and were not even observed on one prototype. However, the microvaristor-filled composite failed in the inclined plane test, which is used to inspect the tracking and erosion performance of high voltage insulating material. The failure raises a major concern on the suitability of the insulator for use in outdoor applications. Furthermore, under steady state operation, continuous power loss will result in such configurations, due to leakage current in the microvaristor compound, and this would not be acceptable to the power utilities.

2.9. CONCLUSION

A broad review of polymeric outdoor insulator performance has been presented. Important aspects concerning in-service stresses and the determination and control of electric field distribution are particularly emphasised.

Factors contributing to premature degradation and ageing of polymeric insulator have been reviewed. The mechanisms leading to insulation failure are now fairly well understood under these conditions. Determination of field distribution along the creepage path and experimental investigation discussed in Chapter 3 (*Investigations Of Electric Field Distribution Over The Surface Of Polymeric Insulators*) provide greater insight into surface discharges and dry band prediction on the insulator surface.

A number of criteria have been taken into account for modelling polymeric outdoor insulators. Consideration of insulator designs, practical installations and weather conditions provide better and more accurate simulation results. The literature review has shown that polluted insulators have been modelled with constant pollution conductivity. This is, however, not usually the case in practice. Therefore, a more realistic pollution model having a non-linear field-dependent conductivity is developed, and it is detailed in Chapter 4 (*A New Dynamic Simulation Model For Polluted Insulator*).

Various techniques for stress control on polymeric insulators, particularly near the terminals, have been demonstrated in a number of research publications. Most of the works focus on field optimisations, while very few explored an alternative grading technique. To address this shortfall, the potential use of non-linear grading material for controlling high fields is proposed in Chapter 5 (*Proposal For Stress Control On Insulator Surface Using ZnO Microvaristor Compounds*) and experimentally verified in

Chapter 6 (*Development Of A Microvaristor-Graded Insulator Prototype And Laboratory Characterisation Under Impulse Conditions*).

CHAPTER 3:

INVESTIGATIONS OF ELECTRIC FIELD DISTRIBUTION OVER THE SURFACE OF POLYMERIC INSULATORS

3.1. INTRODUCTION

Despite the advantages of polymeric insulators over ceramic insulation systems, concerns remain about their performance in contaminated environments. An in-depth understanding of problems such as dry bands and electric discharges can only be achieved through accurate determination of electric field distribution along the insulator surface, and this is a key factor in developing good insulator design for optimal performance under a range of atmospheric conditions.

The measurement of electric fields around practical insulators is difficult, and becomes increasingly complicated under polluted surface conditions. Experimental setups such as the electrostatic probe [110] can be used but these are subject to periodic errors, although this could be improved by using a more advanced field detection system [74]. As an alternative, many researchers have employed numerical simulation techniques using commercially available electromagnetic software which appears to be more practical and cost-effective, avoiding expensive and complex laboratory experiments that are often difficult to carry out. Moreover, rapid growth in computer technology has led to the development of advanced numerical packages that can handle complex models without compromising processing time and accuracy.

In this chapter, computer simulation based on the Finite Element Method is used to compute potential and electric field distributions along the creepage path of weather sheds housing. The insulator model is developed and simulated under dry-clean and wet-polluted surface conditions with simplifying assumptions of a homogeneous and uniform pollution layer. It should be emphasised that, under normal conditions, polymeric insulators would rarely be subjected to a uniform wetted surface situation, due to their excellent hydrophobic surface properties when new or undegraded. Nevertheless, the following simulation results help to identify the high field region that is vulnerable to dry band formations.

Thorough understanding of the mathematical approach was not the main objective of the present study, as this can be explored in great detail in many textbooks, for example [127] and [128]. Instead, this study focuses on the modelling procedures and simulation results which are more beneficial to the field of engineering. The computed electric field and voltage distribution over the insulator surface under both dry-clean and wet-polluted surface conditions are compared and discussed. As a complementary study, experimental investigations through artificial pollution clean fog tests were also carried out in an attempt to establish correlation with the simulation results concerning the high field regions. The complete test programme is described in this chapter.

3.2. INSULATOR UNDER INVESTIGATION

The insulator that was considered in this investigation, and for the entire research programme, is a standard 11 kV polymeric outdoor insulator, shown in Figure 3.1 (a). Although in practice stress grading may not be required for 11 kV systems, the insulator, due to its small size allows easy prototype fabrication and testing in laboratory. For the actual applications, simulations and laboratory tests need to be applied on systems with higher voltage rating, normally greater than 200kV where stress control system is highly required.

The insulator has four equal sheds with a diameter of 90 mm, spaced at a distance of 45 mm along the insulator unit. The sheath thickness is about 5 mm, and the total creepage distance along the insulator surface is approximately 366 mm. The insulation housing is made of silicone rubber having a relative permittivity $\varepsilon_r = 4.3$. Forged alloy is used for the high voltage and ground terminals, which are attached to an 18 mm diameter rod as a core, at a distance of 160 mm. The core, with relative permittivity $\varepsilon_r = 7.1$ is a fibreglass material that is reinforced with epoxy resin for enhanced mechanical strength. Detailed dimensions and the geometrical structure of the insulator are given in Figure 3.1 (b).

3.3. FINITE ELEMENT MODELLING

The modelling and field computations in this study were carried out using a commercial finite element package, COMSOL Multiphysics version 3.5a. The simulation is performed in three consecutive stages namely, pre-processing, solving and post-processing stages. Components of the physical problem such as geometrical structure, material and boundary properties, and meshing criteria are presented as inputs in the pre-processing stage. The mathematical model, normally expressed as differential

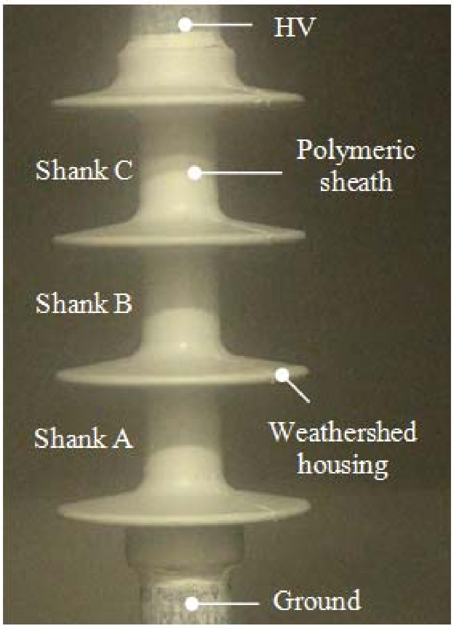

(a)

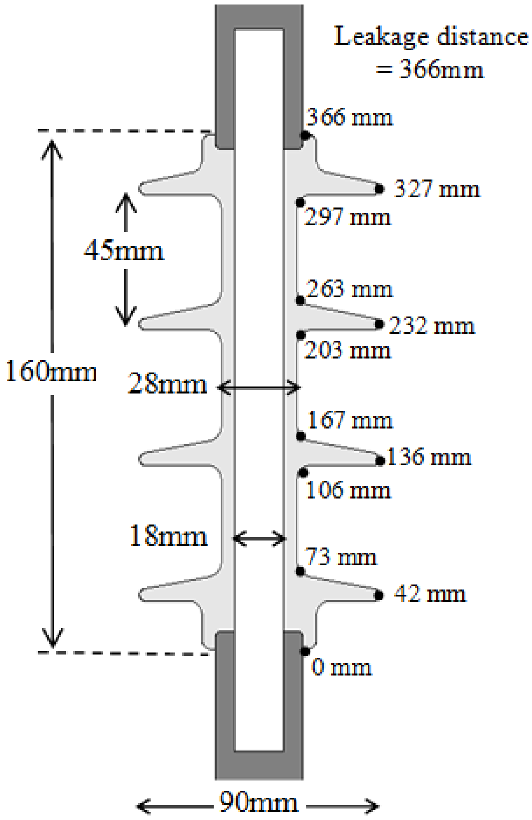

(b)

Figure 3.1: An 11kV polymeric insulator under consideration: (a) practical insulator, and (b) cross-sectional profile and dimensions

equations that describe the physical problem, is executed in the solving stage. Finally, in the post-processing stage, the package allows users to generate a plot of the desired postprocess variables or parameters. The flowchart diagram in Figure 3.2 shows the general FEM procedures for simulation works in this study.

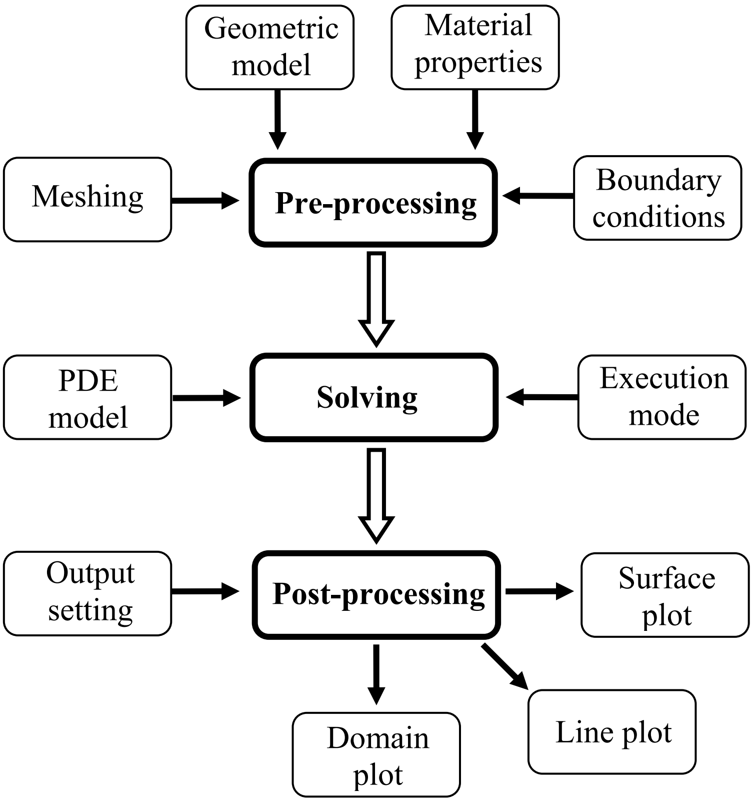

Figure 3.2: General procedures for FEM simulations

3.3.1. Simulated Insulator Model

The model of the polymeric insulator described in Section 3.2 was created using CAD drawing tools available in the FEM package. Since the insulator structure is cylindrical in shape, the modelling can be simplified into a two-dimensional (2D) problem instead of a full three-dimensional (3D) model. This simplification can save considerable memory and processing time without affecting the accuracy of the simulation results. To take advantage of the axis-symmetric property, only half of the insulator shape was created, as shown in Figure 3.3.

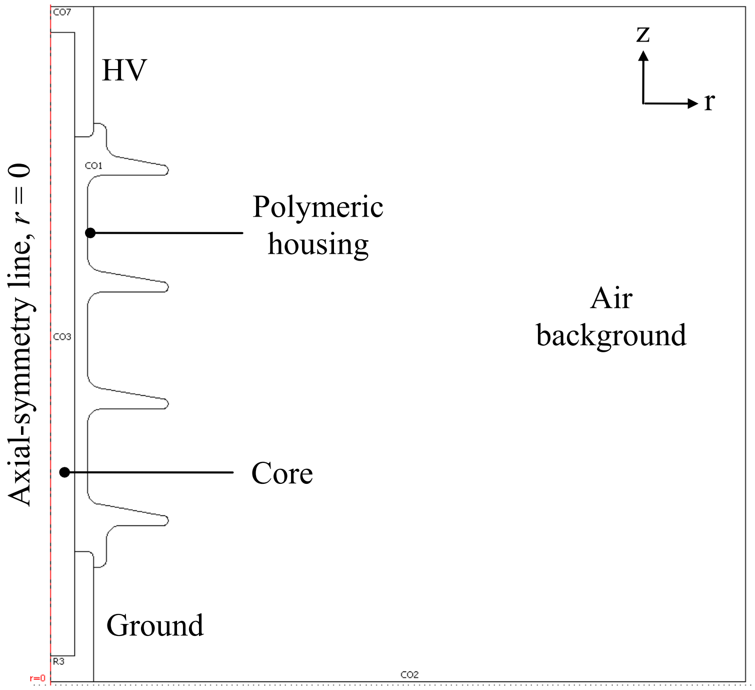

Figure 3.3: A 2D axis-symmetric insulator model on r-z plane in CAD platform

The simulated model adopted in this work is an idealised configuration for the outdoor insulator, but is easily reproducible in the laboratory. It is expected that this configuration would produce the most non-uniform field distribution around the terminal electrodes and, hence, represents the worst case scenario. Application to the numerous practical outdoor insulator configurations with the presence of adjacent equipment and structures would introduce distortions to both potential and electric field distributions.

3.3.2. Material Properties

Each region of the model was specified with appropriate material properties as described in Section 3.2. Both dielectric materials i.e. silicone housing and fibre reinforced (FRP) core were arbitrarily assigned with a low conductivity, $\sigma = 1.0\times10^{-14}$ S/m. The relative permittivity for the pollution layer was assumed to be 80, considering water as the dominant substance when the pollution layer is completely wet and saturated with moisture. The conductivity of the pollution layer was set to 0.6 μS/m, a value adopted from the laboratory measurements reported in [129]. The pollution layer was assumed homogenous and uniformly distributed along the creepage path of the insulator surface, at thickness 0.5 mm. The air region surrounding the insulator was specified with a very low conductivity, $\sigma = 1.0\times10^{-15}$ S/m. The material properties used for insulator modelling in this study are summarised in Table 3.1.

Table 3.1: Material properties used for insulator modelling

Materials	Relative Permittivity, εr	Conductivity, σ (S/m)
Forged steel	1.0	5.9×10^{7}
FRP core	7.1	1.0×10^{-14}
Silicone Rubber	4.3	1.0×10^{-14}
Pollution layer	80	6.0×10^{-7}
Air background	1.0	1.0×10^{-15}

3.3.3. Boundary Conditions

The top high voltage terminal was energised with power frequency A.C. voltage at 18 kV, while the bottom electrode was connected to ground, 0 V. The energisation voltage corresponds to the maximum phase to earth potential when considering the insulator subjected to very heavy pollution conditions, according to BS EN 60815 standard [61]. The air space is made large enough to minimise the effect on the distribution of potential near the electrodes and along the insulator profile. The outer edges of the air background region are assigned with a boundary that assumes zero external current and electromagnetic sources, hence representing physical system that is in an isolated open space background. The symmetry line of the insulator was set to be the axial-symmetric axis on the r-z plane.

3.3.4. Meshing

After completing the initial stage with the model structure, as well as specifying material properties and boundary conditions, the entire domain problem was discretised into non-overlapping triangular elements during the meshing process. To enhance the accuracy of the computed simulation results, meshing refinement in the region of interest was performed by increasing the number of mesh elements along the insulator surface. The refinement which results in a reduced element size can evidently be seen from the concentrated meshing along the leakage path as illustrated in Figure 3.4. The choice of mesh number is important, and must be balanced, as fewer mesh elements may reduce the accuracy of simulation results, while excessive elements lead to high memory consumption and longer processing time. An optimised number facilitates a faster computation time without compromising the accuracy of the result.

3.3.5. Solver Settings

The insulator model was simulated in an AC/DC module using a quasi-static electric current solver, which allows user to specify the conductivity as well as permittivity of a material. In quasi-static, the currents and electromagnetic fields vary slowly [130], which is valid for many high voltage applications including outdoor

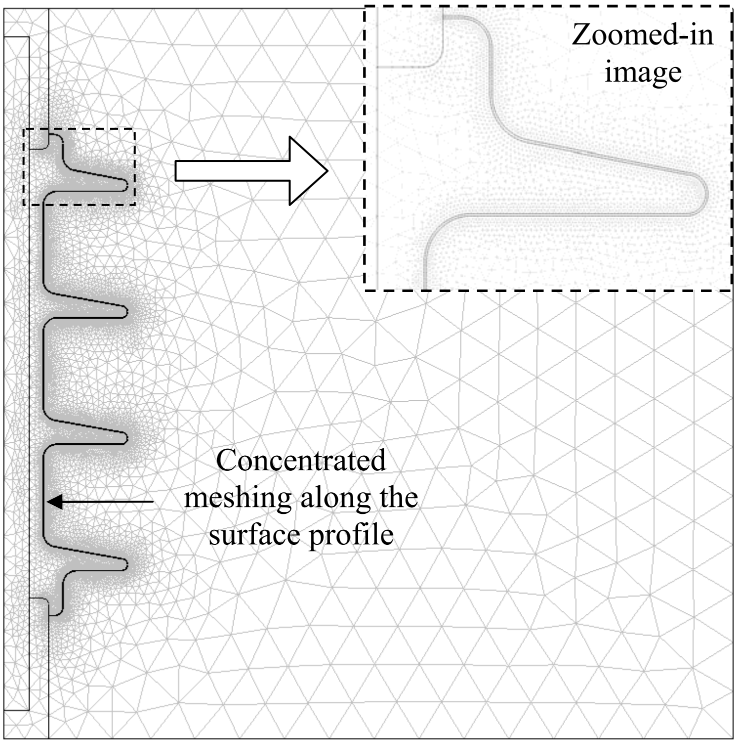

Figure 3.4: Discretisation of domain problem with mesh refinement along the creepage path

insulators that operate at power frequencies of 50-60 Hz. The induced current from magnetic fields, *B* and electric fields, *E* coupling is neglected in the computation. This approximation can be represented by mathematical expression:

$$\nabla \times E = -\frac{\partial B}{\partial t} = 0 \qquad (3.1)$$

Considering $E = -\nabla V$ and applying the divergence to Maxwell-Ampere's law:

$$\nabla \cdot \nabla \times H = \nabla \cdot \left[J + \frac{\partial D}{\partial t} \right] = 0 \qquad (3.2$$

where J and $\partial D/\partial t$ represent conduction current density ($J=\sigma E$) and displacement current density ($D=\varepsilon_r\varepsilon_0 E$), respectively. With Gauss's law, $\nabla\cdot D=\rho$ and equation of continuity, the software solves Equation 3.2 using time step domain to obtain electric potential and field distributions.

$$-\nabla\cdot\frac{\partial}{\partial t}\left(\varepsilon_0\varepsilon_r\nabla V\right)-\nabla\cdot\left(\sigma\nabla V\right)=0 \qquad (3.3)$$

In this expressions, V is the potential difference, σ is the electric conductivity, ε_0 is the vacuum permittivity and ε_r is the relative permittivity of a material.

3.4. SIMULATION RESULTS AND ANALYSIS

3.4.1. Equipotentials and Voltage Distribution

The equipotentials in the vicinity of the polymeric insulator model under dry-clean and wet-polluted surface conditions are shown in Figure 3.5 (a) and 3.5 (b) respectively to allow direct comparison. The lines are plotted at 4% voltage interval, hence producing a total of 25 equipotential lines in the simulation results. As can be observed on both plots, the contour lines are generally concentrated around the metal electrodes, indicating high field regions on the polymeric insulator. The equipotentials under the polluted condition are more uniformly spread compared with those for the dry-clean surface, giving a better field distribution along the creepage profile. This behaviour can be explained by the presence of the resistive pollution layer which helps to redistribute concentrated contours over a wider surface region.

The computed voltage distributions along the leakage path under both surface conditions are compared in Figure 3.6. The leakage distances are measured along the polymeric surface, starting at the ground, and moving up to the high voltage terminal.

As expected, the curves demonstrate an increment trend when shifting toward the energisation terminal. The voltage profile under dry conditions shows a high potential gradient at both insulator ends, illustrating high field regions on the insulator surface. This correlates well with the equipotentials plot in Figure 3.5 (a) that indicates line concentration around the insulator terminals. As for the polluted surface, the voltage profile appears to be more uniform and smoother than the profile for the dry-clean surface. This favourable distribution reflects the equally spread equipotentials given in Figure 3.5 (b).

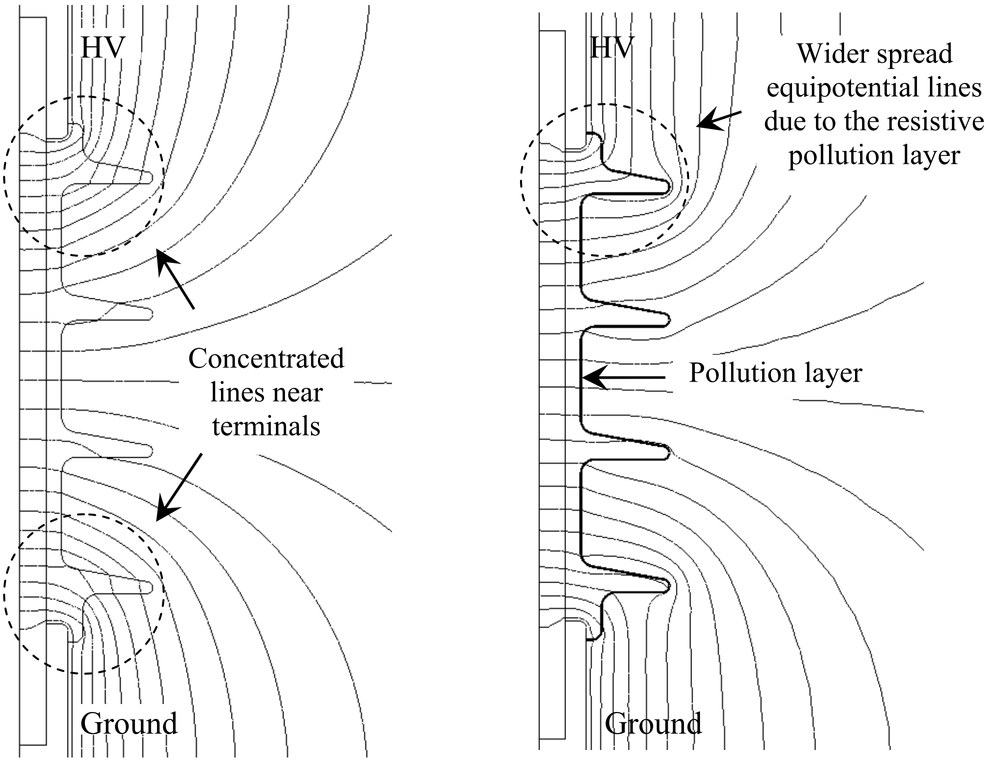

a) Dry-clean surface

b) Wet-polluted surface

Figure 3.5: Equipotentials at 4% interval around polymeric insulator

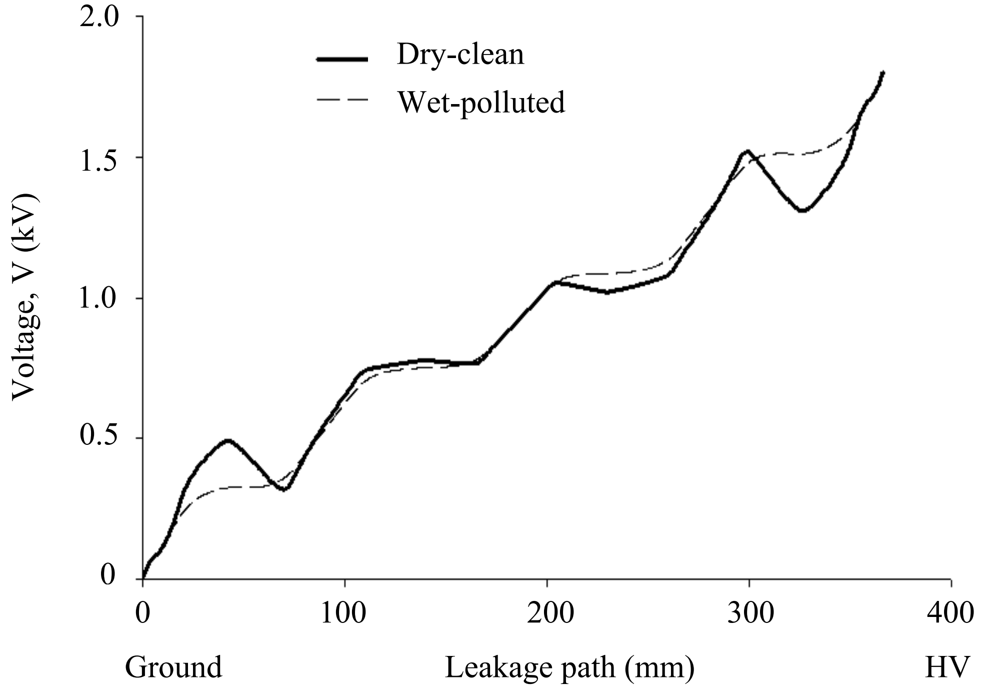

Figure 3.6: Voltage profile along the insulator surface

The dry insulator also exhibits curve undulations particularly at the region near the insulator terminals. Such behaviour can be explained by the equipotential lines that intersect the insulator surface at more than one point, as illustrated in Figure 3.7 (a). The equipotential lines representing 14.8 kV and 14.0 kV, for example, cross the insulator surface at three different locations indicated by points 1, 2 and 3. The same voltage level, therefore, appears at three points along the leakage distance, hence creating a non-smooth potential profile. Undulation was not seen on the voltage profile under the wet-polluted condition because each equipotential line only passes through the surface at one single location, as shown in Figure 3.7 (b).

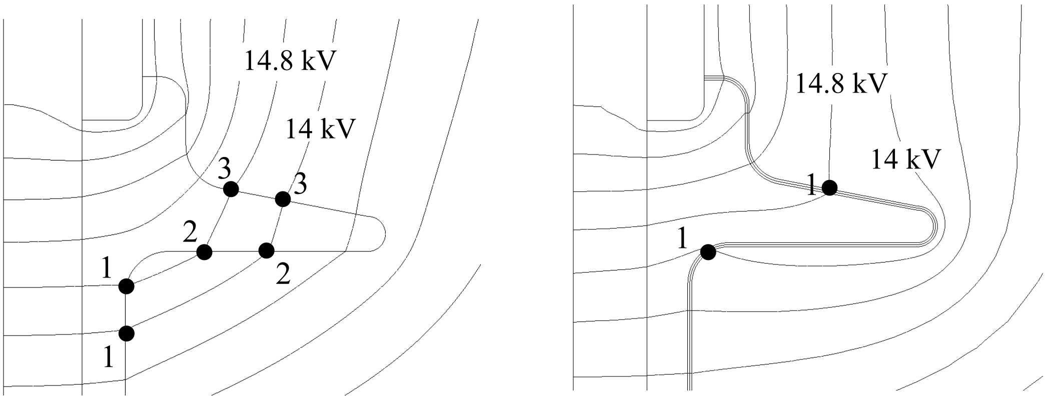

a) Dry-clean surface **b) Wet-polluted surface**

Figure 3.7: Zoomed-in view of equipotentials on the shed near the high voltage terminal

3.4.2. Electric Field Distribution

Figure 3.8 shows the simulation results of electric field distributions along the leakage path under dry-clean and polluted surface conditions. The computed electric field represents the tangential component along the insulator surface. The flow of leakage current on the insulator surface is largely driven by this tangential electric field. The plot in general shows a similar trend of distributions with a symmetric field distribution between both ground and high voltage terminals, as expected. The tangential field magnitude is highest on the surface area near the metal electrodes, with relatively smaller peaks in the shank regions. This shows good correlation with the equipotential plot and voltage profile as discussed in previous sections. Field distribution for the polluted insulator is smoother than that of the dry-clean surface as expected. Again, the presence of a resistive wet pollution layer helps in reducing the high field stress and produces a better and more favourable field distribution over the insulator surface.

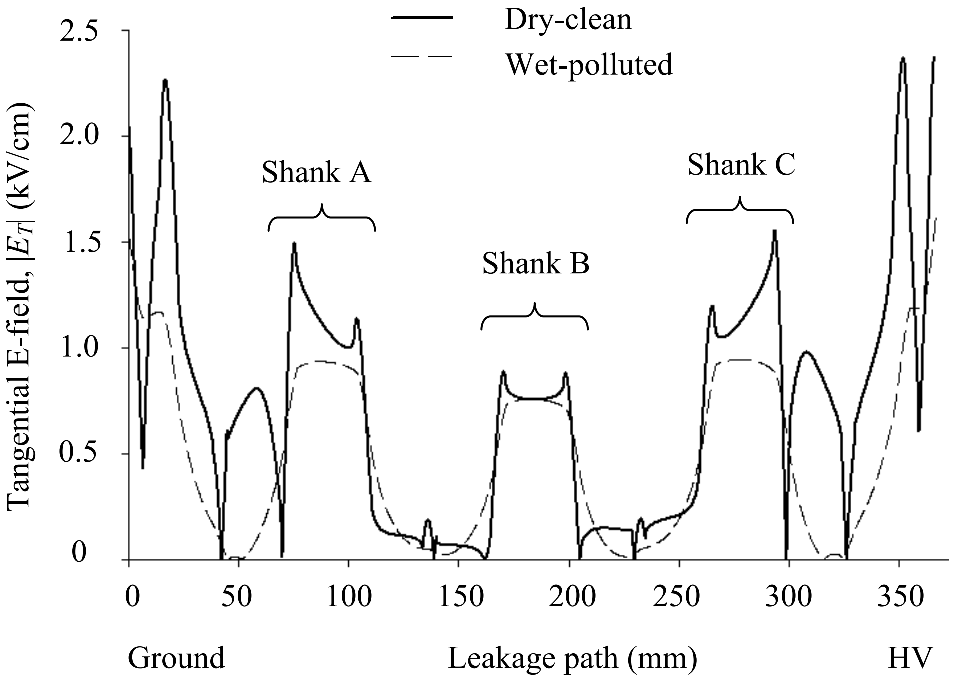

Figure 3.8: Tangential field distribution along the leakage path

From the equipotential contours shown in Figure 3.5, it is identified that electric fields in the shanks regions tend to run tangentially to the insulator surface, thus contributing to a field increase at the surface areas between 73 mm and 106 mm (shank A), 167 mm and 203 mm (shank B) and 263 mm and 397 mm (shank C) along the leakage path (see Figure 3.1 (b)). The peaks as seen on the dry-clean profile occur at the intersecting points between the vertical shank with the horizontal bottom and upper shed surfaces, where the edges are sharp with approximate angles in the range 80˚ to 90˚, hence causing field intensification. Although these peaks do not generate critical stress conditions under dry conditions, they could, however, trigger intense electrical arcs when the insulator is subjected to a wet atmosphere. High electric fields in the region between 42 mm and 73 mm (upper shed surface at ground end) and between 297 mm and 327 mm (bottom shed surface near high voltage electrode) are less significant because the direction of the tangential field is changed in the opposite direction of the leakage current on the polymeric surface. Figure 3.9 provides an illustration of vector field components demonstrating such phenomena.

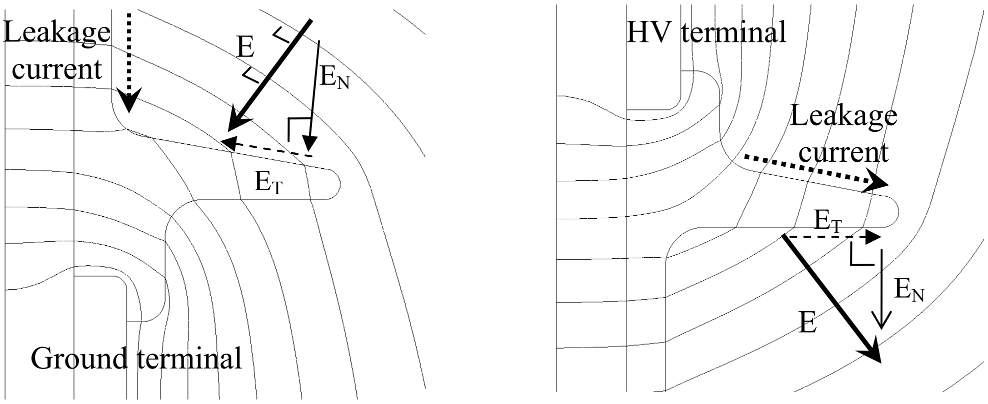

a) Bottom shed at ground end **b) Top shed at high voltage end**

Figure 3.9: Tangential field vectors that are in the opposite direction of leakage current on the insulator surface

Dry band formations and discharge activities on the surface of high voltage insulators are closely associated with high electric fields. Within the conductive pollution layer, the flow of leakage current is mainly driven by the electric field, particularly the tangential component. The leakage current giving current density that is highly non-uniform due to the shape of the polymeric insulator causes uneven surface heating and evaporation, leading to the formation of dry bands. When the localised electric field in the dry region is high enough to exceed the air breakdown threshold, electric discharge will be triggered. From the simulation results, it can be predicted that dry bands and electrical discharges are likely to occur on the polymeric sheath near the terminals and shank regions where the tangential fields are considerably high.

3.5. EXPERIMENTAL INVESTIGATIONS

As a complement to the modelling and simulation work presented in the earlier sections, experimental investigations were carried out on practical insulators to examine visually the electrical stress on the polymeric surface. An artificial pollution test in accordance with the BS EN 60507 standard was performed on the 11 kV polymeric insulator described in Section 3.2. The focus of this investigation was primarily on visual inspections aided by video recording and an infrared thermal camera. Dry band formation and discharge activities during the test period are evidence of high field regions, emphasising the electrical stress on the insulator surface.

3.5.1. Fog Chamber Test Facilities

The experiments were carried out using the existing fog chamber test facility available at Cardiff University. The schematic layout of the fog chamber is shown in Figure 3.10. The chamber is made of the non-corrosive material, polypropylene, and has dimensions of 2 m × 2 m × 3 m, giving a total space measuring approximately 12 m^3. It is equipped with a tubular aluminium rod suspended vertically at the centre as the test voltage point, and an earthed grid covering the base of the chamber. Water is pumped into the chamber through a spray nozzle system mounted on the wall, to generate micron-sized fog particles during the experiment. The detailed construction of this test facility including design considerations and choice of components are provided in [131].

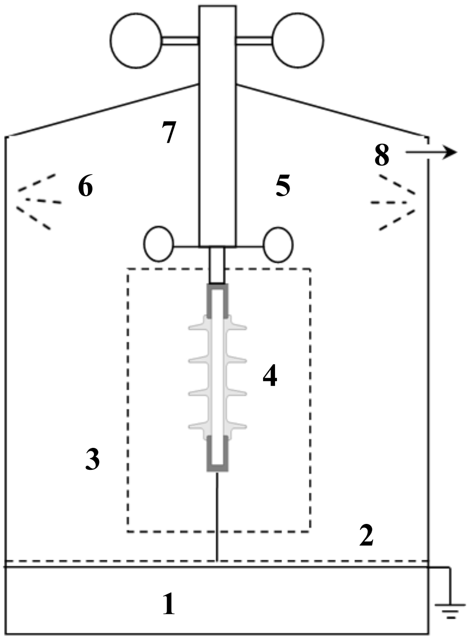

(1) Waste water container, **(2)** Grounded base, **(3)** Transparent viewing door, **(4)** Test insulator, **(5)** Grading ring, **(6)** Spray nozzle, **(7)** HV conductor, and **(8)** Pressure outlet

Figure 3.10: Schematic layout of fog chamber test facilities

3.5.2. Circuit Arrangement

The schematic diagram of the test circuit used in this experiment is shown in Figure 3.11. Test voltage is regulated using a PCL control unit (1), which is connected to a 75 kV high voltage transformer (2) through a Peschel variable transformer (output 0 V to 960 V) (3). The variable transformer (PVT) has a built-in protection system, which provides isolation in the event of transient overvoltage. The PVT features negligible distortion output which ensures improved signal quality presented at the test insulator and also on the visual probe. The voltage across the test insulator was measured through the low voltage arm of the North Star capacitive divider (6), rated at ratio 10,000:1. The leakage current was obtained from the voltage drop across a variable shunt resistor of

1.0 kΩ (7) that is connected in series with the test insulator (8). Both voltage and leakage current measurements are simultaneously displayed and stored using a LeCroy digital storage oscilloscope (DSO) (10). As a precaution, the leakage current was continuously monitored throughout the test period to ensure that the voltage drop presented at the input terminal of the oscilloscope was always in a safe range of ±10 V. In addition, a circuitry overvoltage protection box consisting of a gas discharge tube, a transient suppressor and a zinc oxide varistor is connected in parallel to the shunt resistor as a protection mechanism against surge.

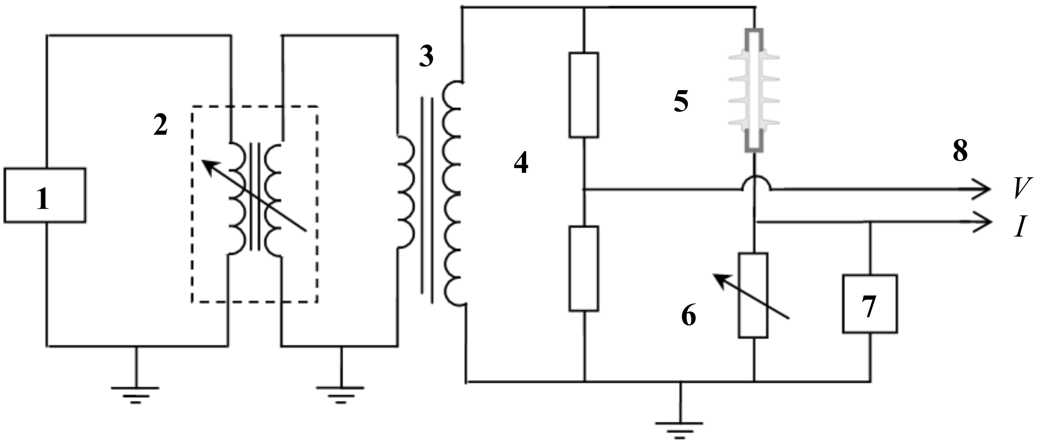

(1) PLC control unit, **(2)** Peschel variable transformer (PVT 0V-960V), **(3)** High voltage transformer (760 V/76 kV), **(4)** Capacitive divider (10,000:1), **(5)** Test polymeric insulator, **(6)** Variable shunt resistor (1 kΩ), **(7)** Protection box, and **(8)** Digital storage oscilloscope

Figure 3.11: Circuit diagram of the experimental setup

3.5.3. Preparation of Artificial Contaminant

The polluted test insulator was prepared using a solid layer method based on kaolin suspension, obtained by dissolving 40 g of kaolin in one litre of demineralised water. A suitable amount of sodium chloride (NaCl) was added to achieve the required volume conductivity of 11.2 S/m at 20˚C, which corresponds to a heavy pollution level in accordance with the BS EN 60507 standard [132]. Iso-octylphenoxypoly ethoxyethanotl, a non-ionic wetting agent Trixton X-100, at a volume concentration of 0.02%, was added to increase the wettability of the hydrophobic polymeric surface. This allows a better and more uniform pollution film without beads over the insulator surface. Prior to the contamination, the test insulator was thoroughly cleaned using water to remove any unwanted powdery stain or pollution traces. The kaolin suspension was applied to the test insulator using a 'flow-on' technique by flooding the pollution slurry over the entire polymeric surface. The insulator was then allowed to dry naturally at room temperature overnight before testing in the clean fog condition.

3.5.4. Low Voltage Test

Low voltage pollution tests based on the solid layer method were carried out to determine the time required for the test insulator to reach its most conductive state on exposure to fog generation. The insulator was hung vertically in the chamber with the top flange attached to the high voltage source, while the bottom end was connected to the ground. The spraying control system consisting of a water pump and air pressure valve was fixed at the preset settings of 3.0 litre/hour and 2.0 bar respectively to generate fog throughout the test period. A low voltage of 300 V rms was used as the source of energisation to trigger current conduction along the pollution layer. This is in accordance with the standard that suggests that the applied voltage should not be lower than 700 V rms per 100 cm of overall leakage distance. The test insulator was energised at 5 minute intervals over a period of 60 minutes from the start of fog generation. The voltage was applied only for a short instant, just sufficient to establish measurable leakage currents. The possibility of resistive heating and drying effects on the polymeric surface can, therefore, be minimised. Voltage drop across the insulator and the resulting leakage current were simultaneously measured and recorded using a digital storage oscilloscope (DSO).

The layer conductance of the pollution layer, G_{LC}, along the insulator surface can be calculated using the following expression:

$$G_{LC} = \frac{I_{LC}}{V_E} \tag{3.1}$$

where V_E and I_{LC} are the energisation voltage and the resulting leakage current flowing through the pollution respectively. Figure 3.12 shows examples of measured plots of layer conductance as a function of time under continuous fog generation.

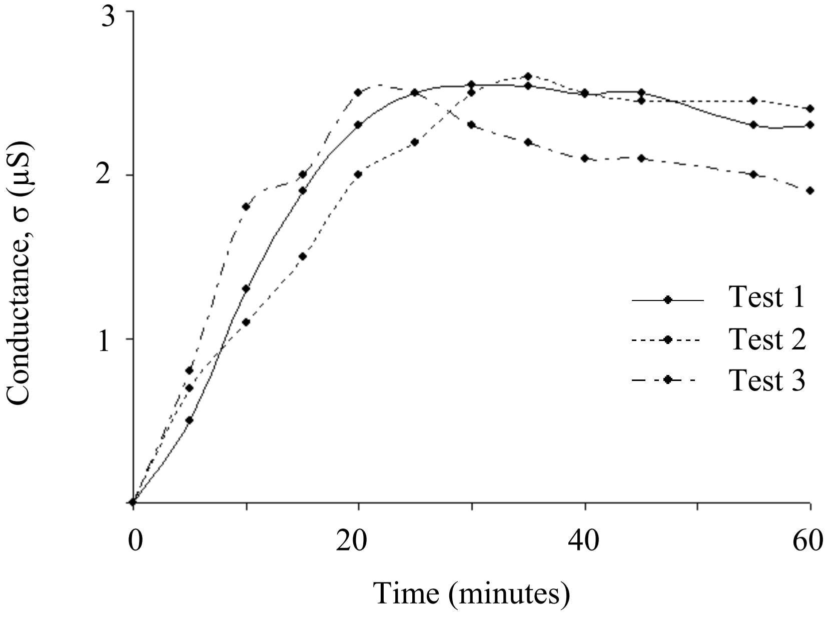

Figure 3.12: Measurements of layer conductance of polluted insulator on exposure to fog generation (water flow: 3 litre/hour, air pressure: 2 bar)

As can be seen on this figure, the conductance level increases with time as the moisture from the fog particles deposits on the polluted surface. It can be estimated that the insulator becomes saturated with water and reaches the highest conductive level after applying fog for about 25 to 30 minutes. This period will be considered as a pre-wetting stage in the high voltage test.

3.5.5. High Voltage Test

Prior to high voltage application, the test insulator was exposed to fog generation for about 25 to 30 minutes in the pre-wetting stage. According to the conductance plot in Figure 3.12, this should provide sufficient time for fog water droplets to deposit on the pollution surface, establishing maximum pollution conductivity. With continuous fog generation, a constant power frequency voltage at 18 kV rms was applied across the insulator immediately after the pre-wetting period. This energisation level is similar to that employed in the previous simulation work, and corresponds to the maximum line to ground voltage for an 11 kV system. The highest possible applied voltage together with the maximum pollution conductivity is expected to resemble the worst scenario in actual practice. A video camcorder (SONY CX190) was used to record visual manifestations of discharge activities during the test period. In addition, surface heating due to leakage current and electrical activities was monitored using an infrared thermal camera (FLIR A325) that was linked to a computer.

3.6. OBSERVATIONS AND DISCUSSION

Electric discharges were first observed on the shank region near the ground electrode (shank A). They appeared about 5 seconds after applying the high voltage source. The discharges with almost constant length were anchored at the intersecting point of the sheath and the bottom shed surface. They occurred and ceased intermittently within less than a second at different locations around the cylindrical surface before gradually elongating longitudinally down the rod in varying lengths. Discharge activity was not seen on other surface areas until electric sparks began to emerge on the bottom polymeric sheath at the ground electrode. A similar trend of arc propagation was observed in this area.

After some time, discharge activities were established at other regions; the middle (shank B) and the top shank region (shank C). Electric discharges were actively occurring on the middle shank but not on the top shank which was subjected to only minimal activity. During the whole of the test period, shank regions were sometimes completely devoid of electrical activity with only minor intermittent bursts. It was also identified that the upper surfaces of the top shed and sheath at the high voltage terminal were almost free of any discharge activity. Figure 3.13 provides snapshots of surface arcing and thermal images indicating the progression of electric discharge over the insulator surface.

The observed electrical discharges are the evidence of dry band formation on the insulator surface. Dry bands are likely to form in areas with the smallest circumference, normally the shank of the insulator structure where current density, and thus power dissipation, is greatest. This corresponds well with the experimental observations in the high voltage tests where electric discharge was first observed and was found to be actively present on the shank regions. Furthermore, regions sheltered by the shed are less wetted by the fog. As the electrical activity was not instantaneous with the voltage application, it is inferred that the initial period, before discharge initiation, corresponds to the time required for surface heating and evaporation to cause dry bands.

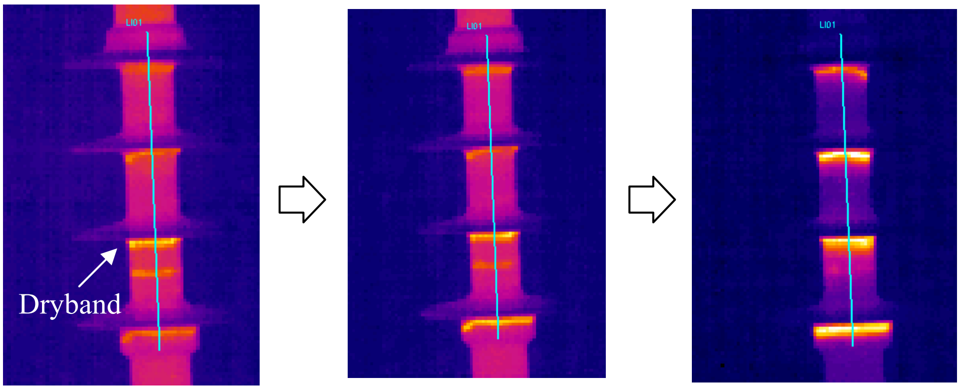

(a) Infrared thermal images

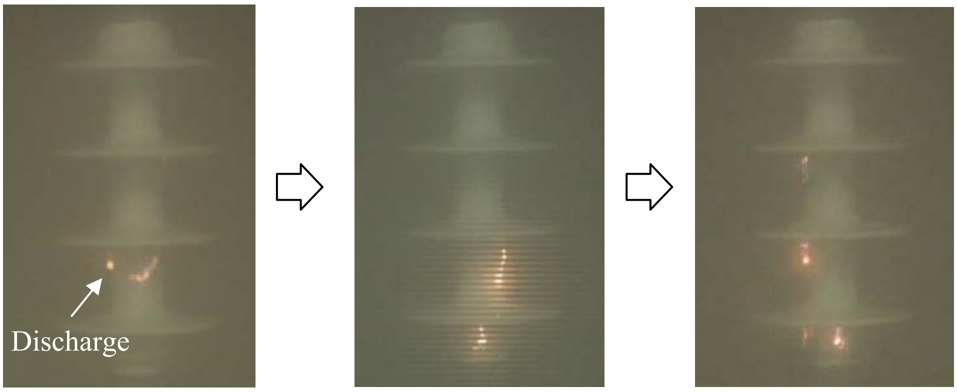

(b) Snapshots from video recording

Figure 3.13: Propagation of surface discharge during artificial pollution test

The polymeric sheath at the ground end was one of the regions being attacked early by electric discharges. Although the region has a slightly larger cylindrical diameter, hence lower current density if compared to the shank region, the high electric field in this region, shown in Figure 3.8, combined with lower wetting, greatly contributes to an increase in power dissipation ($P=EJ$) that leads to dry band formation. Surprisingly, that is not the case for the top sheath at the high voltage terminal. Electric discharge was not visually seen despite the area being subjected to a high electric field.

There are two possible reasons that could explain this unexpected behaviour: i) imbalance in wetting action, and ii) field grading by corona toroid attachment. Fog droplets, due to gravitational force, can easily reach the outward-facing surfaces compared to the hidden areas which are partly sheltered by the weather shed structure. Higher wetting rate with continuous moisture deposition on the upper surface prevents the drying of the wet pollution layer which, therefore, avoids dry band formation and the consequent electric discharges.

In addition, the pre-installed corona ring at the high voltage end effectively minimises high electric fields and, therefore relieves field stress around the top metallic electrode. For verification, insulator was modelled with corona ring structure at the top high voltage terminal, which imitates the arrangement in the fog chamber. The simulation results of equipotentials and electric field distribution are given in Figure 3.14. As can be seen, equipotential contours around the top high voltage terminal, where corona ring is attached to, are less concentrated compared to those at the ground electrode. The electric field strength in this region, as shown in Figure 3.14 (b), is about four times lower than the electric field at the other insulator end.

Reduction in electric field combined with lower current density on this surface region leads to a small and insufficient power dissipation for dry band formation. This could also be the reasons and explanation for the top shank region being subjected to only minimal electrical activity.

Throughout the test period, electric discharges show typical discharge propagation on each shank region. The short electric discharge elongates over the wider surface area and each discharge occurrence seems to trigger the subsequent chain of electric discharges around the circular shank surfaces. This progression behaviour can

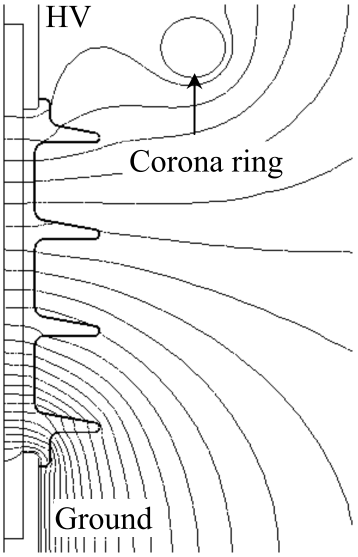

(a) Equipotentials profile

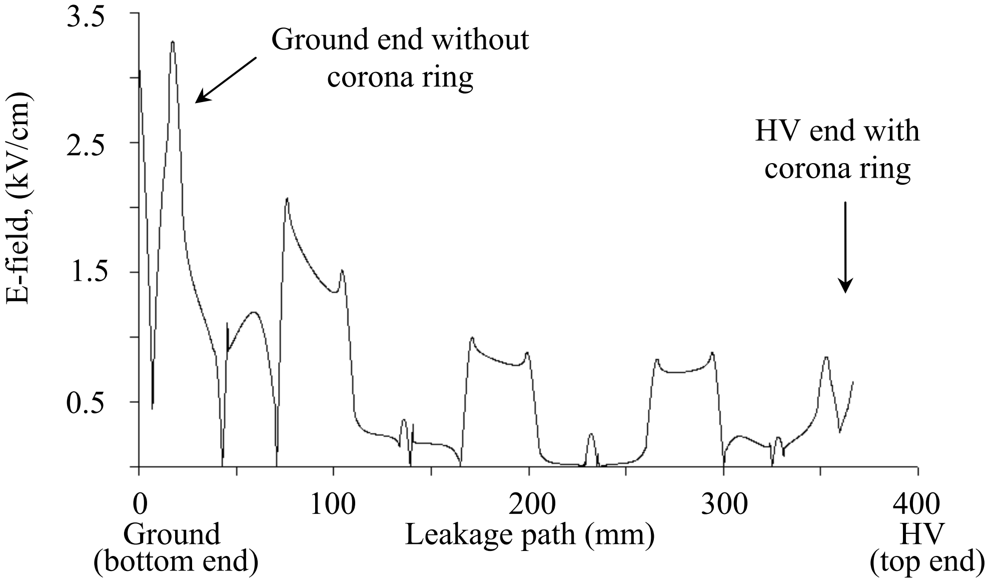

(b) Electric field distribution

Figure 3.14: The effect of stress relief by corona ring structure

be explained by discharges that generate heat, causing further drying of the wet pollution layer on the surrounding area. The dry band is, therefore, widening to promote longer arcing distances and spreading of electric discharges. However, if the dry band is sufficiently large, the electric field across the dry regions could drop below the breakdown threshold, hence inhibiting discharge activity. This accounts for the period during which the shank regions were found free from any electrical activity.

3.7. CONCLUSION

An 11 kV polymeric outdoor insulator has been simulated using a commercial finite element package to determine potential and electric field distributions on the insulator surface. An idealised model has been adopted for an easily reproducible laboratory test.

The simulation results under dry-clean and wet-polluted surface conditions reveal the highly stressed region on the insulator surface, particularly near the terminals and the shank regions. This provides useful information about surface heating that can be used to predict dry band formation along the leakage path.

Experimental investigation through artificial pollution tests has been carried out to practically examine the phenomena associated with high field stress. Electric discharges were found to actively occur on the surface regions as predicted in the simulation results. This favourable finding indicates a good correlation between the two approaches of simulation and laboratory work.

Unexpected negligible discharge activities near the high voltage terminals in the pollution test were considered to be due to two possible causes: i) imbalance in the wetting action, and ii) the field grading effect of the corona ring attachment

Finite element modelling can be a useful technique in predicting the high stress region over the insulator surface. The simulation in this study provides reliable field computations which are in accordance with the laboratory test programme.

CHAPTER 4:

A NEW DYNAMIC SIMULATION MODEL FOR POLLUTED INSULATOR

4.1. INTRODUCTION

It is well known that the performance of outdoor insulators is strongly affected by the severity and type of pollution on their surface. In Chapter 3, an insulator under wet-contaminated surface condition was modelled with a homogeneous pollution layer having a constant conductivity. Similarly in many published articles, authors usually assume a single and linear conductivity for the pollution layer when dealing with insulator modelling. This is, however, not always the case in practice. The surface conductivity will, in fact, vary with the electric field strength, particularly when subjected to electric field effects. The conductivity decreases with time as moisture from the wet pollution layer starts to evaporate and dry out, mainly due to the effect of surface heating arising from leakage current flowing through the pollution layer.

There have been a large number of research works that focus on pollution modelling, but no effort has been made to consider a pollution layer with a non-linear conductivity. In an attempt to address this shortfall, this chapter proposes the use of a pollution model that has a non-linear field-dependent conductivity in computing electric field distribution over the insulator surface. This will account for the drying effect due to electric field strength. The non-linear pollution conductivity is derived from laboratory measurements of low voltage layer conductance tests. Finite element modelling and simulations are performed under fog and light rain conditions which are considered here on the basis of their natural wetting action in practice.

4.2. FIELD-DEPENDENT CONDUCTIVITY OF POLLUTION LAYER

Pollution layer deposited on an energised insulator surface under dry conditions is risk-free, with a negligible capacitive current due to high surface resistance. However, the resistance drops significantly when the pollution layer becomes wet on exposure to humid atmospheres such as fog, mist and drizzle, which may result in a flow of leakage current and, therefore, the current density along the creepage path from the high voltage to the ground terminal. The electric field, E_S, and longitudinal current density, J_S, on the insulator surface are always non-uniform due to the geometrical shape of polymeric weather sheds housing. For a pollution layer with surface resistivity, ρ_S, the surface electric field can be expressed by the following equation:

$$E_S = \rho_S J_S \tag{4.1}$$

The current density which varies with the insulator shape is greatest in the region with the smallest cylindrical surface, i.e. the shank region. An enhanced electric field combined with the high current density leads to an increase in power dissipation, which then becomes the source of energy for surface heating to initiate dry band formation. The power dissipation, P_E, for a conducting pollution layer with uniform volume conductivity, σ_v, can be represented as:

$$P_E = E_S J_S = \frac{{J_S}^2}{\sigma_V} \tag{4.2}$$

Leakage current flowing through the polluted surface is essentially governed by the moisture level within the conducting layer. It becomes significant when the pollution layer is subjected to high humidity. The layer is considered in its most conductive state, hence its highest conductance level, when the surface is completely wet and saturated with water. The conductance level decreases as the wet pollution surface starts to dry out due to joule heating. Considering the power term in Equation (4.2), it can be predicted that the evaporation rate is minimum on exposure to low electric field, and it will increase as the electric field is increased. As such, the conductance level is not significantly changed in the low field region, and it is expected to decrease rapidly when subjected to a high electric field. This general hypothesis can be translated into a graphical representation of the electric field-conductance relationship, as shown in Figure 4.1. Nevertheless, the actual dependency will be determined experimentally and described in the next sections.

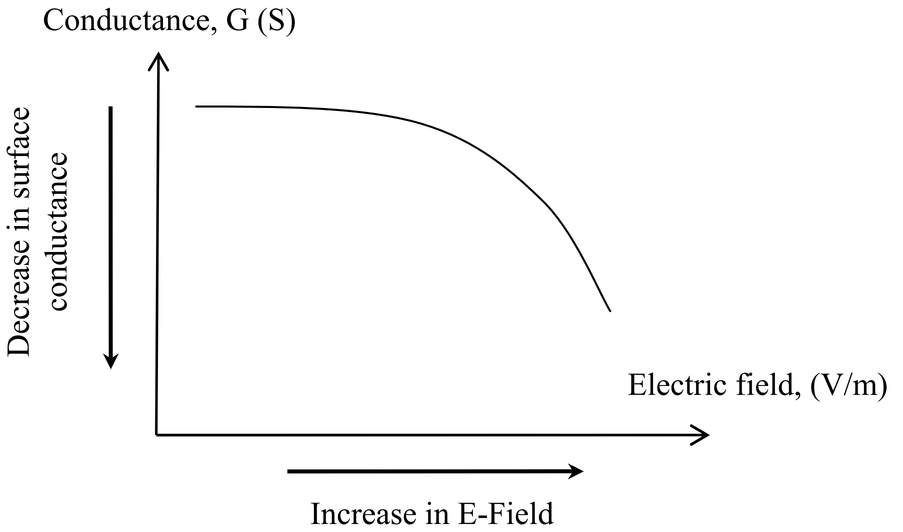

Figure 4.1: Expected general trend for layer conductance on insulator surface

4.3. LAYER CONDUCTANCE TEST

Artificial pollution tests using a low voltage source were carried out to obtain measurements of surface conductance, which were then incorporated into a field-dependent conductivity graph to be used in the pollution model in finite element simulations. The pollution test was performed in the fog chamber, using the same experimental setup as detailed in Section 3.5. The pollution suspension and test insulator were prepared using procedures identical to those described in Section 3.5.3.

4.3.1. Non-Standard Wetting Action

The standard artificial pollution experiment requires the test insulator to be wetted by fog generated using a spraying system. However, there is a significant concern regarding the possibility of washing effects when the clean-fog solid layer method is employed. Pollution on the insulator surface may gradually be washed-off on exposure to continuous fog generation, and this could contribute to a reduction in surface conductance. Instead, the pollution layer was uniformly wetted by submerging the test insulator in water, which is similar to the ‘flow-on’ technique when applying the pollution suspension. This is an alternative approach to rule out the possible washing effect of the pollution layer.

Considerable care was taken to ensure the pollution coating remained on the polymeric surface as it could be washed off during the dipping process. The insulator is considered at its maximum layer conductance when the pollution is completely wet and saturated with water, representing the most severe operating condition in practice. The advantage of using this wetting procedure is that the amount of water deposited on the entire surface can be standardised and controlled more effectively without having to consider the time to reach the maximum conductance level when using continuous fog generation as discussed in Section 3.5.4.

4.3.2. Non-Standard Test Procedures

After being uniformly wetted using the submerging technique, the test insulator was suspended vertically in the fog chamber for voltage application. Fog generation was not used in this experiment to avoid the possibility of the washing effect as explained in the previous section. To ensure an accurate examination of the effect of joule heating and surface evaporation to the layer conductance level, the low voltage test procedures as per BS EN 60507 Standard were modified. Instead of energising the test insulator at five minute time intervals as suggested in the standard, a constant and continuously low voltage source, starting at 300 V, was applied across the insulator unit. Both applied voltage, V_E, and the resulting leakage current, I_{LC}, were displayed and monitored using an oscilloscope.

The measurements were recorded every minute, starting at the point of voltage energisation for the entire test duration. The test was terminated when leakage current became negligible and a series of spikes due to electric discharges started to dominate the current waveform. The insulator was then thoroughly washed before applying a new pollution suspension for the next test. This experimental procedure was repeated with different energisation levels at 600 V, 900 V, 1.2 kV and 1.5 kV, where a 'fresh' polluted insulator was used for each test cycle.

To ensure good uniformity of the pollution layers, each insulator was subjected to a pre-test conductance measurement before commencing the actual test. The polluted insulator was energised with the lowest permissible voltage level (700 V rms per metre of overall creepage distance) at 250 V rms, applied just long enough to establish a measureable leakage current. If the computed layer conductance deviated considerably from the average value, the insulator was to be cleaned off and re-polluted until the desired starting conductance level was achieved.

4.4. DEVELOPMENT OF NON-LINEAR POLLUTION MODEL

4.4.1. Experimental Results and Analysis

Figure 4.2 shows examples of A.C. waveforms of the applied voltage and the resulting leakage current when energised with 900 V rms (1.27 kV peak). The waveforms under dry surface conditions were recorded only for comparison purposes. As can be seen on the figures, the leakage current is very small in magnitude and predominantly capacitive with 90° phase shift on a dry surface. However, there is a significant change in both magnitude and phase shift when the insulator surface is wet. The current magnitude increases from approximately 21 μA rms (30 μA peak) to 1.15 mA rms (1.65 mA peak), and the phase difference with the applied voltage is reduced to zero indicating resistive current conduction.

The layer conductance, G_{LC}, of pollution covering insulator surfaces can be computed using the following expression:

$$G_{LC} = F \times \frac{I_{LC}}{V_E} \tag{4.3}$$

where, V_E and I_{LC} are the applied voltage and the resulting leakage current flowing along the creepage of polymeric housing respectively. F is known as the geometrical form factor, a dimensionless numerical value that represents the overall surface area with regard to the shape of the polymeric insulator. It is unique for each insulator design, and can be determined using Equation (4.4):

$$F = \int_0^L \frac{l}{2\pi r(s)} ds \tag{4.4}$$

where *2πr(s)* is the circumference of the insulator surface at distance *l* along the creepage path. Form factor for the polymer insulator considered in this study is 2.94.

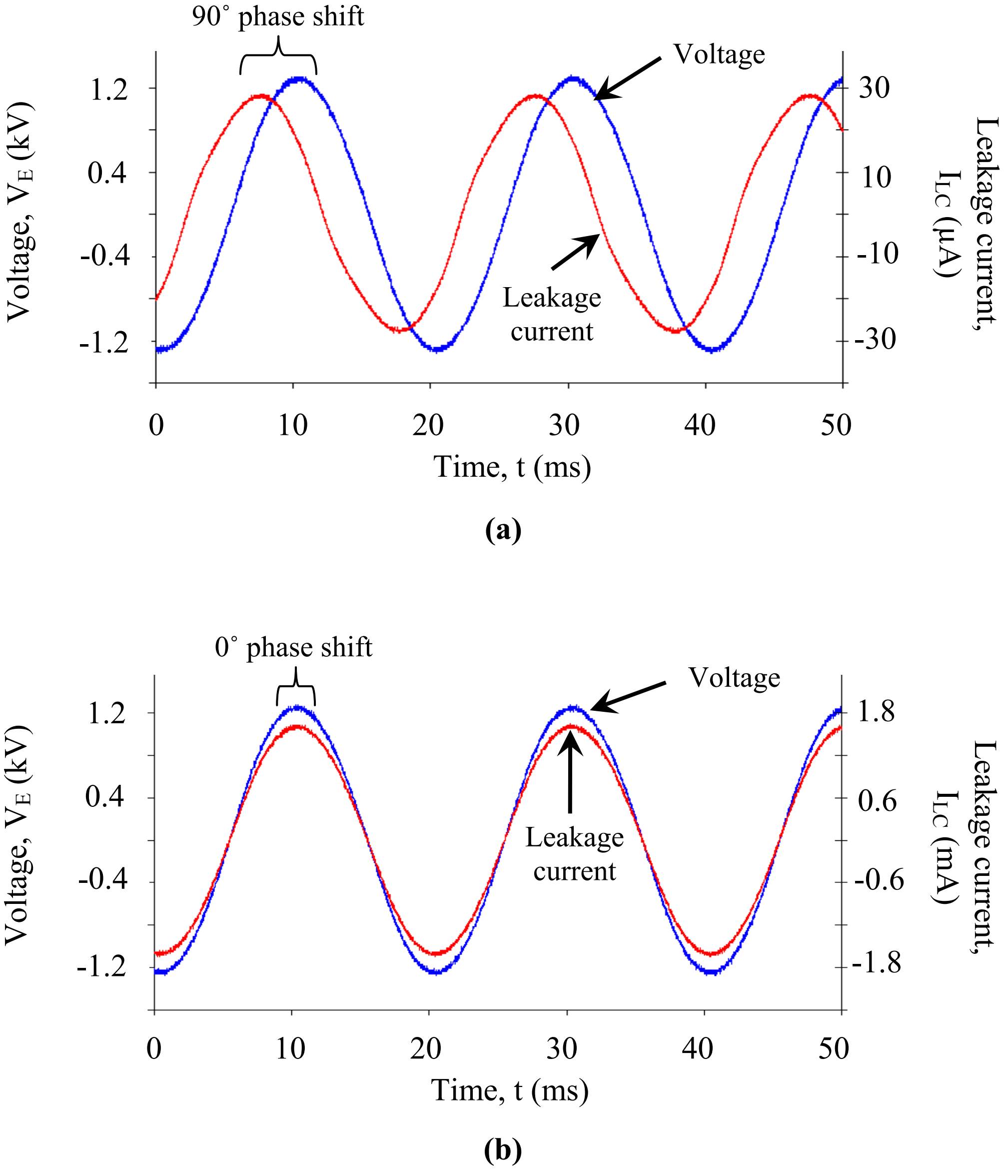

Figure 4.2: Example of voltage-current traces from oscilloscope for insulator with (a) dry-clean, and (b) wet-polluted surface

The leakage current and the corresponding surface conductance obtained in the test are tabulated in Table 4.1. Insulators A, B, C, D and E in this case represent polluted insulator used for energisation levels at voltage 300, 600, 900, 1200 and 1500 V rms respectively. The small differences between the measured layer conductance values indicate marginal discrepancy in the pollution layers, which give clear evidence of excellent consistency for all test insulator surfaces.

Table 4.1: Measurement of initial conductance prior to the test investigating drying effect on conductance (test voltage 250 V rms)

Test insulator	Ins. A	Ins. B	Ins. C	Ins. D	Ins. E
Leakage current (mA)	0.327	0.336	0.319	0.305	0.323
Conductance (µS)	3.845	3.951	3.751	3.587	3.798

Ins. = Insulator

Figure 4.3 shows the plot of leakage current for different energisation levels obtained in the low voltage test, and the corresponding layer conductance obtained using Equation (4.3), is presented in Figure 4.4. The conductance curve is normalised to its initial conductance value. These two parameters i.e. leakage current and normalised conductance are plotted as a function of the duration of the test period. As can be seen, the curve for all voltage levels in both figures shows a general reduction trend throughout the test period. The leakage current and layer conductance are highest at the point of energisation (t = 0 s) and then gradually decrease with time before a sudden fall towards the end. At this point, it is thought that a dry band is formed, preventing flow of current in each test. The maximum leakage current and layer conductance indicate that the polluted insulator is in its most conductive state after being uniformly wetted prior to the start of the test. The reduction in these parameters is the evidence of surface heating that evaporates water from the pollution layer during current conduction.

The steep gradient in the early voltage applications suggests an accelerated evaporation process due to high power dissipation ($P=EJ$) that facilitates the drying of the wet pollution layer. As the water level on the insulator surface continues to decrease, the resulting leakage current, which is relatively low in magnitude, requires a longer time to generate adequate heating energy to cause further evaporation. Therefore, minimal change in both leakage current and layer conductance due to the low evaporation rate is observed after about 5 minutes of voltage energisation. The subsequent sudden drop at the end of each curve can be accounted for by the formation of dry bands that prevent the flow of leakage current over the insulator surface. The time taken for this to happen varies depending on the applied voltage. The higher the voltage level, the shorter the time required for dry band formation. Higher voltage, as expected, generates greater heating energy that would speed up the drying process. The series of steep falls, as can be seen on the plot at higher voltage levels of 1.2 kV rms and 1.5 kV rms, suggests discontinuous current conduction in the early stage of dry band formations.

4.4.2. Proposal for the Derivation of Field Dependent Conductivity of the Pollution Layer

According to the hypothesis described in Section 4.2, surface conductance will decrease on exposure to high electric field. This is primarily due to the joule heating that causes drying of pollution layer. In this section, the intention is to establish a relationship of non-linear pollution conductivity as a function of applied electric field.

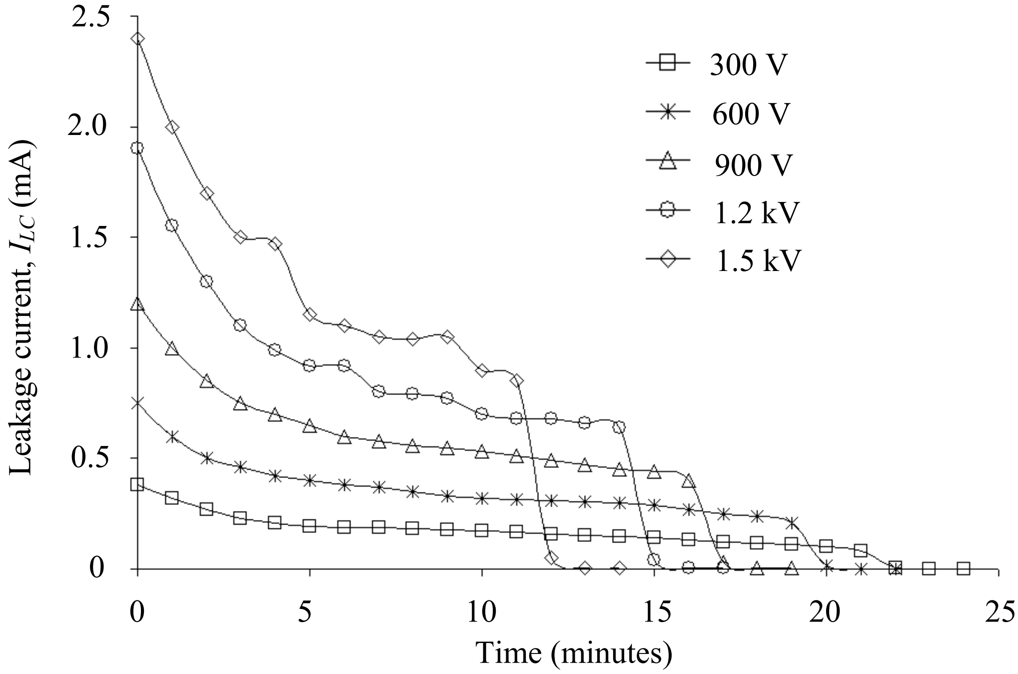

Figure 4.3: Measurements of leakage current for different energisation voltages

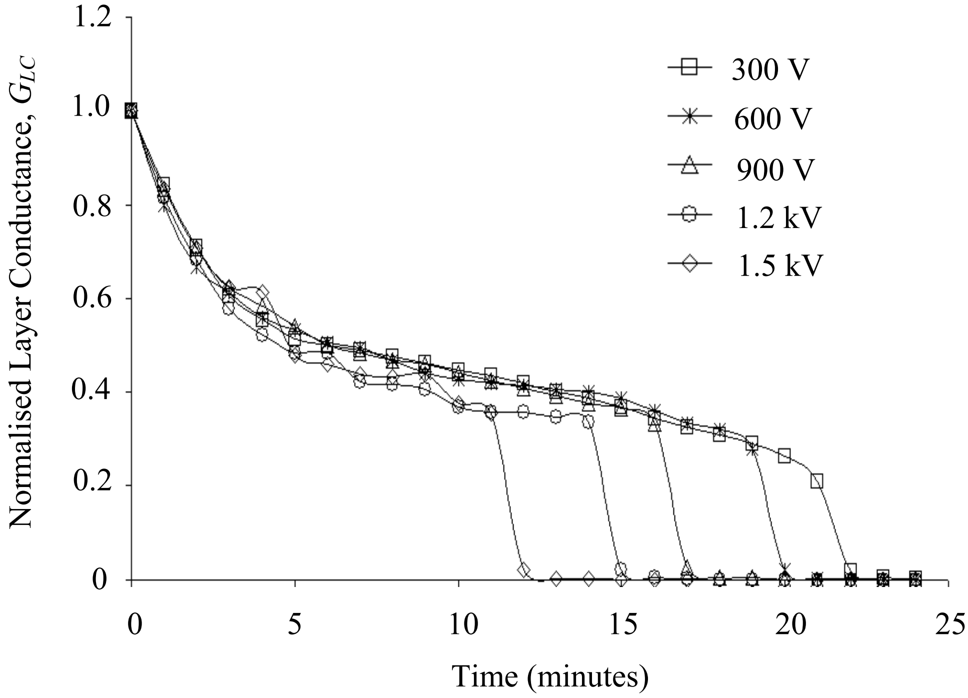

Figure 4.4: Normalised layer conductance for the leakage current measurements given in Figure 4.3

For a very simplistic model, the average electric field, E, on the insulator surface, can be approximated by the following equation:

$$E = \frac{V_E}{d_C} \tag{4.5}$$

where V_E is the energisation voltage and d_C is the total creepage distance of polymeric housing. In this study, the change in surface conductance is termed as 'conductance index', ΔG, and is defined as the difference between the maximum (G_{max}) and the minimum (G_{min}) conductance levels measured during the low voltage test. It is calculated using Equation (4.6):

$$\Delta G = G_{\max} - G_{\min} \tag{4.6}$$

Assuming the conductance is negligible (i.e. zero) when the dry band occurs, the conductance index, ΔG, for the complete drying process is, therefore, equal to the maximum conductance level, G_{max}, when the pollution layer is saturated with water. If the flow of leakage current requires a certain period of time, t, to cause a complete dry band, the rate of reduction in surface conductance, $R_{\Delta G}$ (S/min), can be expressed as:

$$R_{\Delta G} = \frac{\Delta G}{t} = \frac{G_{\max}}{t} \tag{4.7}$$

Figure 4.5 shows the plot of $R_{\Delta G}$ as a function of the average field, E, developed from the experimental result of layer conductance measurement. As can be seen, the rate of reduction in layer conductance, which corresponds to the evaporation/drying rate, increases as the specific creepage field increases. This dependency confirms the hypothesis described in the earlier section. A high electric field generates greater heating energy that leads to an accelerated drying of the pollution surface layer on the insulator surface.

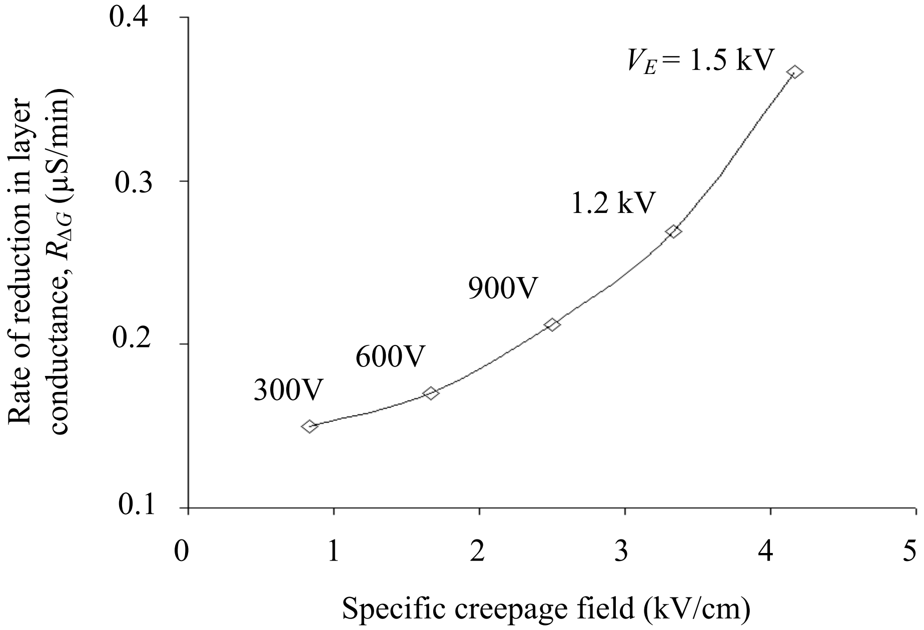

Figure 4.5: Rate of change in surface conductance as a function of specific creepage field

The plot of pollution conductivity as a function of electric field is shown in Figure 4.6. This relationship is established using the experimental results with some simplifying assumptions. In order to generate this plot, polluted test insulators are assumed to have uniform and identical pollution conductivity. That means, the initial surface conductance at t = 0 minute for all test insulators will be the same. Here, the value of initial conductance is assumed maximum at 4.2 µS (the average value obtained from the laboratory measurements). This initial conductance is assumed to correspondingly decrease by $R_{\Delta G}$ within a minute when subjected to the electric field (refer Figure 4.5), hence giving the field dependent conductance curve as shown in

Figure 4.6. It can be seen that the surface conductance decreases with an increase in the electric field. However, the relationship at higher fields, i.e. greater than 5 kV/cm, could not be plotted due to lack of experimental data at higher voltage levels. Measurement of leakage current for insulator with energisation level greater than 1.5 kV could not be carried out due to difficulties in obtaining accurate readings from the oscilloscope. Active electric discharges on the insulator surface greatly distorted the sinusoidal leakage current waveforms, with a series of peaks that could lead to significant errors.

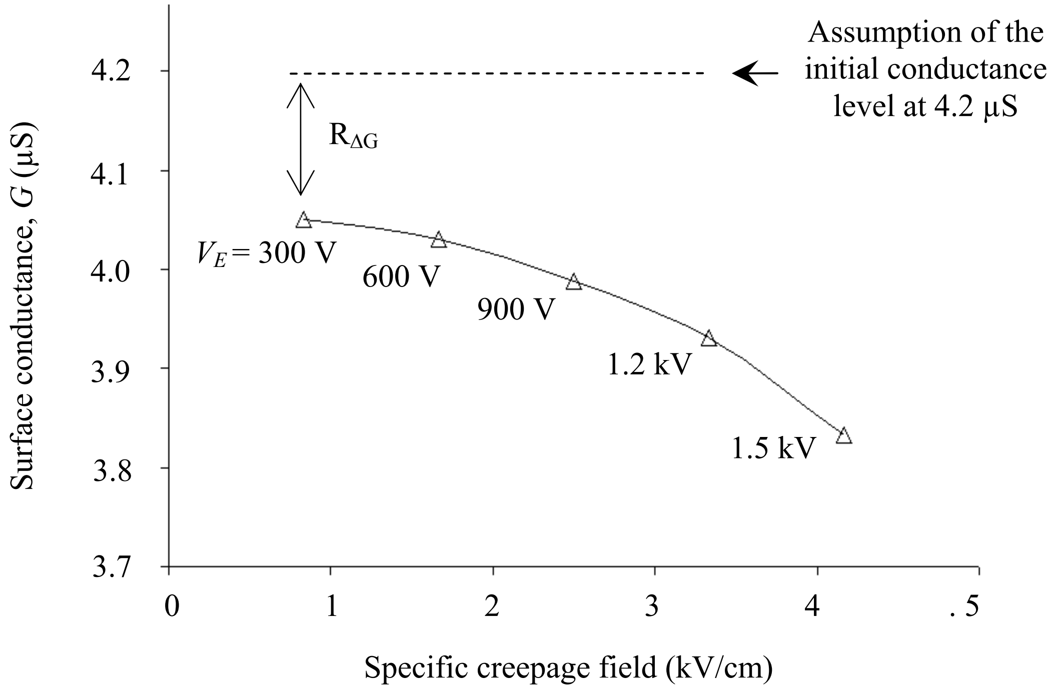

Figure 4.6: Surface conductance as a function of average field on polluted insulator

As an approach to obtain the dependency at higher field level, a curve extrapolation method has been adopted using the available curve fitting tool in MS Excel. Figure 4.7 presents the extrapolation plot of field-conductance relationship over a wider range of electric fields approaching air breakdown threshold at about 10 kV/cm. The trend of the curve on the log-log scale plot shows an exponential decay, which was approximated by an empirical general mathematical expression as given by Equation (4.8):

$$G = \sigma_0 \; e^{\tau(E)} \tag{4.8}$$

where σ_0 represents the initial conductivity value, while τ defines the rate of change in conductivity at the switching threshold level. From Figure 4.7, the following values were obtained; σ_0 = 4.2 μS and, $\tau = -6.7\times10^5$. This extrapolation plot will be adopted to characterise the pollution model in the numerical simulations.

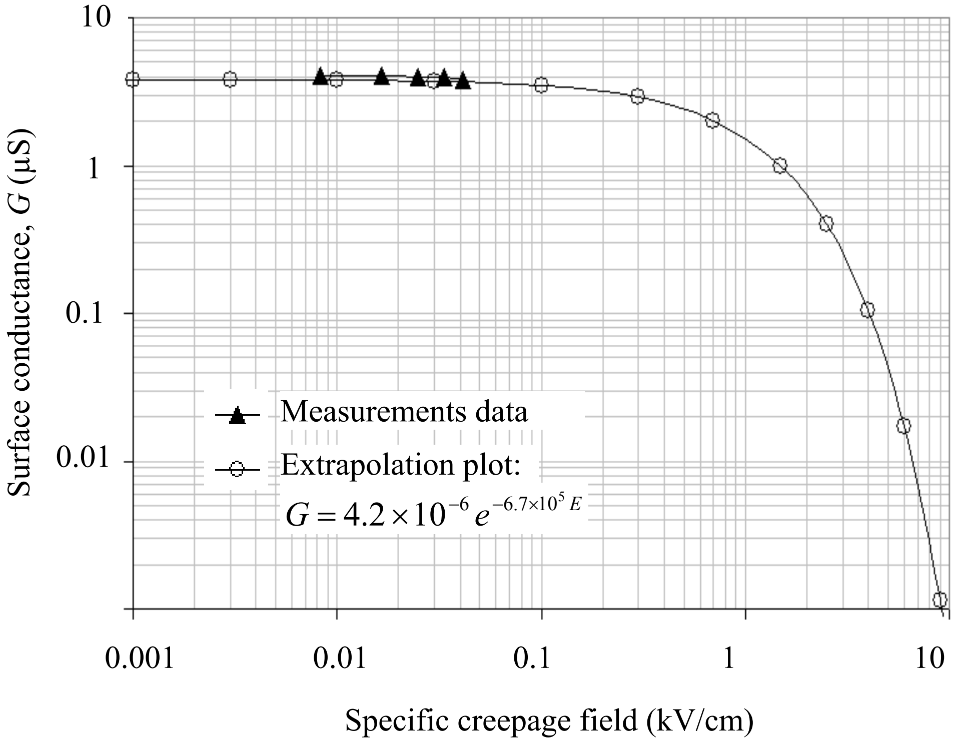

Figure 4.7: Proposed pollution layer conductance as function of electric field

4.5. CLASSIFICATION OF POLLUTION MODEL

Dry band formation on polymeric outdoor insulators is governed by two important factors: i) the dissipated power that leads to surface heating and evaporation (drying rate), and ii) the rate of moisture being deposited on the polluted surface (wetting rate). Occasionally, dry bands will occur when the drying rate is equivalent to, or greater than, the wetting rate. Under heavy rain conditions where the insulator is subjected to a high wetting action, dry bands may not have a chance to establish on the insulator surface. The rain could re-wet the dry region, or wash away the deposited pollutants, to prevent a continuous conductive layer along the leakage path. However, outdoor insulator is at high risk of dry band formation if exposed to moderate humidity such as light rain and fog-atmosphere. For better understanding, a pollution model under fog and light rain conditions is developed for simulation of electric field distribution over the insulator surface. The pollution model represents uniform (fog) and non-uniform (light rain) wetting scenarios.

4.5.1. Model Under Fog Condition (Uniform Wetting)

Under the fog condition, tiny water droplets move slowly in random motion in the atmosphere. They could reach the insulator surface from almost any direction. Therefore, the wetting of the pollution layer under fog conditions is assumed to be constant and uniform along the leakage path. The proposed field-dependent conductivity for the pollution model under fog conditions is given by the extrapolation curve plotted in Figure 4.7, which was obtained from the low voltage experiment using uniform wetting procedures.

From the figure, it can be seen that the conductivity is maximum and nearly constant in the low electric field region. The pollution layer in this case is saturated with water, and the dissipated power which would cause water evaporation is negligible, due to the low electric field. The conductivity gradually decreases as the electric field increases, indicating the effect of surface heating that evaporates water from the pollution layer. With a continuous drying process, when the electric field exceeds a certain threshold level, the conductivity drops rapidly, as clearly shown in the field region above approximately 1.0 kV/cm. The surface conductivity is considered zero in the higher field region above 10 kV/cm, reflecting a complete drying process which turns the wet conductive region into a dry and high resistive area on the polymeric surface.

4.5.2. Model under Light Rain Condition (Non-Uniform Wetting)

In contrast to the fog condition, deposition of water under light rain conditions varies depending on the region of the polymeric insulator. Surface areas that face the rainfall are subjected to a higher wetting rate compared with those in the sheltered regions (under shed surfaces). For modelling purposes, the uniform pollution layer along the creepage path is subdivided into three main regions namely: H (high), M (medium), and L (low) as illustrated in Figure 4.8. Each region is categorised based on the wetting action in practice. Region H, assigned to the upper surface, represents a highly wetted area. Water from the rain can easily reach this area without any obstacles. Half of the under sheds close to the tip, indicated by region M, are classified as a region with medium wetting rate while the remaining regions down to the shank, marked by region L, are considered to be the least wetted areas on account of their sheltered location protected by the sheds.

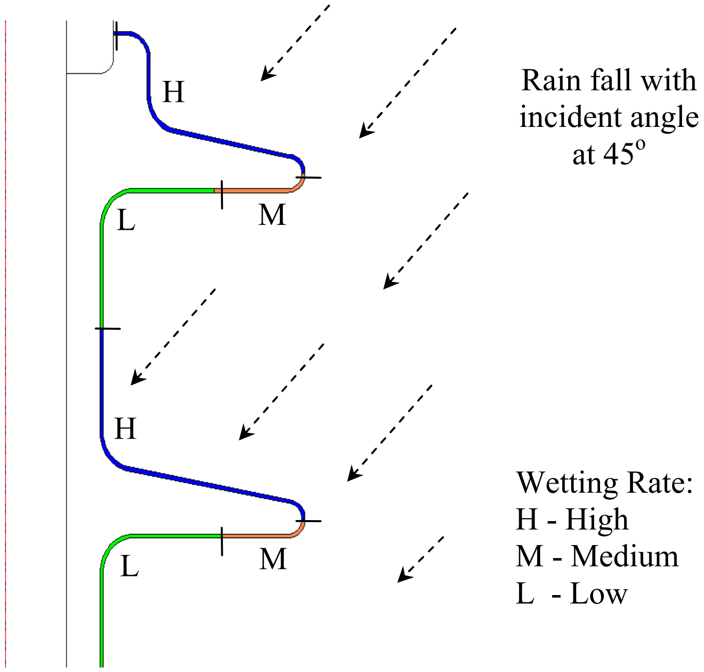

Figure 4.8: Subdivision of pollution layer under light rain conditions according to wetting level

Figure 4.9 shows three independent surface conductivity curves proposed to characterise the pollution layer under light rain conditions. Each curve, marked by H, M and L, is assigned to the pollution model in regions H, M and L respectively. These curves replicate the general reduction trend of the plot considered under fog conditions. The small difference in the maximum conductivity and the field threshold at which the conductivity starts to decrease rapidly accounted for the variation of water deposition under the described light rain conditions. Curve H is assigned with the highest surface conductivity, initial 4.2 µS/m, considering region H as the most water-saturated area. The medium and least saturated areas M and L are characterised by a slightly lower initial conductivity of 3.0 µS/m and 2.0 µS/m respectively. The region with a low field threshold represents a less wetted area and, therefore, is subject to a higher probability of dry band formation. Therefore, the pollution model in region L is associated with the lowest threshold level, followed by region M and H respectively with the moderate and the highest threshold levels, indicating surfaces that are exposed to a greater wetting level.

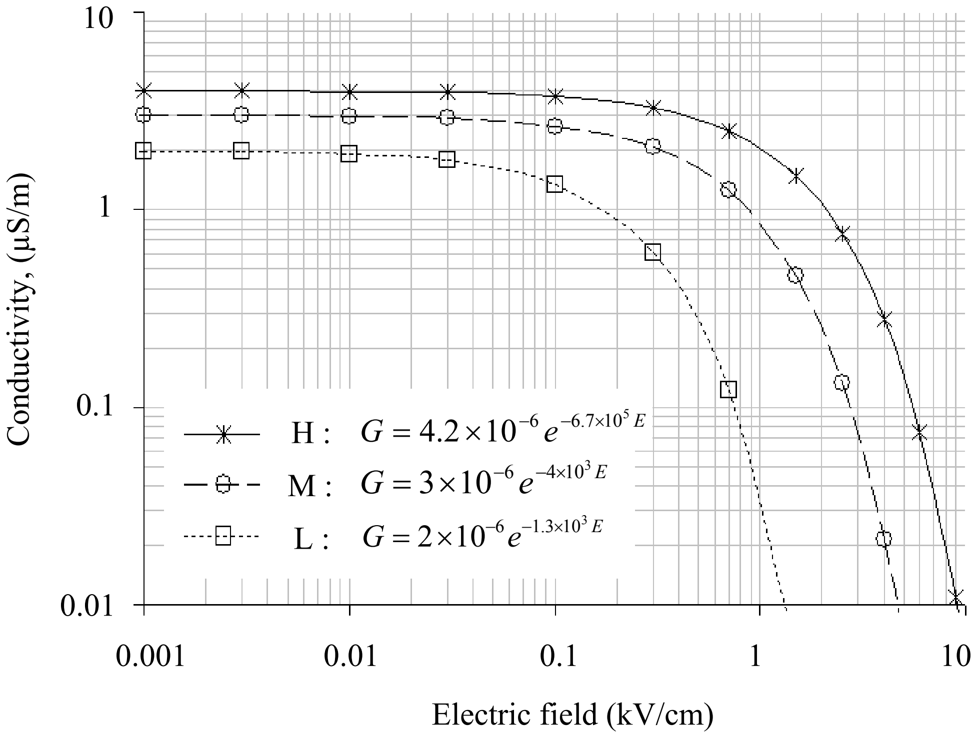

Figure 4.9: Field-dependent conductivity for the pollution model under light rain conditions (non-uniform wetting)

4.6. COMPUTATION OF ELECTRIC FIELD USING THE PROPOSED NON-LINEAR POLLUTION MODEL

Field distributions along the creepage path were computed under wet weather conditions; fog and light rain conditions, using the proposed non-linear pollution models. It is expected that a better and more realistic field distribution, that could be useful for dry band prediction, would be obtained using this approach when compared with commonly used single value conductivity of the pollution layer.

4.6.1. FEM Modelling

Similar modelling setup and procedures to those described in Section 3.3 were adopted in this simulation work. The non-linear property for the pollution layer was specified as an exponential function, as shown in Figure 4.7 (fog model) and Figure 4.9 (light rain model).

4.6.2. Simulation Results and Analysis

For comparison purposes, simulation results of electric field under polluted surface conditions presented in Chapter 3 were considered as a reference. The pollution layer that has been modelled with linear conductivity is an example of the common modelling practice found in most of the available literature, where the effects of wetting and drying processes, and hence the variations of layer conductance with the electric field, are not taken into account.

The computed field distribution from the proposed non-linear pollution model under fog conditions (uniform wetting) is compared with the linear model in Figure 4.10. The pollution is characterised by a non-linear field-dependent conductivity shown in Figure 4.7. It is evident in the figure that there is a slight difference between the two field profiles. The non-linear model indicates a redistribution of the electric field, where the local stress near the terminals is raised from a normal value of 1.2 kV/cm to approximately 1.6 kV/cm, representing about 33% field enhancement. A moderate field increase, nearly 10%, is also observed on the bottom and top shank regions i.e. shank A and shank C respectively. The rise in electric field, when considering the non-linear pollution model, can be explained by the reduction in surface conductivity as the computed field reaches the drying threshold. Such results could be interpreted as an acceleration process for dry banding, as higher fields appear due to redistribution resulting from heating effects. The profile on the middle shanks is almost unchanged because the computed electric field is not high enough and remains in the constant conductivity region similar to the standard model.

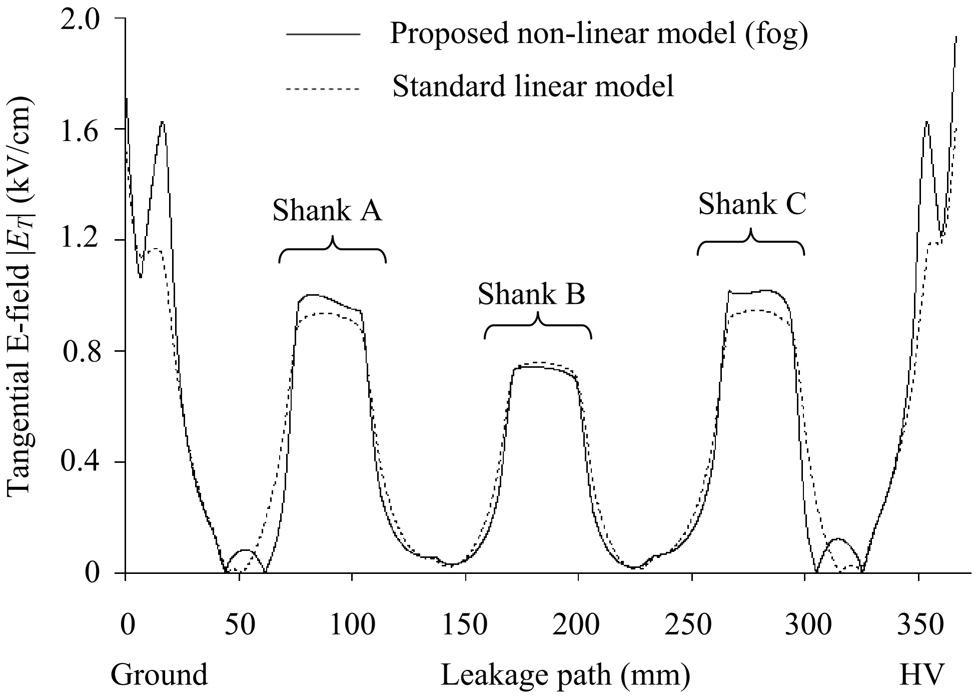

Figure 4.10: Comparison of field distributions from the proposed non-linear pollution model (fog condition) with the single value conductance model

Figure 4.11 shows a comparison of field distribution when simulating the non-linear pollution model under light rain conditions (non-uniform wetting). The pollution layer in this case is characterised by three different layer conductance characteristics as described in Section 4.5.2. The proposed non-linear model provides field distribution with a series of peaks at different locations along the creepage distance. The peaks show a significant field increase, more than double the magnitude of the linear model. Similar to the explanation for the increase under fog conditions, the peaks appear when the electric field is high in a region, resulting in decreased conductivity due to the drying effect that was considered in the proposed model. It is clear that discharge will occur on the surfaces at the bottom terminal as well as the sheltered shank regions, represented by region L in Figure 4.8, where the wetting rate is minimum. These are the regions that are susceptible to dry band formation and discharge activities, as observed in the laboratory and as reported in most of the published literature.

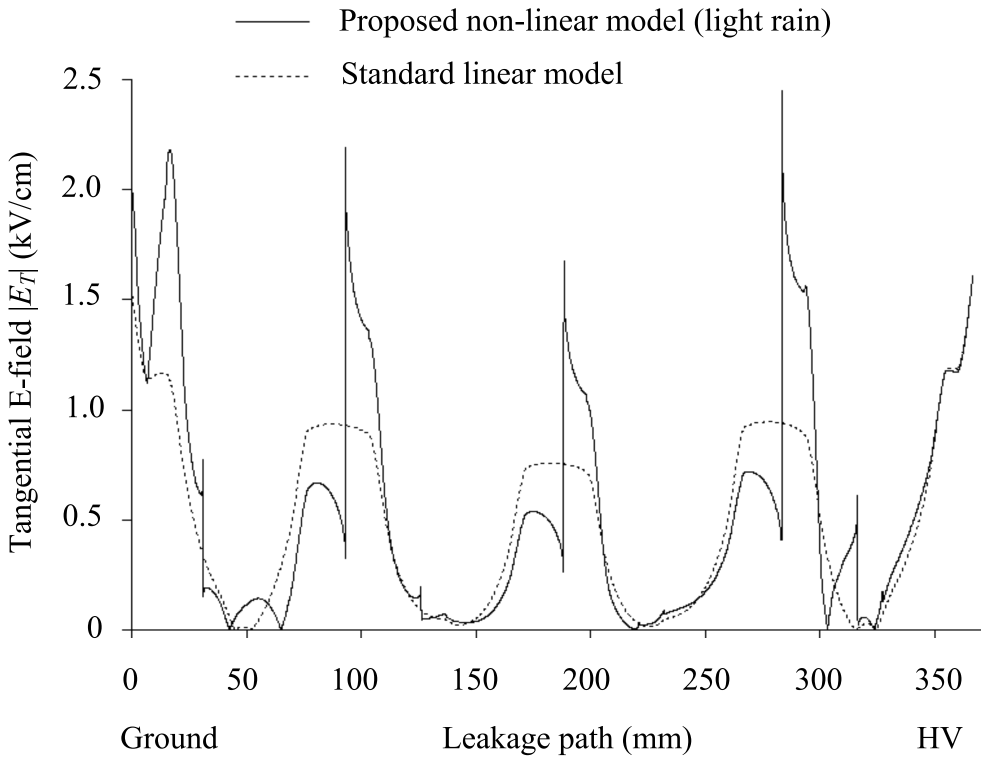

Figure 4.11: Comparison of field distributions from the proposed non-linear pollution model (light rain) and standard linear model

On the contrary, the upper shed surfaces, indicated by region H, show a slight decrease in the electric field if compared to the standard model. Such behaviour is evidence of higher conductivity and higher drying thresholds which account for surface regions with high wetting action. Field enhancement is, therefore, not observed in the top shed region at the high voltage end.

The field comparative study clearly shows that the use of non-linear pollution models leads to detailed and more realistic field profiles compared to conventional modelling with typical assumptions of linear and constant conductivity. The presence of peaks in the distribution provides better understanding of field response on insulator surfaces which are important for dry band prediction. In addition, the simulation results from the proposed non-linear models show a good correlation with the experimental observations in Section 3.5, where, as expected, dry band and electric discharges were actively present at the bottom ground terminal and on the sheltered shank surfaces.

4.7. CONCLUSION

Low voltage artificial pollution tests, based on the BS EN 60507 solid layer method, have been carried out on 11 kV polymeric insulators to measure leakage current at various energisation levels. Non-standard approaches were adopted in the experimental procedures to allow an investigation into the effect of surface drying on the layer conductance.

A new field-dependent conductivity for characterising non-linear pollution models has been successfully developed from the experimental results. Pollution models under fog and light rain conditions have been proposed to simulate the electric field distribution along the leakage path and its effect on the drying of the pollution layer. The models represent uniform as well as non-uniform wetting behaviour in practice.

The simulation results from the proposed non-linear model have demonstrated a detailed and more realistic field distribution with the presence of peaks, which do not appear on the profile from the standard single conductivity model. The spike in the electric field profile suggests a drop in surface conductance at the high field region, and this is attributed to evaporation and heating effects that were examined in this study. This is particularly useful to locate dry band formation on the insulator surface where discharge may occur.

CHAPTER 5:

PROPOSAL FOR STRESS CONTROL ON INSULATOR SURFACE USING ZNO MICROVARISTOR COMPOUNDS

5.1. INTRODUCTION

One of the major threats to polymeric outdoor insulators is the localised high electric field on the insulator surface, in particular at the high voltage electrode and ground terminals. They could result in significant electric discharges when subjected to moisture. In favourable conditions, on exposure to severe polluted environments under prolonged wetting conditions, a high field that facilitates the propagation of electric discharges on the insulator surface could trigger complete insulator flashover. Moreover, continuous discharge activity leads to material degradation through surface tracking and erosion that will reduce the flashover voltage and insulation performance. Considering these undesirable consequences, effective stress control and field grading is extremely important to alleviate the effect of such detrimental discharges on polymeric outdoor insulators.

The use of non-linear field grading materials on many high voltage applications such as cable terminations and motor windings has been successful in minimising high electrical stress on the insulation surface [118], [120]. This encouraging realisation has triggered research investigations to examine the feasibility of this grading material on polymeric outdoor insulators.

In this chapter, the effect of microvaristor utilisation as a means of controlling electric stress on polymeric outdoor insulators is investigated. This new approach is to provide an alternative for the existing grading techniques using hardware fittings, i.e. corona ring. In the proposed design, a short length of microvaristor-based compound is applied onto the core of the insulator near the high voltage and ground terminals, which is then encapsulated within the silicone rubber housing for protection against various environmental effects. The field grading and optimisation principles to allow better performance are investigated in an attempt to improve the insulator performance under steady state operation and surge conditions. The insulator equipped with microvaristor layers is modelled under dry-clean and uniformly polluted surface conditions and the simulation results are compared with those obtained from a standard insulator design without field grading material. In addition, the dissipated power and associated heat are derived to analyse surface heating and losses in the graded regions.

5.2. PROPOSAL FOR MICROVARISTOR-GRADED INSULATOR

One of the effective approaches for minimising local discharges on polymeric insulation for many high voltage applications is to suppress high field regions on the surface. This can be successfully achieved through the application of stress grading material using capacitive, resistive or non-linear materials. Among these options, the non-linear material grading solution appears to be a promising method for use on outdoor polymeric insulators.

5.2.1. Microvaristor Characteristics

In recent years, ZnO microvaristor, micro-scaled electroceramic particles exhibiting highly non-linear electrical properties, similar to the varistor in high voltage arrester applications, have been developed [111]. The non-linear switching characteristics can always be tailored to any desired threshold level using sophisticated manufacturing processes, giving flexibility for the material to be used in a wide range of applications [115]. At present, microvaristor-filled composites are commercially produced for grading purposes mainly for indoor applications such as machines and cables. Figure 5.1 shows a measured electrical characteristic of microvaristor compound provided by a German manufacturer [133], which was also used for designing and building an insulator prototype as described in Chapter 6. As can be seen on the figure, this is reminiscent of the highly non-linear characteristic of ZnO material used for high voltage surge arresters.

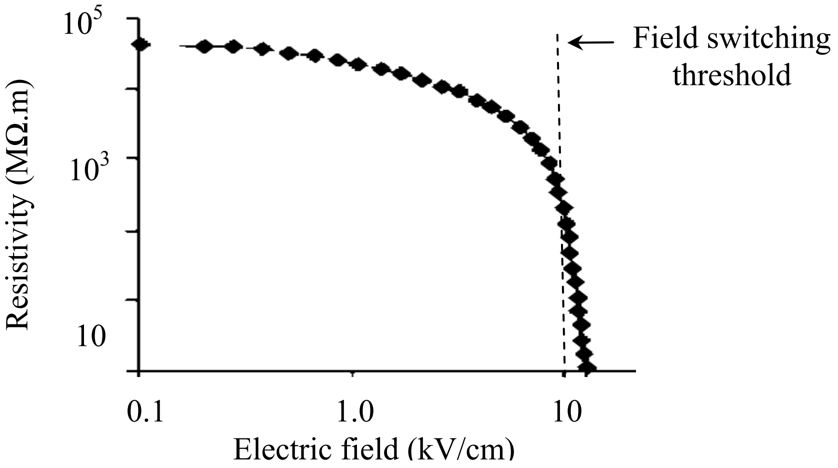

Figure 5.1: Resistivity of microvaristor compound with field conduction switching threshold at 10 kV/cm [133]

5.2.2. Options for New Insulator Design

Different promising design options for implementing the microvaristors on the polymeric insulator were considered:

i) One option is to apply a thin grading layer on the insulator surface. With this arrangement, the electric field along the creepage path is expected to be uniform, even with the presence of a discontinuous wet pollution layer. As the field across the dry areas reaches the switching threshold, the grading material starts to conduct, hence bridging the dry regions. Consequently, damaging electric discharges on the surface may be avoided. The implementation, however, may not be suitable for outdoor applications. Constant conduction together with the impact from the environment can lead to other problems such as losses and thermal damage which, consequently, may result in tracking/erosion and possible premature failure.

ii) Another option is to utilise a thin cylindrical microvaristor coating along the full length of the insulator core structure, which will then be covered by the silicone housing. With the ability to conduct when reaching a set electric field threshold, the material is expected to suppress high fields on the insulator, giving a better and improved field distribution. It should be stressed, however, that with this design, there is a concern on the long-term performance. Continuous leakage current will cause unacceptable power losses along the overhead lines or even at a particular substation application. More importantly, internal heating would certainly lead to internal damage and eventually to insulation failure. In the worst case scenario, the coating may even short-circuit the insulation material, allowing current flow directly from the high voltage terminal to the ground terminal.

iii) The design approach adopted in this investigation is to avoid the shortfalls described above. The grading material is, therefore, applied at the interface between the core and the silicone housing only near the insulator high voltage and earth terminals. The material is coated onto the fibre-reinforced core with a cone-like graded thickness towards the middle part of the insulator, as illustrated in Figure 5.2. The microvaristor grading coating, which is thicker at the electrode ends, is designed to handle the high field in these regions. With the proposed cone-shaped geometry, concentrated equipotentials near the insulator terminals can be gradually redistributed away from these overstressed areas. The microvaristor layer is also intentionally extended to the sheds region in the middle to provide a smooth transition of the displaced equipotentials, thus reducing electrical stress on the critical shank regions.

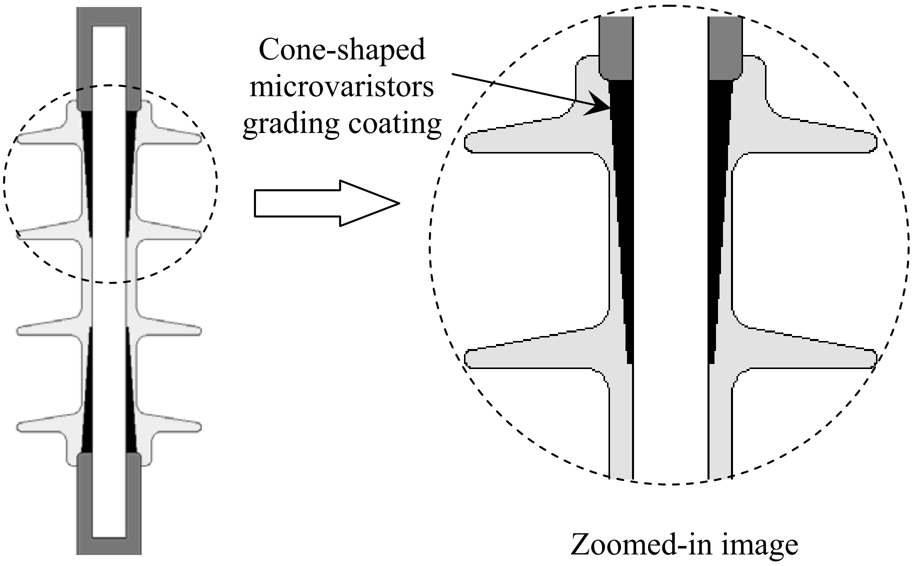

Figure 5.2: Proposed design of microvaristor-graded insulator

5.3. OPTIMISATION OF MICROVARISTOR CHARACTERISTICS

For optimum stress grading performance, it is important to identify suitable conduction field characteristics of the microvaristor material for each specific application. In this way, tailor-made compounds can be requested from the manufacturer for specific applications.

5.3.1. Consideration for Field Switching Threshold

Electrical stress control on polymeric insulators can only be successfully realised by using microvaristors with switching properties within the limits of the electric field appearing along the insulator under the applied voltage conditions. The electric field along the axial line at the core-silicone interface, as shown in Figure 5.3, is utilised to specify an appropriate switching threshold for the 11 kV insulator under investigation.

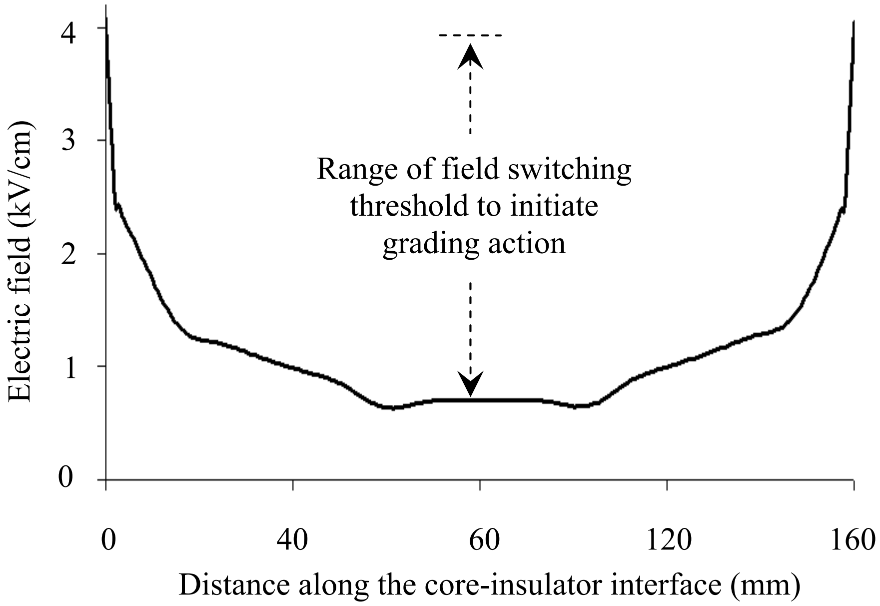

Figure 5.3: Field distribution at the interface between core and polymeric housing

According to the field profile, the conduction switching threshold of the microvaristors should be lower than 4 kV/cm to allow the initiation of microvaristor conduction and, therefore, trigger its grading actions. On the other hand, a sufficiently high threshold value needs to be chosen so that the switching level is not too low, as this may result in constant current conduction and overstress the middle part of the insulator, where no grading material is used.

The conductivity of a microvaristor-based compound that exhibits a highly non-linear behaviour can be represented by a general exponential function, as given in Equation (5.1) [134].

$$\sigma(E) = \sigma_0 \, e^{\alpha E} \qquad (5.1)$$

In this equation, σ_0 represents the initial conductivity, while the constant α determines the field switching threshold at which the material changes its electrical properties from an insulator to conductor.

Figure 5.4 shows three examples of the microvaristor material conductivity-electric field characteristics, constructed in this work in order to optimise the grading effect on the electric field distribution along the insulator surface. Each curve is designated by its switching threshold field, E_0, above which a significant conduction increase occurs for a small change in electric field magnitude. This is equivalent to the concept of ‘turn-on’ voltage used for the voltage-current characteristic of ZnO surge arrester materials.

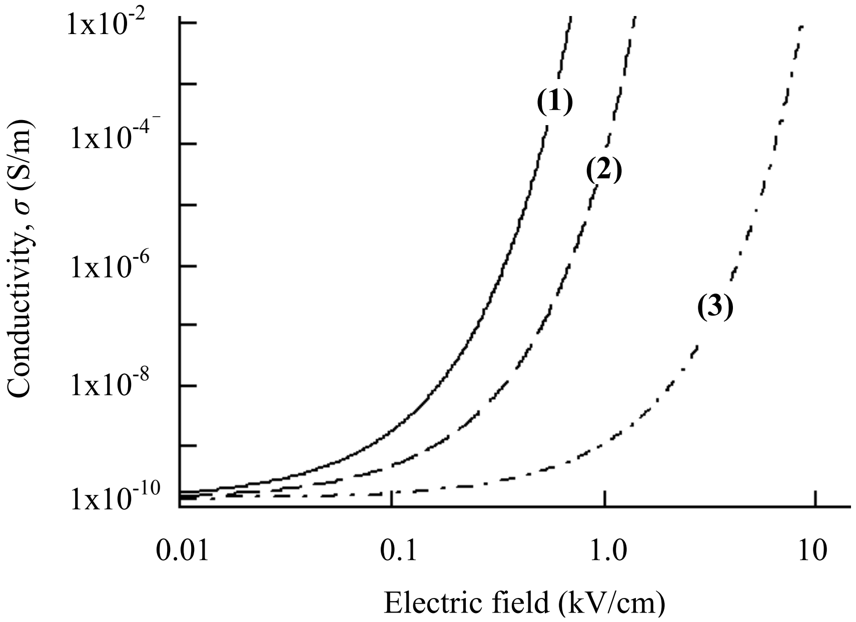

(1): $\sigma = 1\times10^{-10}\cdot e^{\left(5\times10^{-5}\right)E}$ **(2)**: $\sigma = 1\times10^{-10}\cdot e^{\left(2\times10^{-5}\right)E}$

(3): $\sigma = 1\times10^{-10}\cdot e^{\left(5\times10^{-6}\right)E}$

Figure 5.4: Proposed microvaristor characteristics with different switching thresholds. (1) E_0= 0.5 kV/cm, (2) E_0=1.0 kV/cm and (3) E_0=5.0 kV/cm

5.3.2. Effect of Microvaristor Characteristics on Field Distribution

In this investigation, the same modelling procedures including insulator design and properties as described in Chapter 3 were adopted for simulation of the microvaristor-graded insulator. Tapered geometry sections to represent the proposed microvaristor coating were introduced in the region between the core and silicone housing at both insulator ends, as illustrated in Figure 5.2. The conductivity of the grading material, having relative permittivity ε_r =12 [133], is specified as a function of electric field, $\sigma = f(E)$, provided in Figure 5.4.

Figure 5.5 reports the computed tangential field along the leakage path of polymeric insulators, equipped with microvaristor grading exhibiting the electrical properties given in Figure 5.4. The leakage distances are measured along the polymeric surface from the ground up to the high voltage terminal.

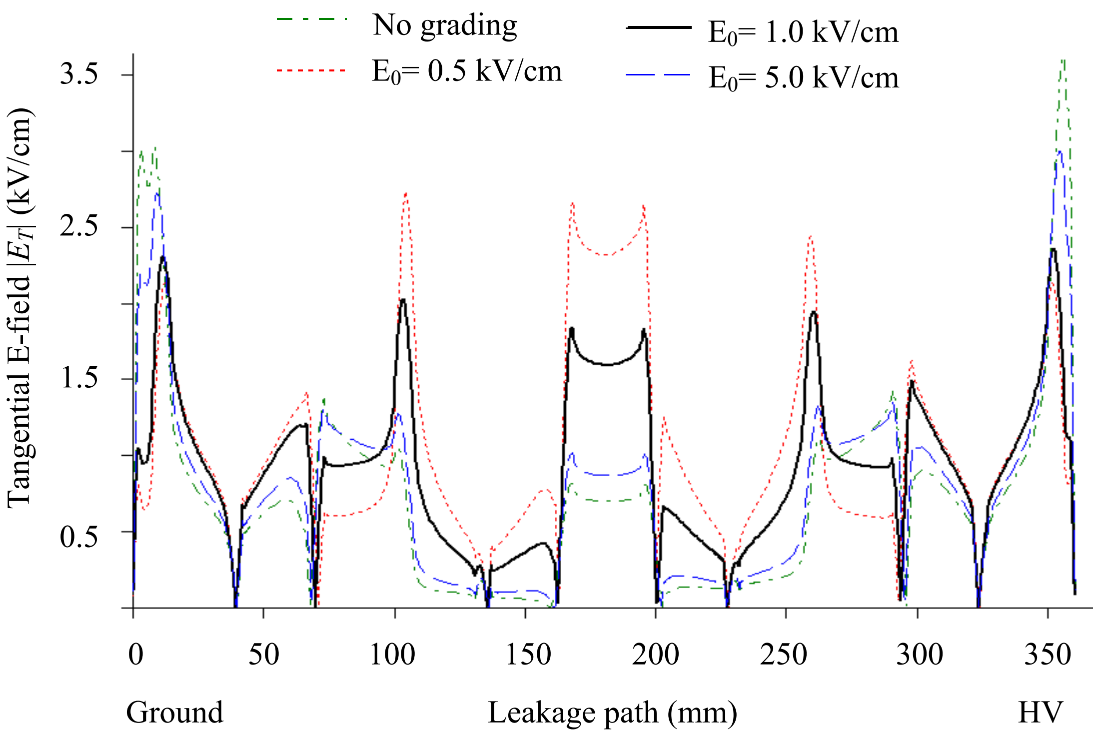

Figure 5.5: Computed tangential electric field profiles along the insulator surface for different microvaristor switching thresholds, E_0

As can be seen on the figure, the tangential electric field magnitudes at the two terminals are excessively high when no grading is used. However, the introduction of the grading material reduces these peaks significantly as the switching threshold of the microvaristor grading material is lowered from 5.0 kV/cm to 0.5 kV/cm. As the field magnitude is reduced at the terminals, the field level at other locations around the middle area of the insulator increases correspondingly. This is due to the displacement of equipotentials from the terminals towards the middle parts of the insulator. Once the microvaristor compound is turned-on, the voltage along its length is redistributed to near-uniform distribution which results in a reduced field near the terminals and increased magnitude away from the grading material. The results shown in Figure 5.5 indicate that a material with a 1.0 kV/cm switching threshold results in a distribution that generates comparable field magnitudes at the terminals and around the middle of the insulator (see continuous curve). The favourable distribution can be clearly observed on the corresponding equipotential plots in Figure 5.6, where the equipotential lines along the surface are distributed more evenly. This demonstrates that the redistribution

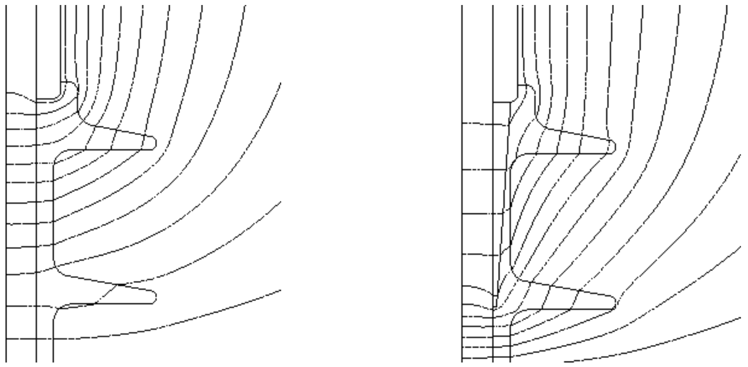

No grading

E_0=0.5 kV/cm

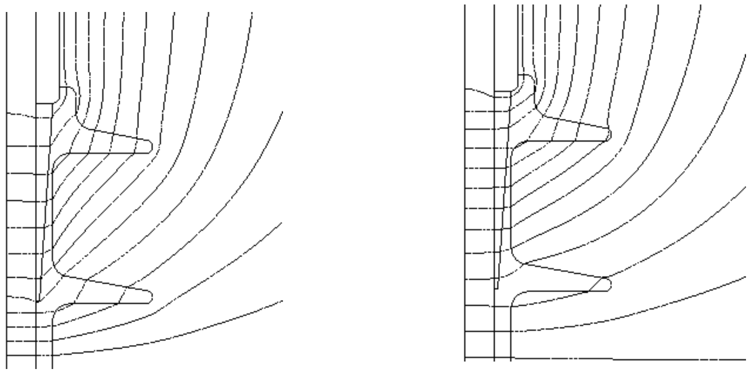

E_0= 1.0 kV/cm

E_0= 5.0 kV/cm

Figure 5.6: Equipotentials at 4% interval around high voltage electrode for different microvaristor switching thresholds, E_0

can be adjusted to the required application depending on the exact configuration of the installed insulator in the field by a suitable selection of the characteristics of the microvaristor grading material.

Table 5.1 summarises the highest tangential field values at different regions on the dry-clean insulator surfaces. From careful analysis, the computed values clearly indicate that the grading material with $E_0 = 1.0$ kV/cm has the smallest variation in peak values, and offers the best surface field distribution for the insulator. A grading material with this conduction threshold was, therefore, selected for further investigation of field-control concept.

Table 5.1: Peak magnitude of tangential field on the surface of dry-clean insulator

Region on insulator surface (leakage distance)	With no grading (kV/cm)	Grading E_0=0.5 kV/cm (kV/cm)	Grading E_0=1 kV/cm (kV/cm)	Grading E_0=5 kV/cm (kV/cm)
Ground end (0 – 42 mm)	3.03	2.70	**2.31**	2.12
Shank A (73 – 106 mm)	1.38	1.30	**2.03**	2.72
Shank B (167 – 203 mm)	0.82	1.02	**1.84**	2.66
Shank C (263 – 297 mm)	1.41	1.35	**1.95**	2.43
HV end (327 – 366 mm)	3.62	3.01	**2.38**	2.13

5.4. EVALUATION OF MICROVARISTOR PERFORMANCE

To appreciate the benefit of field grading using microvaristors, simulation results from the proposed microvaristor-graded insulator are compared with those from the standard non-graded insulator. In this case, the optimum microvaristor characteristic, E_0=1.0 kV/cm, determined in the previous section, was used to characterise the microvaristor grading material in polymeric insulator. The performance of microvaristor application is assessed in two important aspects: i) field distribution and ii) power dissipation. The pollution layer in this simulation is considered uniform with constant single conductivity, as adopted in Chapter 3.

5.4.1. Field Control Under Dry-Clean and Wet-Polluted Conditions

Figures 5.7 provides the comparison of equipotential distributions under dry-clean and uniformly wet-polluted conditions respectively. As can be observed on the figures, the introduction of microvaristor grading under both surface conditions improves the potential profile around the insulator terminal ends. The redistribution results in a wider spread of equipotentials compared with the insulator having no grading material. In particular, this action is more effective when the grading material switches into conduction state as the local applied field magnitudes reach or exceed the microvaristor's switching threshold, thereby improving the electrical stress control. The equipotentials for a wet-polluted insulator, as expected, show a more favourable distribution due to the presence of resistive pollution layer, where the lines are farther apart compared to those under dry-clean surfaces.

Figures 5.8 (a) and 5.8 (b) show the corresponding electric field profiles along the leakage path for the clean and polluted insulators. The field distributions on the insulator equipped with grading material under both surface conditions are improved, which correlate well with the computed equipotentials plot. The field distribution appears to be more uniformly distributed along the leakage path, thus avoiding excessive stress at specific vulnerable areas on the insulator surface. The maximum fields in the critical high field regions at both insulator terminals are successfully reduced. Under dry-clean surface conditions, peak magnitudes are lowered from 3.62 kV/cm to 2.38 kV/cm at the high voltage electrode, and from 3.03 kV/cm to 2.31 kV/cm near the ground, which respectively represent 34.3% and 23.8% of field reduction. The performance under wet-polluted conditions is even better, with the improvement around 40% at both insulator terminals. This encouraging improvement, as summarised in Table 5.2, is expected to minimise the probability of surface discharges and also increase the flashover voltage level, which consequently enhances the long-term performance of the insulator.

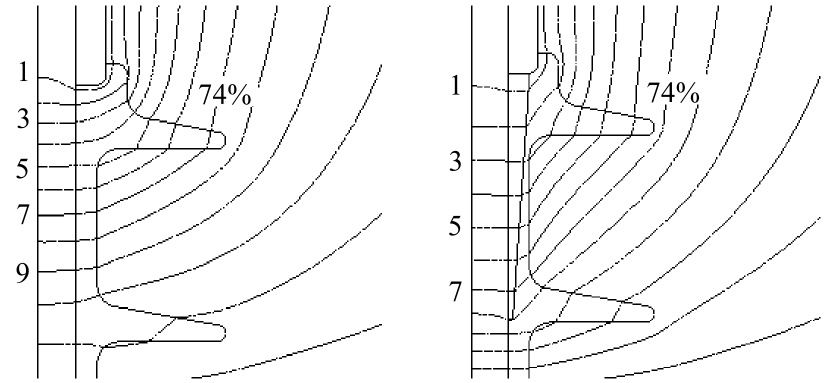

Non-graded insulator

Microvaristor-graded insulator

(a)

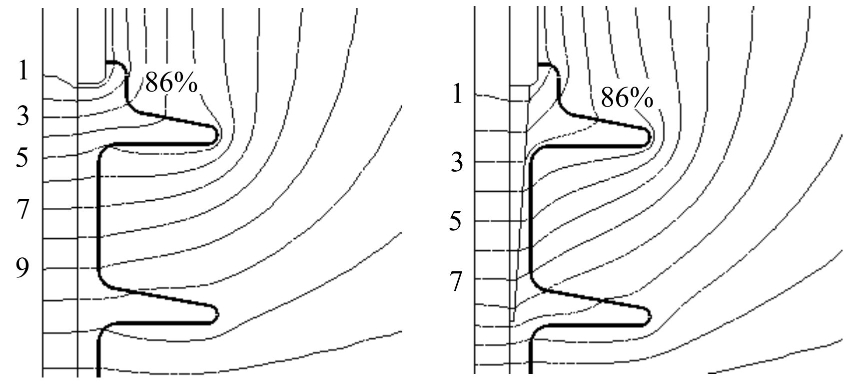

Non-graded insulator

Microvaristor-graded insulator

(b)

Figure 5.7: Equipotential lines at 4% interval around polymeric insulator under (a) dry-clean, and (b) wet-polluted surface condition

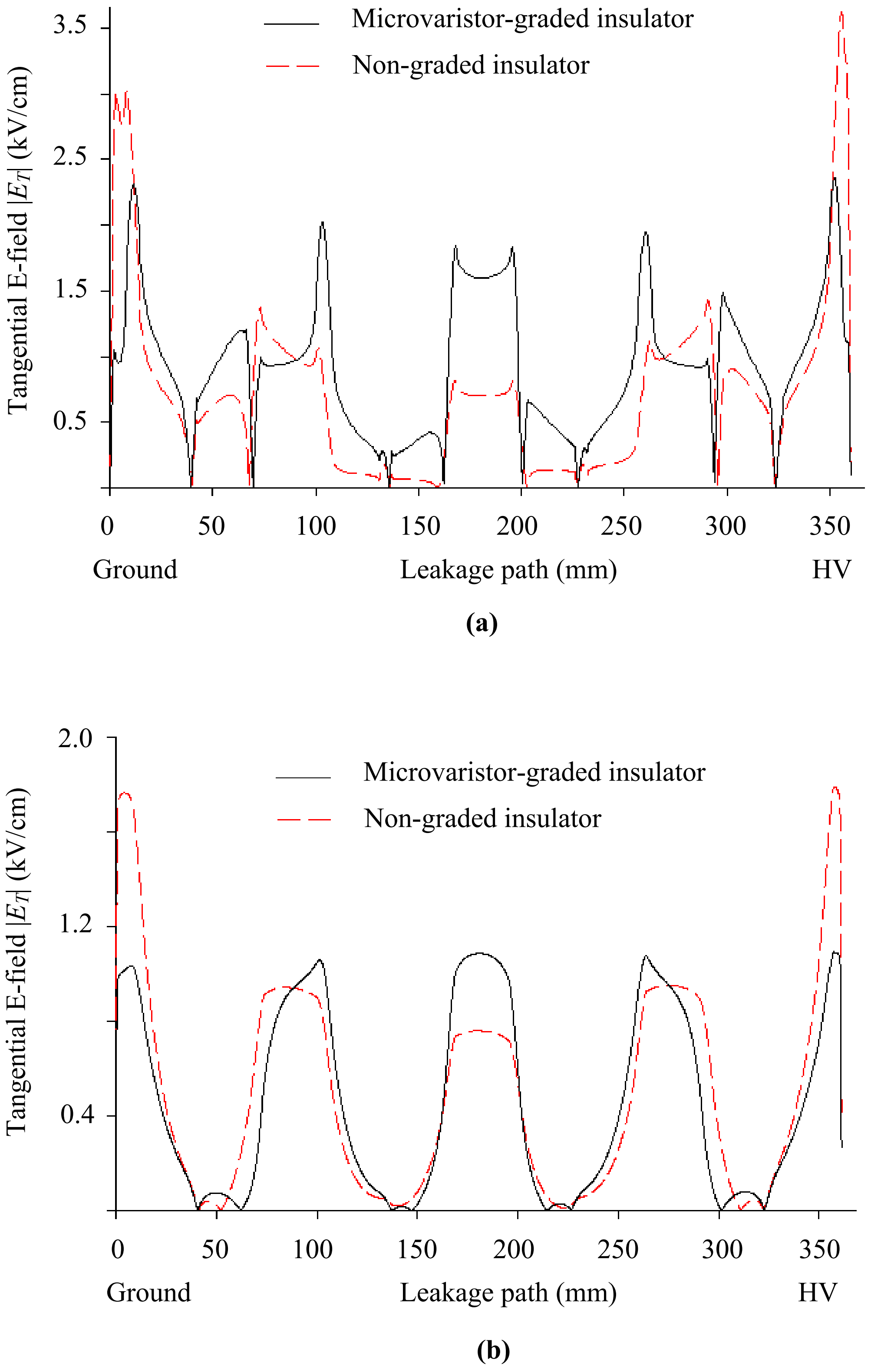

(a)

(b)

Figure 5.8: Comparison of tangential field along the leakage path for insulators under (a) dry-clean, and (b) wet polluted surface condition

Table 5.2: Peak magnitude of tangential electric field on polymeric surface near both insulator terminals

Surface condition	**Dry-Clean**		**Wet-Polluted**	
Terminal	**HV**	**Ground**	**HV**	**Ground**
Non-graded insulator	3.62 kV/cm	3.05 kV/cm	1.79 kV/cm	1.76 kV/cm
Microvaristor-graded insulator	2.37 kV/cm	2.31 kV/cm	1.08 kV/cm	1.05 kV/cm
Improvement due to grading effect	34.3%	23.8%	39.7%	40.3%

5.4.2. Power Dissipation and Heating Assessment

The most onerous condition for outdoor insulators is the effect of surface leakage current on the covering wet pollution layer. Such a phenomenon will cause power dissipation leading to resistive heating in the pollution layer which, in turn, could dry out the water, and hence contribute to the formation of dry bands on the insulator surface. At any location of the insulator along its creepage path, the power dissipation in a thin pollution layer of thickness, t_p, is proportional to the resistance of the pollution layer, R_p, and the magnitude of the leakage current, I_{lc}. The total power dissipation, P, is written as:

$$P = R_p \times I_{lc}^{\ 2} \qquad (5.2)$$

The resistance of the pollution layer of length, ℓ, is expressed as:

$$R_p = \left(\frac{1}{\sigma}\right) \times \left(\frac{\ell}{S}\right) \qquad (5.3$$

with σ the conductivity of the pollution layer (S/m), and assuming that the thickness is very small compared to the radius of the insulator, *r*, the pollution section area, *S*, at any point along the creepage path can be expressed as:

$$S = 2\,\pi\, r\, t \tag{5.4}$$

Noting that the tangential electric field, E_t, drives the surface leakage current, the resulting pollution layer current density, *J*, in this case can be expressed as:

$$J = \frac{I_{lc}}{S} = \sigma E_t \tag{5.5}$$

Combining Equations (5.2) to (5.5) yields the power dissipation expression as a function of the insulator geometrical parameters:

$$P = 2\pi\, r\, \ell\, \sigma E_t^2\, t_p \tag{5.6}$$

Using $A=2\pi\ r\ell$ to represent the total surface area of the insulator profile, power dissipation in the pollution layer per unit surface area along the creepage path is given by:

$$P_\Omega = \frac{P}{A} = \sigma E_t{}^2 t_p \tag{5.7}$$

The power dissipation per unit volume of the pollution layer can, therefore, be expressed as:

$$P_V = \frac{P_\Omega}{t} = \sigma E_t{}^2 \tag{5.8}$$

Equations (5.7) and (5.8) are particularly useful to estimate the power dissipation on outdoor insulators, and facilitate the prediction of dry band formations on the surface.

5.4.2.1. Power Dissipation in the Pollution Layer

The surface power dissipation in the pollution layer along the creepage path, as shown in Figure 5.9, is calculated using Equation (5.7) with the tangential electric field results presented in Figure 5.8 (b). The power calculations were carried out through programming of the equation within the COMSOL user interface and also verified using simple spreadsheet calculations. Good agreement was obtained between the two computation approaches.

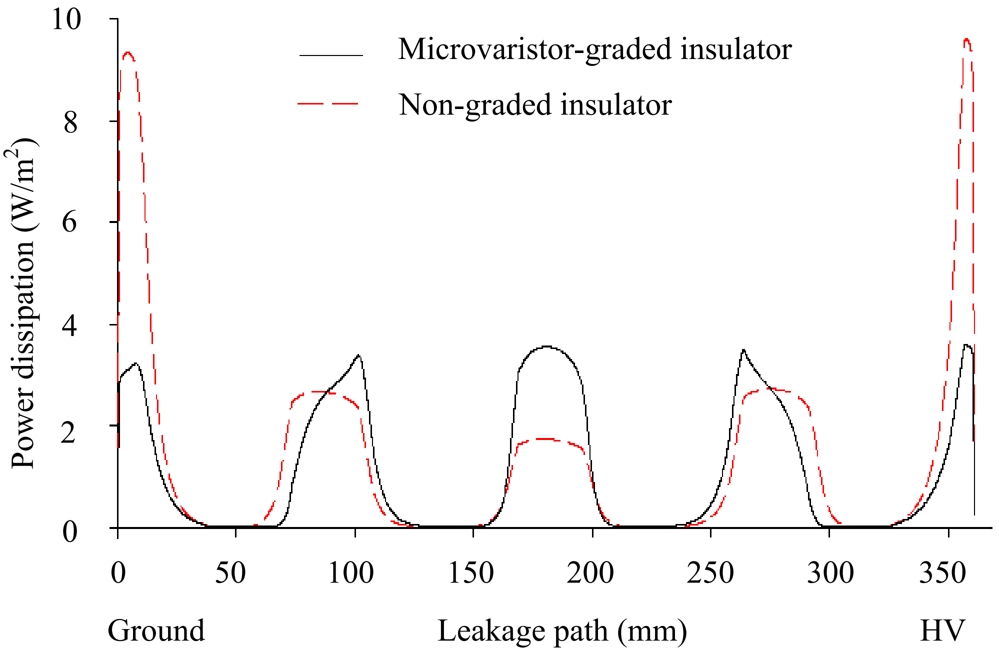

Figure 5.9: Surface power dissipation in the pollution layer along the insulator surface

As can be seen on the figure, there are two peaks near the insulator end terminals when no grading material was introduced. At these insulator surface zones, discharge activity is likely to occur since dry band formation is expected due to prolonged excessive heating. However, when the proposed grading with the microvaristor layer is introduced, the high power dissipation in these regions is effectively reduced by more than 60%, from approximately 9.6 W/m^2 down to around 3.6 W/m^2 at the high voltage electrode, and from 9.3 W/m^2 to 3.2 W/m^2 at the ground end.

The power dissipation due to leakage current flow per unit volume of the pollution layer, referred to here as resistive heating, is obtained using Equation (5.8) and is illustrated in Figure 5.10. Only the pollution layer near the first shed close to the high voltage terminal is shown to improve clarity. Moreover, the heating on the other insulator end is expected to behave in a similar way due to the symmetrical distribution of power dissipation along the leakage path. The highest thermal stress is clearly seen near the high voltage terminal as can be observed in Figure 5.10 (a). This hot spot, however, is suppressed with the graded insulator design, shown in Figure 5.10 (b). The highest value of heating in this region is reduced from 19.2 kW/m^3 to around 7.2 kW/m^3, representing about 62.5% of improvement.

Table 5.3 summarises the computed electric field and thermal heating at high voltage end for both non-graded and graded insulators. The findings, with an improvement of over 60%, clearly demonstrate that the electric field grading of outdoor insulators using a ZnO microvaristor compound can provide a significant improvement in the pollution performance of polymeric insulators through the reduction of both the electric field and the thermal stresses on the surface.

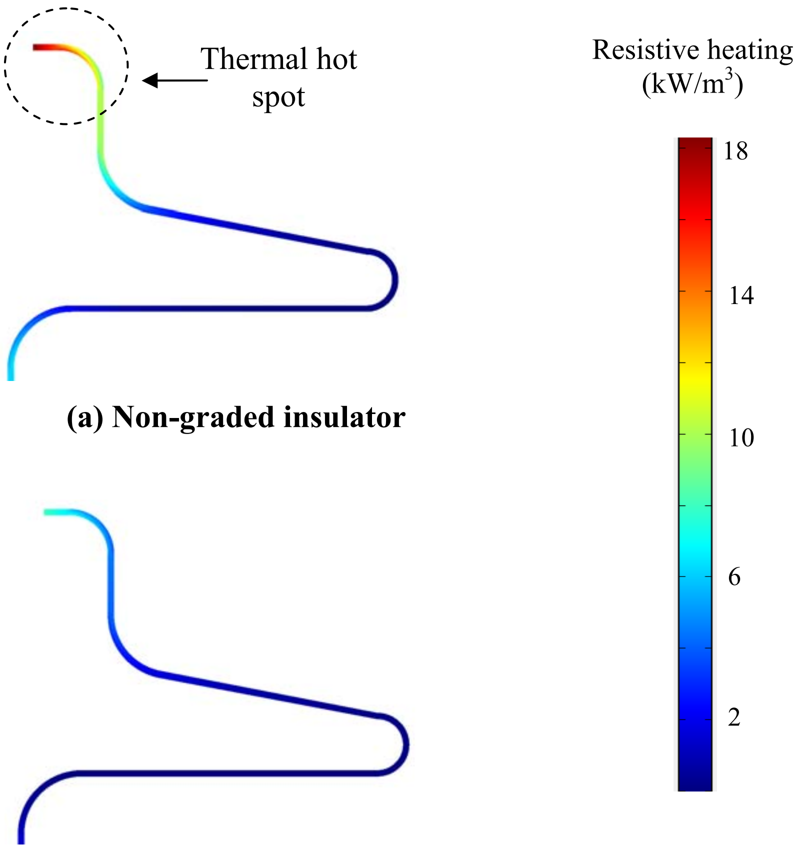

(a) Non-graded insulator

(b) Microvaristor-graded insulator

Figure 5.10: Power dissipation per unit volume in the pollution layer near the high voltage terminal

Table 5.3: Summary of thermal heating performance on polluted insulator

Heating	**Surface heating**		**Volume heating**	
Terminal	**HV**	**Ground**	**HV**	**Ground**
Non-graded insulator	9.6 W/m^2	9.3 W/m^2	19.2 kW/m^3	18.6 kW/m^3
Microvaristor-graded insulator	3.6 W/m^2	3.2 W/m^2	7.2 kW/m^3	6.4 kW/m^3
Improvement due to grading effect	62.5%	65.6%	62.5%	65.6%

5.4.2.2. Heat Assessment in Microvaristor

The volume resistive heating in the microvaristor compound for the cases of dry-clean and polluted insulators is illustrated pictorially in Figure 5.11. As shown, the heating in both cases is highest around the middle of the insulator where the microvaristor coating is thin. This is due to concentration of stress towards the end of the microvaristor region. If required, this can be mitigated by modifying the end shape of the microvaristor compound to reduce high electric field occurrences. The microvaristor compound, as can be observed, absorbs more energy under polluted surface conditions compared with the dry-clean insulator case.

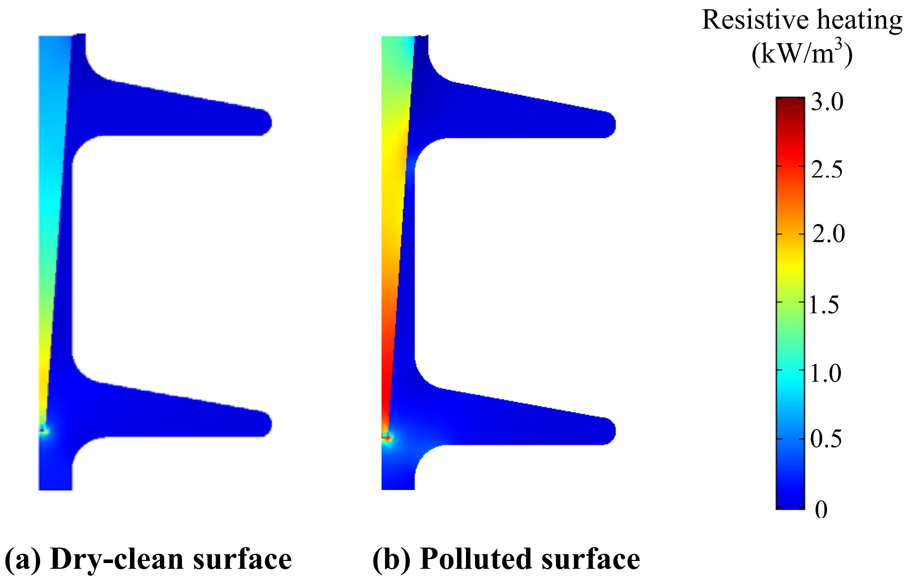

(a) Dry-clean surface **(b) Polluted surface**

Figure 5.11: Resistive heat mapping on the cross section of the microvaristor-graded insulator

5.5. CONCLUSION

An approach for electric field stress control along insulator surfaces has been proposed. The method consists of inserting a ZnO microvaristor compound layer near the high and low voltage terminals of the insulator. The design principles for the proposed field-grading techniques have been described and evaluated.

It has been demonstrated that high field stress at both insulator ends near the insulator terminals can be successfully reduced by adequate design and characteristic optimisation of microvaristor compounds for effective field control. In such a way, appropriate grading concerning the optimum design to be considered in practice can be obtained.

The theoretical analysis of the proposed model has been provided through a number of simulation scenarios. The integration of microvaristors as field grading material improves the electric field distribution along the insulator profile, which in turn, reduces hot spots and the probability of dry band formation. The graded insulators exhibited superior performance, reducing the highest tangential electric field and surface heating near the high voltage and ground terminals.

CHAPTER 6:

DEVELOPMENT OF A MICROVARISTOR-GRADED INSULATOR PROTOTYPE AND LABORATORY CHARACTERISATION UNDER IMPULSE CONDITIONS

6.1. INTRODUCTION

Electric discharges on the surface of high voltage insulators occur when the localised electric field is sufficiently high, exceeding the air breakdown threshold. This field enhancement is mainly due to the combined effect of wet environmental conditions and the highly non-uniform field distribution along the creepage path of the insulator. Although a polymeric insulator can take advantage of its superior water-repellent property in a humid atmosphere, the insulation material may temporarily or permanently lose its hydrophobicity when subjected to intense and prolonged surface discharge activities [135]. This is even more critical in the event of transient overvoltage such as lightning strikes in which the voltage varies widely in magnitude and rise time. The surge could result in a significant rise of electric field along the surface of the insulator, particularly near metal terminal areas. Efficient electrical stress control is, therefore, highly desirable to minimise the possibility of power disruptions, especially in modern power equipments which are designed to be smaller and more compact while the operating voltage is increased for maximum performance.

The integration of a microvaristor composites layer, as reported in Chapter 5, provides a promising approach for achieving stress relief on polymeric outdoor insulators. In continuation of the previous theoretical studies, this chapter investigates the performance of practical insulators equipped with microvaristor material when subjected to fast transient energisation, i.e. lightning impulse voltage. A simple A.C. test is carried out on the microvaristor sample to determine the switching characteristic of the material. In-house vacuum casting facilities are used to fabricate a full insulator prototype for laboratory testing. A microvaristor grading layer is introduced at the interface between the core and the silicone housing near the high voltage and ground terminals, similar to that described in Section 5.3.

U_{50} breakdown tests were carried out using lightning impulse voltages on two different surface conditions: dry-clean and uniformly wet-polluted insulators. The experimental setup and test procedures are presented in this chapter. As a complementary study, computations of electric field distribution through finite element modelling and simulations under lightning impulses are provided in an attempt to corroborate the results from the experiment and also to examine field response under such conditions.

6.2. MICROVARISTOR GRADING MATERIAL

In recent years, microvaristor-filled elastomers, which are relatively new to the market, have been commercially produced only for a selected range of applications with standard field grading properties. Grading compounds for specific requirements, such as in the case of this study, need to be specially fabricated. Due to time constraints and some technical limitations, the allied manufacturer, a large German company, was unable to provide the tailor-made compound with the requested switching properties. Instead, they supplied a standard microvaristor compound with a higher field switching threshold than the required one for distribution voltage applications. Figure 6.1 shows the microvaristor grading compound, in the form of a rectangular silicone sheet that was used to fabricate the prototype of a graded polymeric insulator used for preliminary laboratory characterisation.

Figure 6.1: Microvaristor grading sheets supplied by manufacturer

6.3. CHARACTERISATION OF MICROVARISTOR COMPOUND

A.C. tests were carried out to obtain experimental data over a range of voltages and current magnitudes in order to determine V-I characteristics and electrical properties of the microvaristor grading material. The experiment allows better understanding of the non-linear behaviour under A.C. energisation through the V-I curve and voltage-current traces.

6.3.1. Test Electrodes Cell and Sample

The test electrode system, which was specifically designed and constructed for the A.C. test, is shown in Figure 6.2. It comprises two aluminium plate electrodes and a nonconductive polypropylene structure as a support system to hold the electrodes and the sample in place during testing. The electrodes have a flat surface area of 10 mm in diameter and smooth rounded edges to avoid the possibility of field enhancement that can lead to electric discharge. The space between the two electrodes can be adjusted to a specific thickness using the associated screw-thread system. A specimen for the test was prepared by cutting the microvaristor sheet into the shape of a disc 10 mm in diameter, which creates a perfect contact with the flat electrode surfaces.

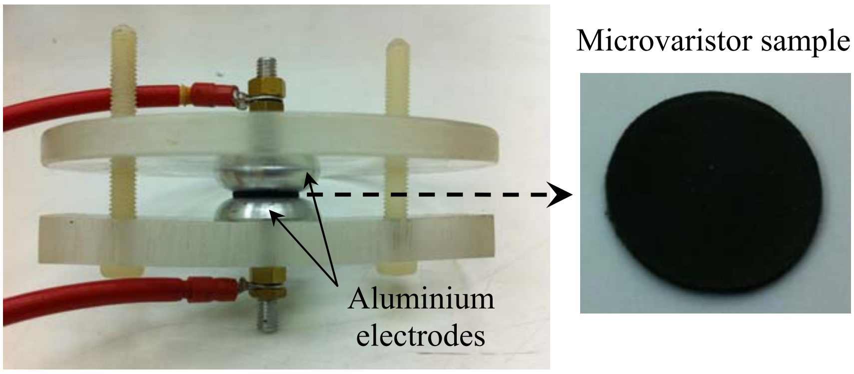

Figure 6.2: Test electrodes system and disc-shaped microvaristor specimen for A.C. test

6.3.2. Experimental Setup and Test Procedures

A circuit arrangement similar to that described in Chapter 3 was adopted to perform the A.C. test on the microvaristor sample. The simple representation of the test circuit is shown in Figure 6.3. The power frequency alternating source is supplied and controlled by a voltage regulator, connected through a step-up 7.5 kV high voltage transformer. The voltage across the sample is measured using a capacitive divider with a ratio of 2000:1, while the current is obtained by measuring voltage drop across a shunt resistor of 1.0 kΩ. Voltage and current waveforms are simultaneously displayed and recorded using an oscilloscope. The measurements of peak voltage, V_{pk}, and the corresponding instantaneous current, I_{Vpk}, for each energisation level are recorded to obtain the V-I characteristic. The applied voltage, starting at 500 V rms, is increased in steps of 500 V rms until high resistive current conduction is obtained, which indicates that the material has reached its conduction turn-on state.

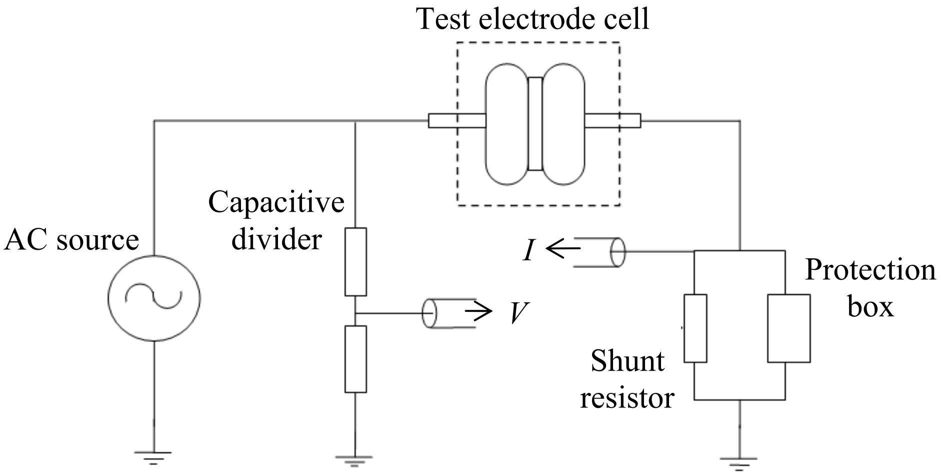

Figure 6.3: Simple layout of the experimental setup for A.C. test

6.3.3. Experimental Results and Analysis

The waveform in Figure 6.4 (a) and 6.4 (b) is an example of voltage and current traces in the pre-breakdown region for the microvaristor grading sheet under investigation.

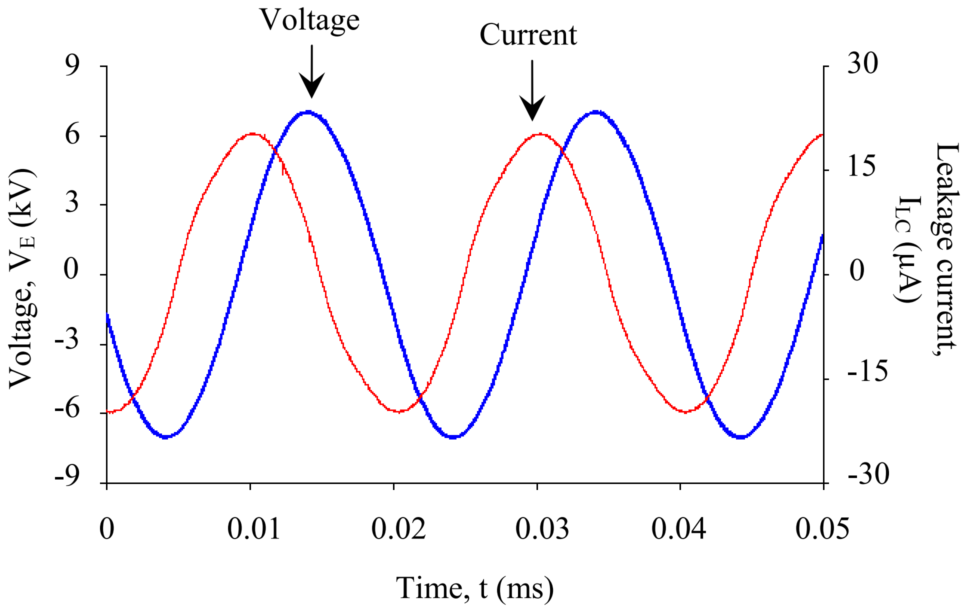

(a) Capacitive current waveform

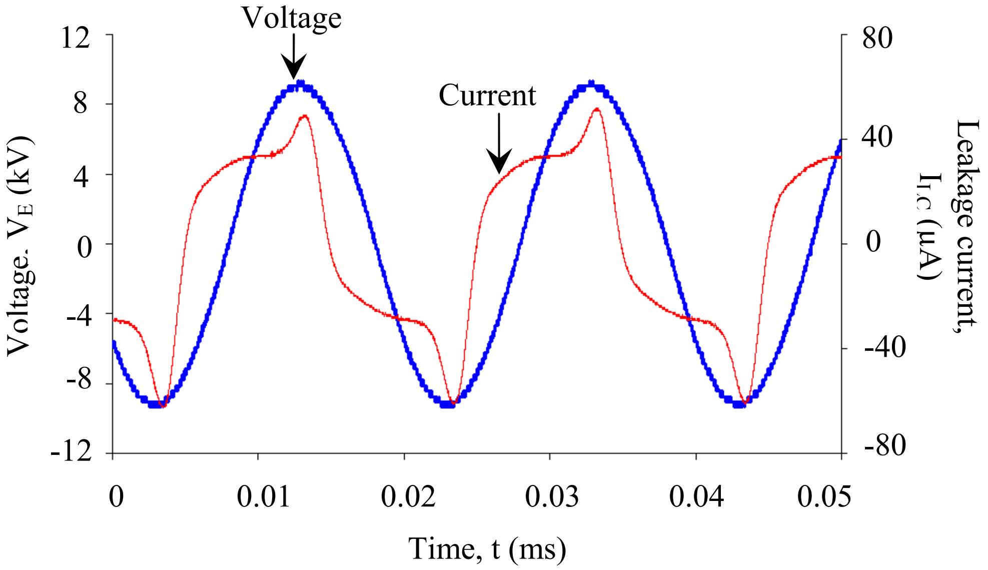

(b) Current waveform at a point just before the conduction

Figure 6.4: Voltage and current traces under A.C. energisation obtained in the pre-breakdown region

As can be seen from the figure, the current is purely capacitive with 90° phase shift when energised with 7.0 kV peak. The microvaristor in this case shows a strong dielectric property and behaves as a perfect insulator. However, the perfect sinusoidal current waveform is distorted, as shown in Figure 6.4 (b), when the voltage level is increased to a higher voltage level at 9.0 kV peak. Such behaviour indicates that the material has nearly reached its knee point of conduction, where the microvaristor is about to change its electrical properties from that of an insulator to that of a conductor. This means that the applied electric field has reached the switching threshold level. If the energisation voltage is further increased, the microvaristor is expected to conduct a high magnitude of resistive current.

Figure 6.5 shows the V-I characteristics in the pre-breakdown region for the microvaristor composites used in this study. As can be observed, the V-I curve shows a near-linear dependency in the low voltage regime below 8 kV peak. The curve starts to exhibit a strong non-linear behaviour when the energisation voltage approaches 9 kV peak in the regime above 10 μA. Beyond this point, small changes in the applied voltage will result in a significant increase in the current magnitude.

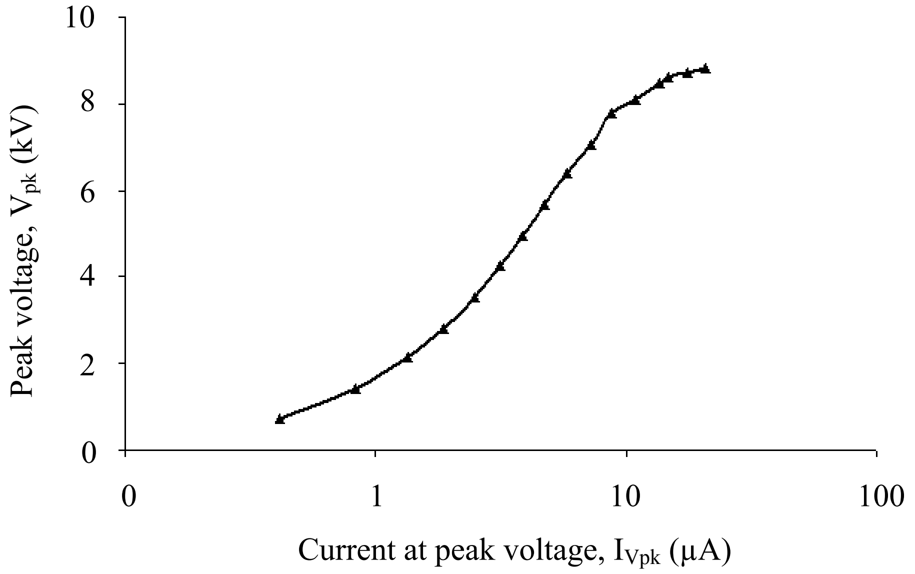

Figure 6.5: Plot of V-I characteristic for microvaristor composite in the pre-breakdown region

6.3.4. Determination of Field Switching Threshold

In this A.C. test, a disc-shaped microvaristor sample is sandwiched between the parallel plate electrodes at separation distance, *d*, which corresponds to the thickness of the microvaristor sample. If the electrode terminal is applied with a potential difference of *V*, the resulting electric field, *E*, can be expressed as:

$$E = \frac{V}{d} \qquad (6.1)$$

The conductivity of the microvaristor sample can be computed using Equation (6.2):

$$\sigma = \frac{I}{V}\frac{d}{A} \qquad (6.2)$$

in which *I* is the magnitude of the flowing current and *A* represents the surface area that is in contact with the plate electrodes. With the computation of the above two variable parameters, the switching characteristic of the microvaristor compound can be obtained.

Figure 6.6 shows a plot of electric conductivity as a function of the electric field, indicating the switching threshold level for the microvaristor compound to enable its grading action. In the linear region of the plot, the increase in the electric field causes a minimal change in conductivity. It can be predicted that microvaristors in this ‘low’ field region operate as perfect insulators to allow negligible capacitive current flowing through them. However, the conductivity increases rapidly when the electric field reaches the threshold level at around 14 kV/cm, indicating the transition of the microvaristor to become a conductor. This dramatic change in electrical behaviour is evidence of the strong non-linear characteristic imposed by the microvaristor composites.

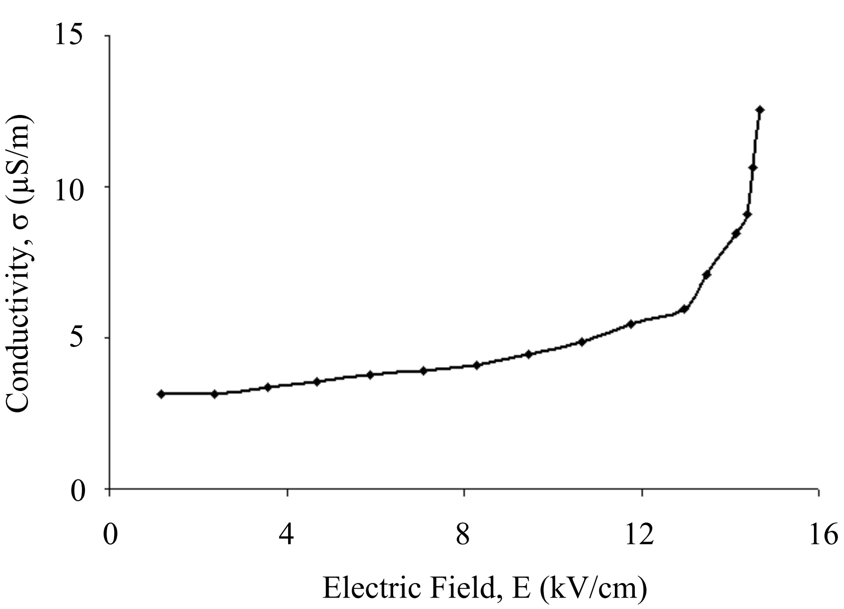

Figure 6.6: Measured switching characteristics of the microvaristor composite

6.4. FABRICATION OF MICROVARISTOR-GRADED INSULATOR PROTOTYPE

6.4.1. New Insulator Design

A new polymeric insulator design has been proposed to control high electric fields near the high voltage and ground electrode by using a tapered microvaristor compound. The grading material is introduced at the interface between the core and the silicone housing near the terminals as illustrated in Figure 6.7. With the cone-shaped grading structure, the concentrated field around the terminals can be re-distributed accordingly on the insulator surface as it advances away from the high field regions of the insulator terminals. The prototype of this new insulator design equipped with microvaristor grading coating was fabricated in-house using a vacuum casting facility.

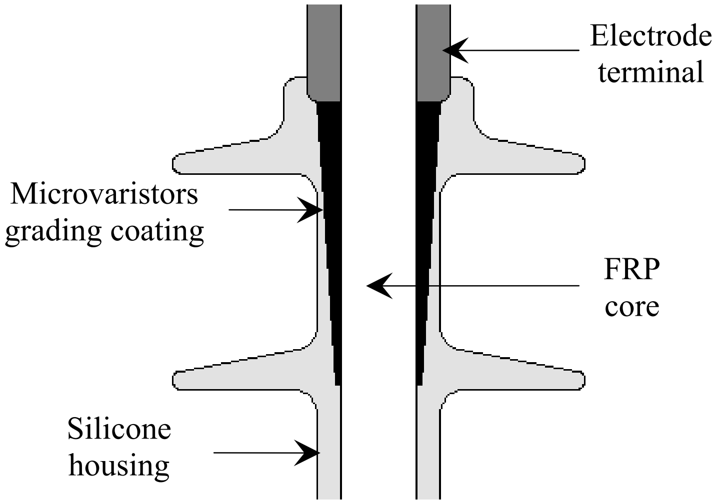

Figure 6.7: New insulator design with microvaristor grading coating

6.4.2. Preparation of Microvaristor Grading Coating

Ideally, the grading material should be coated onto the FRP core with a smooth graded thickness toward the middle. However, this cone-like shape could not be realised effectively due to limitations of the in-house facilities, and technical difficulties. As an alternative, the cone-shaped structure was made using stacked layers of microvaristor composite compound as shown in Figure 6.8 (a). Grading sheets of 1 mm thickness of varying length were tightly wrapped layer by layer onto the core at different lengths of 2 cm, 4 cm and 6 cm. Silicone adhesive was used to ensure good physical contact while preventing undesirable air traps between the grading layers. Particularly in this early development and prototyping stage with limited resources, this alternative approach provides an acceptable tapered effect for the grading coating on the insulator prototype suitable for the research investigation.

6.4.3. Moulding of Weather Shed Insulation Housing

The weathershed insulation housing was fabricated using the in-house casting facility; MCP vacuum machine, oven, and aluminium mould. After preparing the ‘tapered’ microvaristor coating at both insulator ends, the flange was carefully placed in an aluminium cast tooling block as a negative mould for the weather shed insulation housing, as shown in Figure 6.8 (b). The polymeric housing was made of liquid silicone-rubber HV 1540/10P supplied by Dow Corning Ltd. UK. The mechanical and electrical properties of the silicone material are given in Appendix 1. The flow chart in Figure 6.9 (a) illustrates the procedure for casting the polymeric weather shed housing of the insulator prototype.

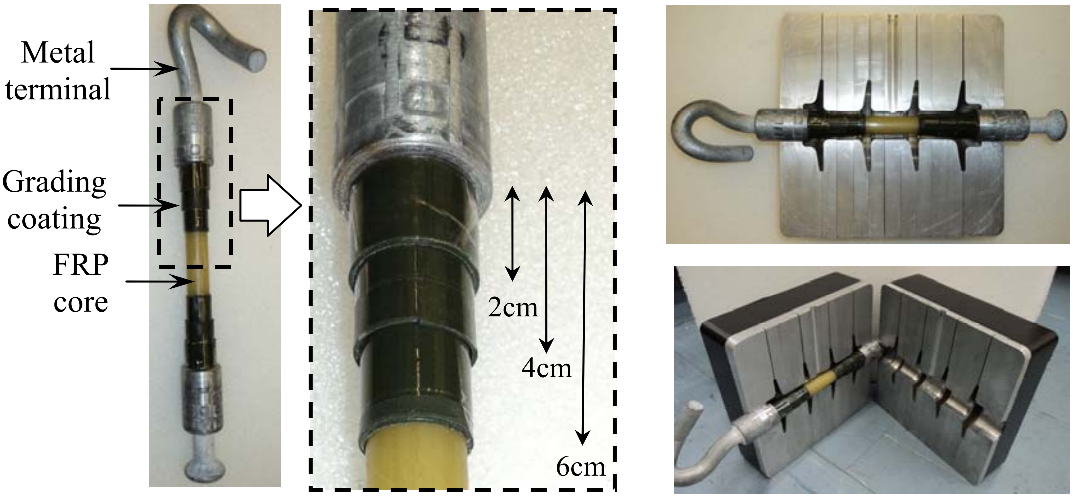

(a) The cone-shaped microvaristor coating near insulator terminals

(b) Aluminium mould used for fabricating weather shed housing

Figure 6.8: Preparation for moulding graded insulator prototype in laboratory

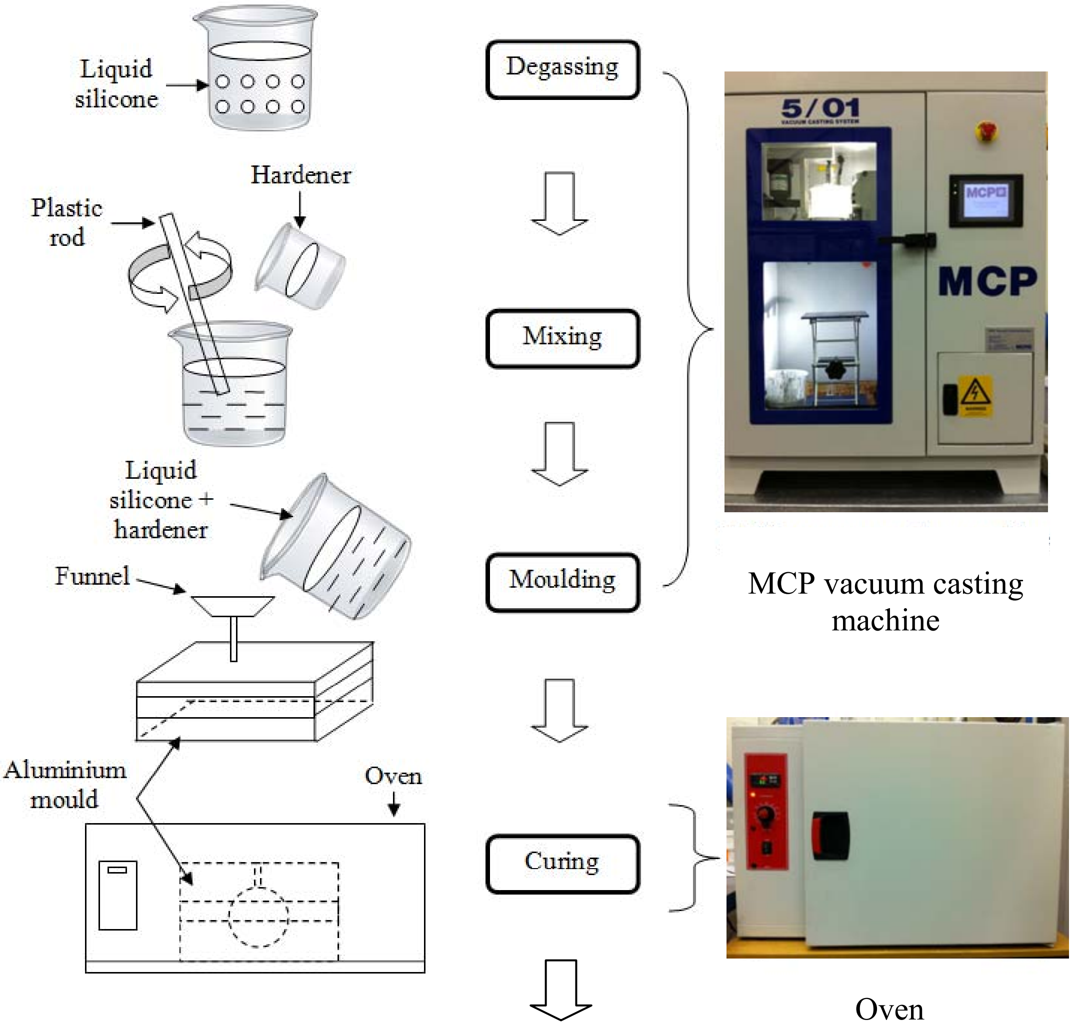

MCP vacuum casting machine

Oven

Cured weather shed housing before trimming the silicone excess

Polymeric insulator ready for laboratory test

Figure 6.9: Fabrication procedure in developing insulator prototype

Fabrication of the polymeric housing was achieved using an injection moulding technique in the vacuum casting machine. At the start of the process, trapped air was removed from the required amount of liquid silicone by pre-degassing for about 5 minutes in the vacuum chamber. A curing agent in a weight ratio of 1:9 was then added as a catalyst to harden the silicone rubber. Then, the mixture was continuously stirred and degassed for another 10 minutes before it was poured into the prepared aluminium mould through a funnel using a pre-assembled controlled mechanical system in the machine. In the final stage, the liquid silicone in the mould was cured in an oven at 50°C for 24 hours, followed by 3 hours post-curing at 120°C.

6.5. LIGHTNING FLASHOVER TESTS U_{50} ON PROTOTYPE GRADED AND NON-GRADED INSULATORS

The microvaristor compound used on the fabricated prototype has a switching threshold at approximately 14 kV/cm, as indicated in Figure 6.6. However, the results from theoretical studies given in Chapter 5 clearly showed that the electric field may not reach such high threshold levels under normal operating conditions. Therefore, a standard A.C. test with nominal system voltage is not sufficient for investigating the effect of the grading layer on practical insulators. A lightning impulse test is more appropriate, since it will stress the insulator to a level where the microvaristors are triggered into the conduction state, to enable field grading action. As a result, the U_{50} breakdown test was carried out to evaluate the performance of breakdown voltage for an insulator equipped with microvaristor material compared with the normal non-graded insulator under both dry-clean and wet-polluted surfaces. This experimental arrangement also permits comparison with the predicted model from simulation studies.

6.5.1. Experimental Setup

A general circuit arrangement for the lightning impulse breakdown test is shown in Figure 6.10. The test insulator was suspended vertically in a designated grounded cage where the top and the bottom flanges were connected to the impulse source and the ground respectively. A six-stage impulse generator with an output up to 300 kV peak was used to generate the required impulse voltage. The system consisted of a voltage regulator, automatic earth stick, DC charging unit with output voltage of 55 kV DC, high voltage stage capacitors 0.14 µF 65 kV, triggering unit and wave shaping resistors *R1* and *R2*. The bank capacitors were charged in parallel after which they were discharged in series through the front and tail resistors into the test insulator by means of an external electric spark. The output voltage was measured on the low voltage arm of the capacitive voltage divider with a ratio of 27931:1. The impulse waveform was captured and stored using a digital oscilloscope.

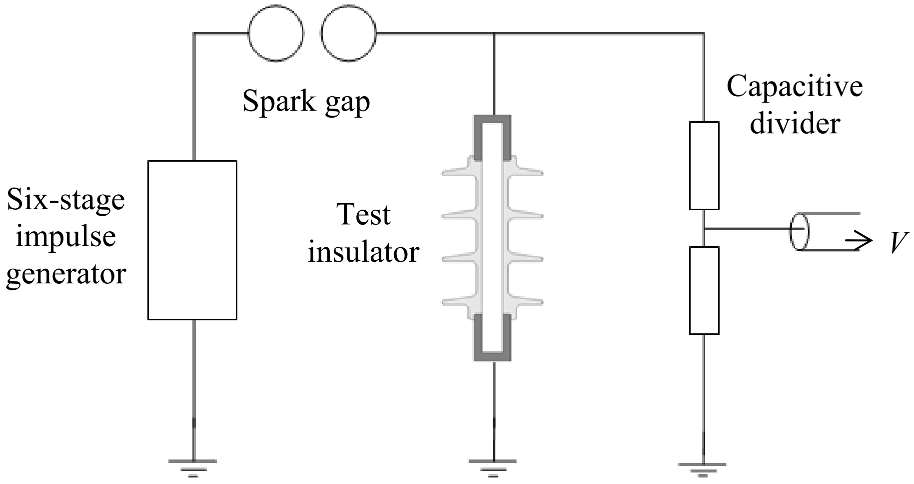

Figure 6.10: Simple layout for lightning impulse test

6.5.2. Test Procedures

In this experiment, a positive lightning impulse 1.2/50 µs was used as the energisation source. The impulse flashover voltage was determined by the 50% probability breakdown, U_{50}, which was carried out using the 'up and down' method in accordance with BS EN 60060 Standard [136]. The test insulator was first stressed with an estimated impulse breakdown voltage, V_k. The magnitude for the subsequent impulse application depends on whether a breakdown occurs in the present application. If the insulator survives the impulse stress without breakdown, the following impulse is increased by ΔV_k, which is typically in the range of 3% to 5% of U_k. However, if a breakdown occurs, the next impulse magnitude is reduced by ΔU_k. This procedure was repeated for a total of 20 impulses, as this figure is known to provide a substantial breakdown certainty [137]. The U_{50} breakdown voltage can be determined using the mathematical expression given by Equation (6.3), where n_i represents the number of impulse applications for the same impulse magnitude of U_k:

$$U_{50} = \frac{\sum n_i U_i}{\sum n_i} \tag{6.3}$$

The same procedures as detailed in Section 3.5 were used to prepare the wet-polluted insulator for the impulse test. When a breakdown occurs, most of the wet regions on the insulator surface may dry out due to the effect of excessive thermal heating from the intense electric discharge and the high current magnitude. Therefore, a portable spraying bottle was used to re-wet the insulator surface after each impulse application, prior to subsequent energisation. This procedure ensured that a uniform wet-polluted surface could be re-established, which would provide good consistency of the surface condition for each consecutive impulse application.

6.6. EXPERIMENT RESULTS AND DISCUSSIONS

The magnitude of voltage drop across the insulator for each impulse application during the U_{50} flashover test is plotted in Figure 6.11. As expected, the dry-clean insulator gives a higher flashover voltage compared with the insulator under wet-polluted conditions. The presence of the conductive pollution layer on the insulator surface allows significant current conduction along the leakage path during impulse energisation. High leakage current leads to the drying of the wet surface, which in turn causes field distortion around the insulator. Field intensification across the established dry regions, together with the highly non-uniform field distribution, contributes to a breakdown at much lower voltage.

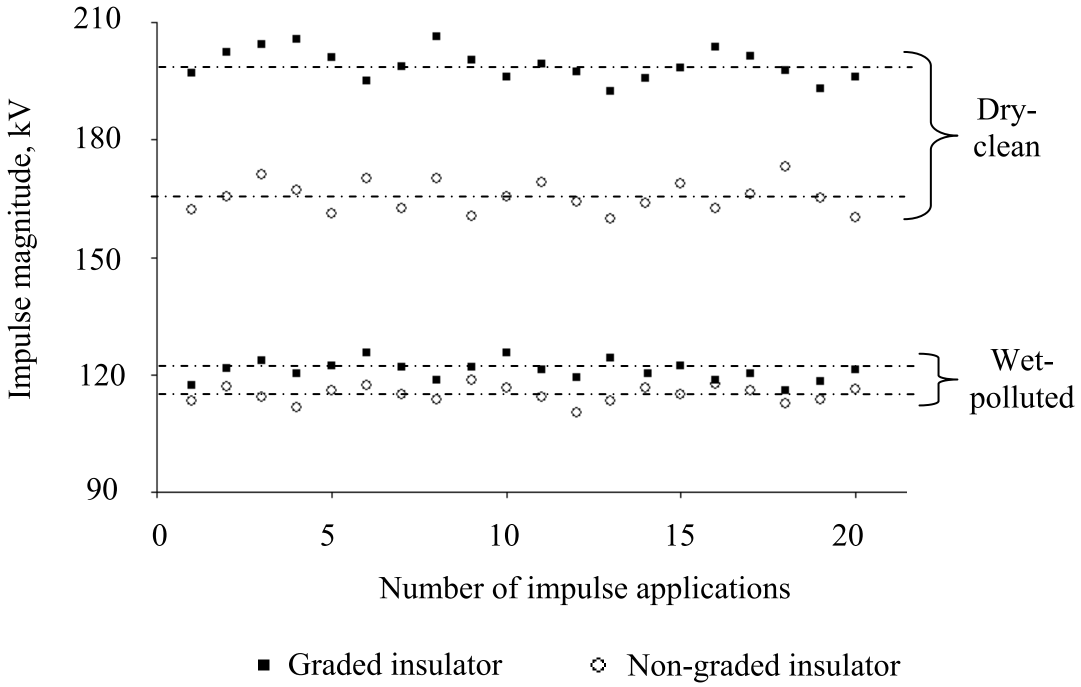

Figure 6.11: Voltage magnitude for 20 impulse applications in the U_{50} insulator flashover tests

The result of U_{50} flashover voltage with a sample size of 20 impulses, computed using Equation (6.3), is given in Table 6.1. In general, the presence of microvaristor grading material enhances the breakdown performance of polymeric outdoor insulator under both dry-clean and wet polluted surface conditions. The results from the impulse test conducted under dry-clean surface conditions indicates a considerable increase in the breakdown voltage, from 164 kV to 199 kV, representing an improvement of approximately 21%. This is illustrated in the typical records of withstand and breakdown waveforms obtained from the standard non-graded insulator and the microvaristor-graded prototype, shown in Figure 6.12. It is inferred that the microvaristor material in this case is switched on to allow the grading action which helps to regulate and minimise high electric field near insulator terminals. The field intensity at these terminals is responsible for the initiation of the flashover process.

Under the wet-polluted condition, the insulator with the microvaristor coating, however, shows only marginal improvement in the breakdown voltage, from 115 kV to 120 kV. The small improvement of just over 5% suggests that the grading material is less effective when the pollution layer has reduced the non-uniform field distribution at lower impulse voltages. In this case, the insulator may not be sufficiently stressed up to the required switching threshold level that could successfully trigger the grading effect.

Table 6.1: The computed 50% breakdown voltage, U_{50}

Surface conditions	Non-graded prototype	Microvaristor-graded prototype	Improvement due to grading effect
Dry-clean	165 kV	199 kV	21%
Wet-polluted	115 kV	122 kV	6%

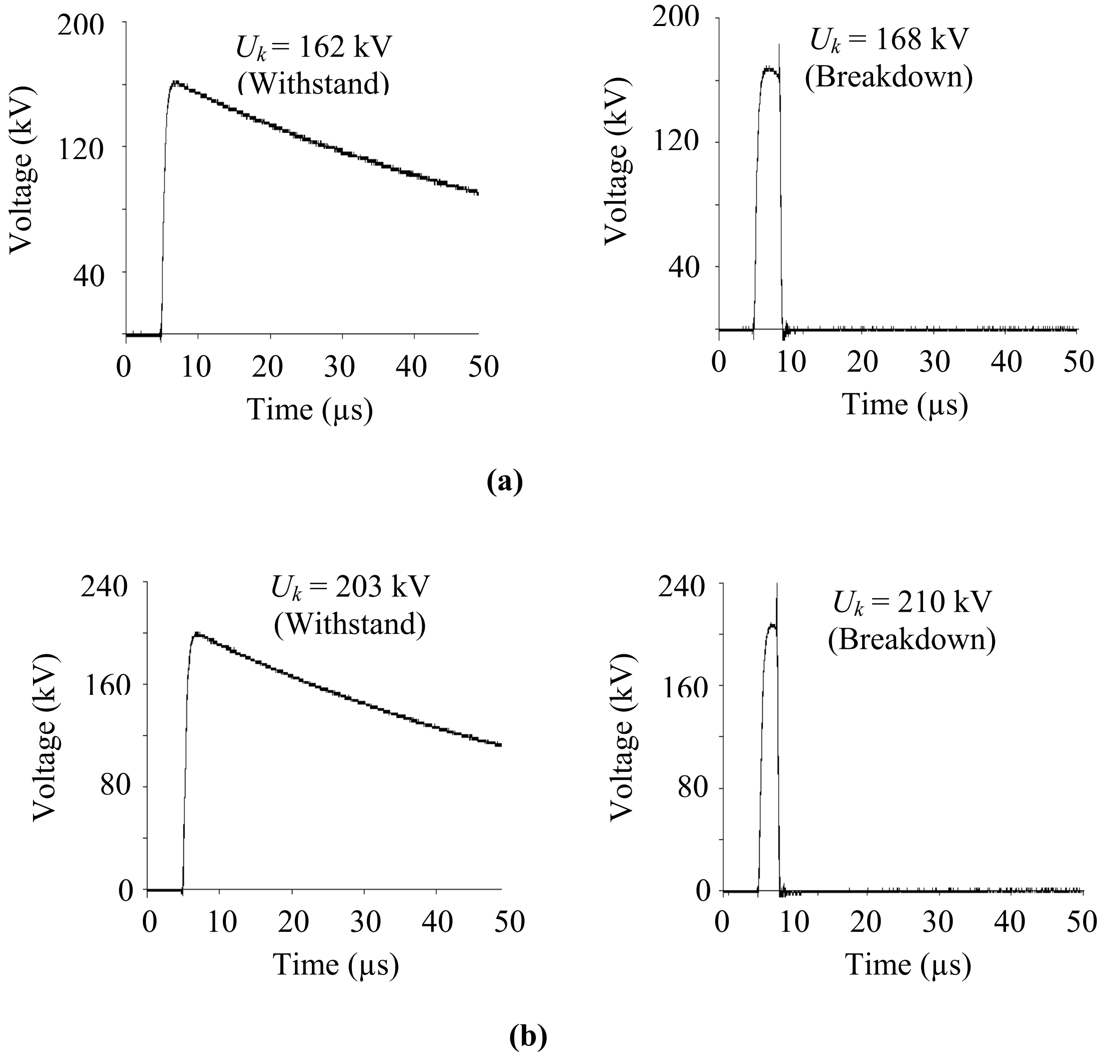

(a)

(b)

Figure 6.12: Example of voltage waveform under dry-clean surface conditions for (a) standard non-graded insulator, and (b) microvaristor-graded insulator

6.7. COMPUTER MODELLING AND SIMULATION STUDIES

As a complement to the earlier laboratory work on the U_{50} flashover test, computational simulation studies were carried out to examine field response under impulse energisation. This could provide a better understanding of the non-linear grading effect for the enhanced insulator flashover performance. The insulator design, material properties and modelling procedures are similar to those described in Chapter

5. To replicate laboratory conditions during the breakdown test, the high voltage terminal was energised with 160 kV and 115 kV of 1.2/50 μs lightning impulse source for dry-clean and wet-polluted surfaces respectively. Field switching threshold for the grading material was specified at 14 kV/cm, similar to the characteristic of the microvaristor compound which was used in constructing the graded insulator prototype.

6.7.1. Equipotential and Electric Field Distribution

Equipotential distributions around the standard non-graded insulator and the proposed microvaristor-graded insulator under dry-clean surface conditions are illustrated in Figure 6.13 (a) and 6.13 (b) respectively. Only half of the insulator profile at the high voltage terminal is shown in the figure to improve the clarity of the contours.

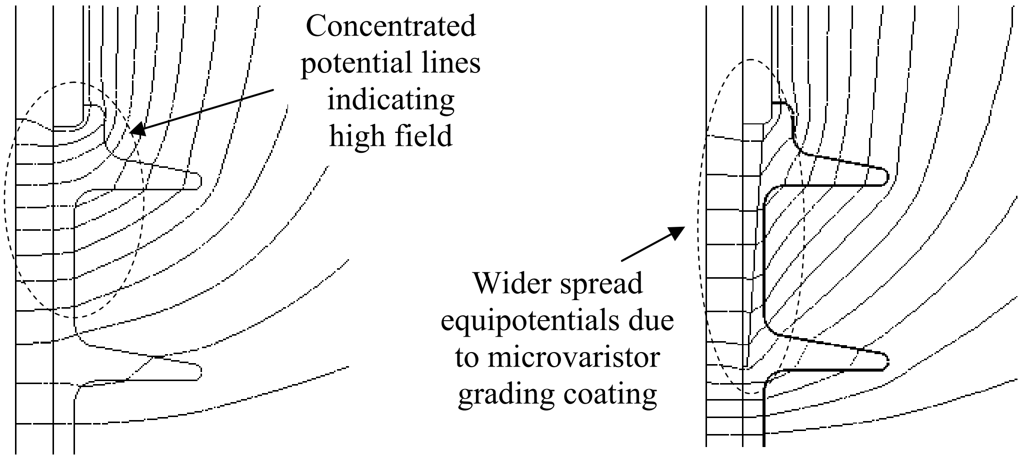

(a) Non-graded insulator

(b) Microvaristor-graded insulator

Figure 6.13: Equipotentials around the high voltage end at impulse instant 1.2 μs with peak voltage of 160 kV

The distributions were plotted at the impulse instant of 1.2 μs, where the voltage magnitude is highest, at 160 kV. As can be observed, the insulator with microvaristor coating demonstrates a better equipotential profile with wider and more equally spread contours. The grading material, in this case, is in its conduction state when the electric field reaches the switching threshold, thereby causing a re-distribution of the concentrated lines over the insulator surface and away from the high field regions.

The corresponding tangential field distributions along the creepage of the insulator for the equipotentials in Figure 6.13 are compared in Figure 6.14. As expected, the electric field on the microvaristor-graded insulator exhibits an improved field distribution compared to that without grading material. Peaks near the insulator terminals are reduced and well distributed over the leakage path to give a more uniform distribution at comparable magnitude around 17.5 kV/cm. The improvement due to the microvaristor grading effect represents nearly 30% of stress reduction at both insulator terminals. This considerable improvement explains the 21% increase in flashover voltage during lightning impulse tests.

Comparison of tangential field distributions for the wet-polluted insulator, energised with a 120 kV lightning impulse source, is shown in Figure 6.15. In contrast to the dry-clean surface situation, the presence of microvaristor grading material results in only a slight redistribution of electric field along the creepage path. High fields near the high voltage and ground terminals are reduced by 11.8% and 9.7% respectively. This small improvement indicates that the grading material is not effectively triggered to enable its grading action, which accounts for the 6% increase in the flashover voltage. The performance of microvaristor stress grading material, energised with lightning impulse sources, is summarised in Table 6.2.

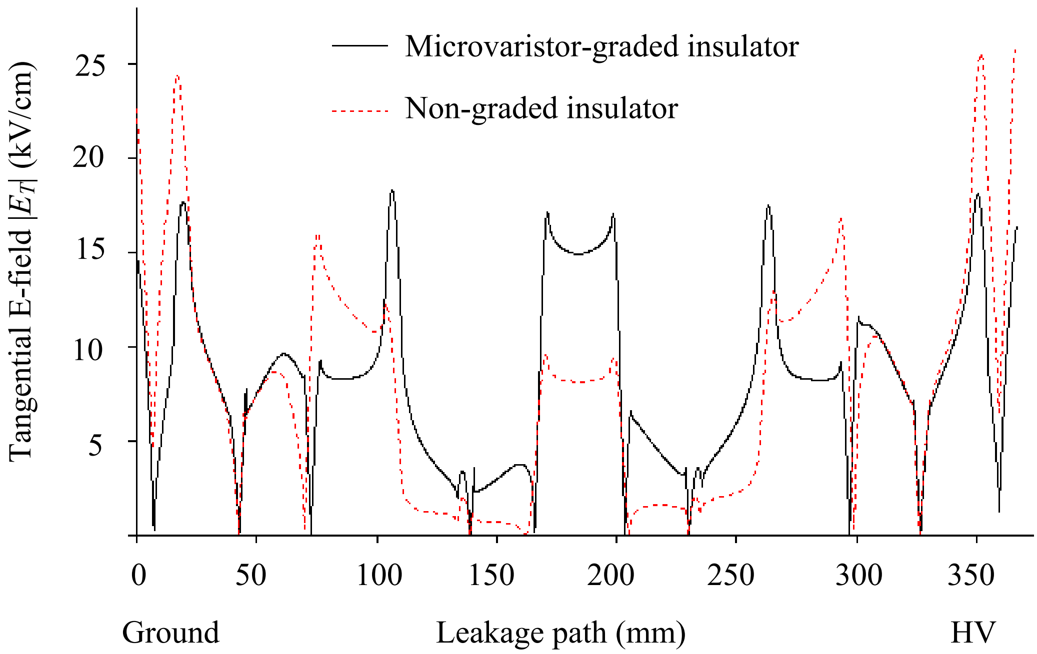

Figure 6.14: Tangential field distribution along the leakage path at impulse instant of 1.2 µs with peak voltage 160 kV (dry-clean insulator)

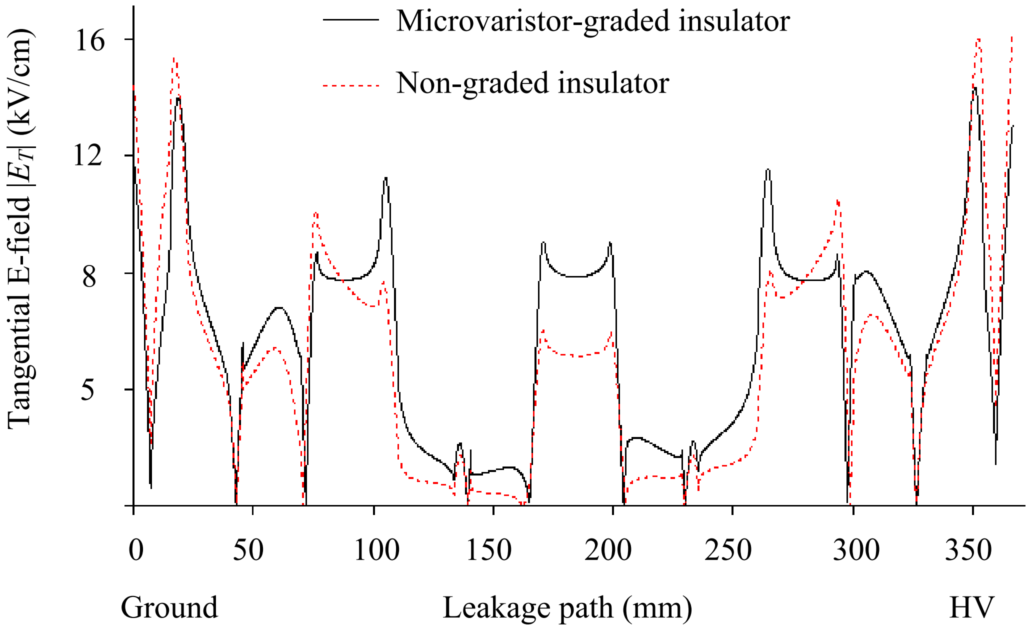

Figure 6.15: Tangential field distribution along the leakage path at impulse instant of 1.2 µs with peak voltage 115 kV (wet-polluted insulator)

Table 6.2: Stress grading performance under impulse energisation at 160 kV

Surface condition	Dry-Clean (160 kV)		Wet-Polluted (120 kV)	
Terminal	**HV**	**Ground**	**HV**	**Ground**
Non-graded insulator	25.5 kV/cm	24.3 kV/cm	16.1 kV/cm	15.4 kV/cm
Microvaristor-graded insulator	18.2 kV/cm	17.7 kV/cm	14.2 kV/cm	13.9 kV/cm
Improvement due to grading effect	28.6%	27.2%	11.8%	9.7%

6.7.2. Grading Effect during Impulse Rise Time

To examine the field response and grading effects in more detail, the equipotential distribution under dry-clean conditions was plotted at three different instants of the impulse front: 100 ns, 600 ns and 1.2 μs, presented in Figure 6.16 for direct comparison. As can be observed, the contour lines around the metal terminal are most concentrated on the profile at the time instant of 100 ns, where the corresponding voltage magnitude is about 30 kV, estimated from the lightning impulse waveform. At a relatively low voltage level, the insulator is not sufficiently stressed to trigger the grading effect of the microvaristors. As the voltage magnitude continues to rise, the electric field becomes higher, and therefore drives the microvaristors into their conduction state. As a result, the denser potential lines in the high field regions are relaxed and spread further apart, as shown by the equipotentials plot at impulse instants of 600 ns and 1.2 μs.

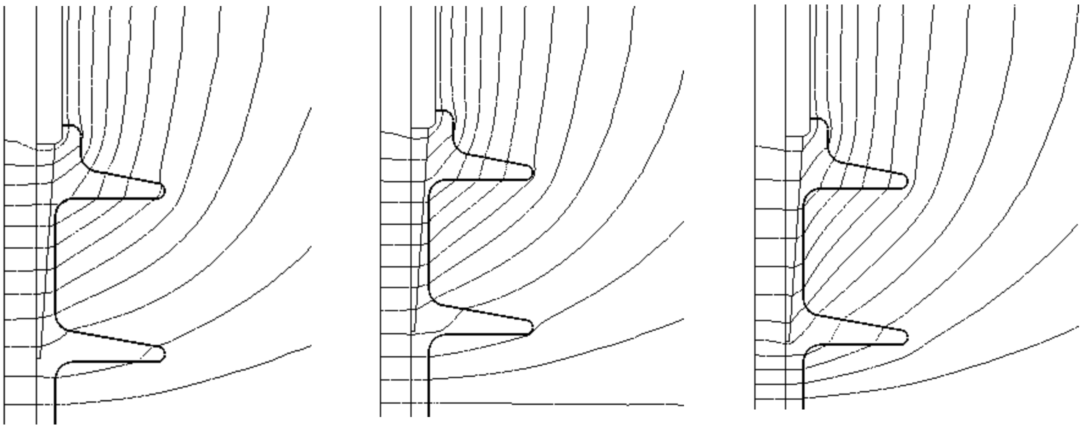

(a) 100 ns (~30 kV) **(b) 600 ns (~90 kV)** **(c) 1.2 μs (~160 kV)**

Figure 6.16: Equipotential around insulator at different instant rise times during transient voltage (dry-clean insulator)

Figure 6.17 shows the corresponding field distribution along the leakage path for the equipotentials in Figure 6.16. At the instantaneous time of 100 ns, the electric field on the insulator surface is generally low, and hence the grading effect is not seen due to the local field that does not reach the conduction threshold. As the voltage rises with time, the electric field increases until the conduction threshold of the grading material is reached, gradually redistributing the equipotential contours at 600 ns and 1.2 μs. The electric field distribution is clearly more uniform at the instant of maximum impulse voltage, i.e. 160 kV. Furthermore, the electric field peaks seen at 100 ns and 600 ns were successfully suppressed at 1.2 μs when the microvaristor material was effectively turned on. It is noteworthy that the highest field magnitude at 600 ns (90 kV instant voltage), i.e. 16 kV/cm, is very close to the peak value for the energisation of 160 kV (1.2μs instant time), i.e. 17.5 kV/cm. The result demonstrates the redistribution effect on the high field regions which also confirms the computed equipotentials in Figure 6.16.

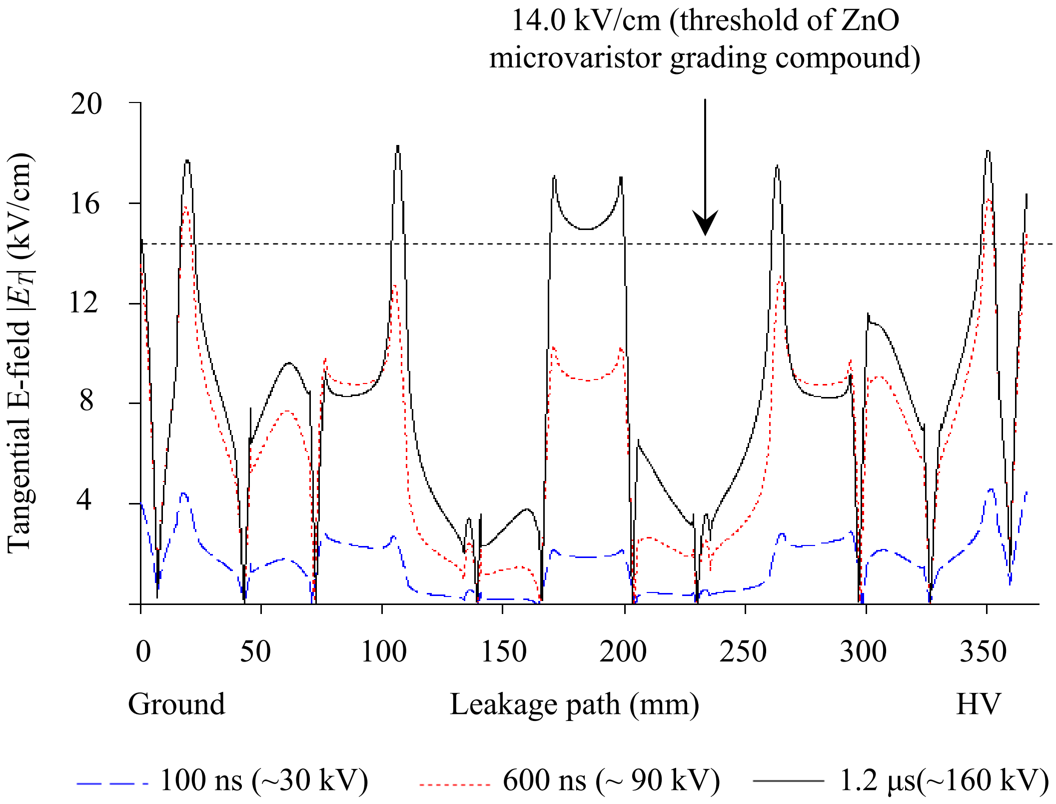

Figure 6.17: Tangential field distribution along insulator surface at different impulse instants (dry-clean insulator)

The field grading effect during the impulse front rise time (0 - 1.2 µs) can be observed more clearly in the time domain plot as shown in Figure 6.18. Electric field distributions for microvaristor graded insulator appeared to be more uniform with comparable peak magnitudes that are lower than those on the insulator without grading material. Excellent field control with the self-recovery approach realised by non-linear grading material is evidence of the improvement in the flashover performance during the impulse flashover test. The equipotentials and electric field response for the wet-polluted surface condition are not evaluated and discussed in further detail, as the microvaristor compound was not effectively triggered to allow its grading action.

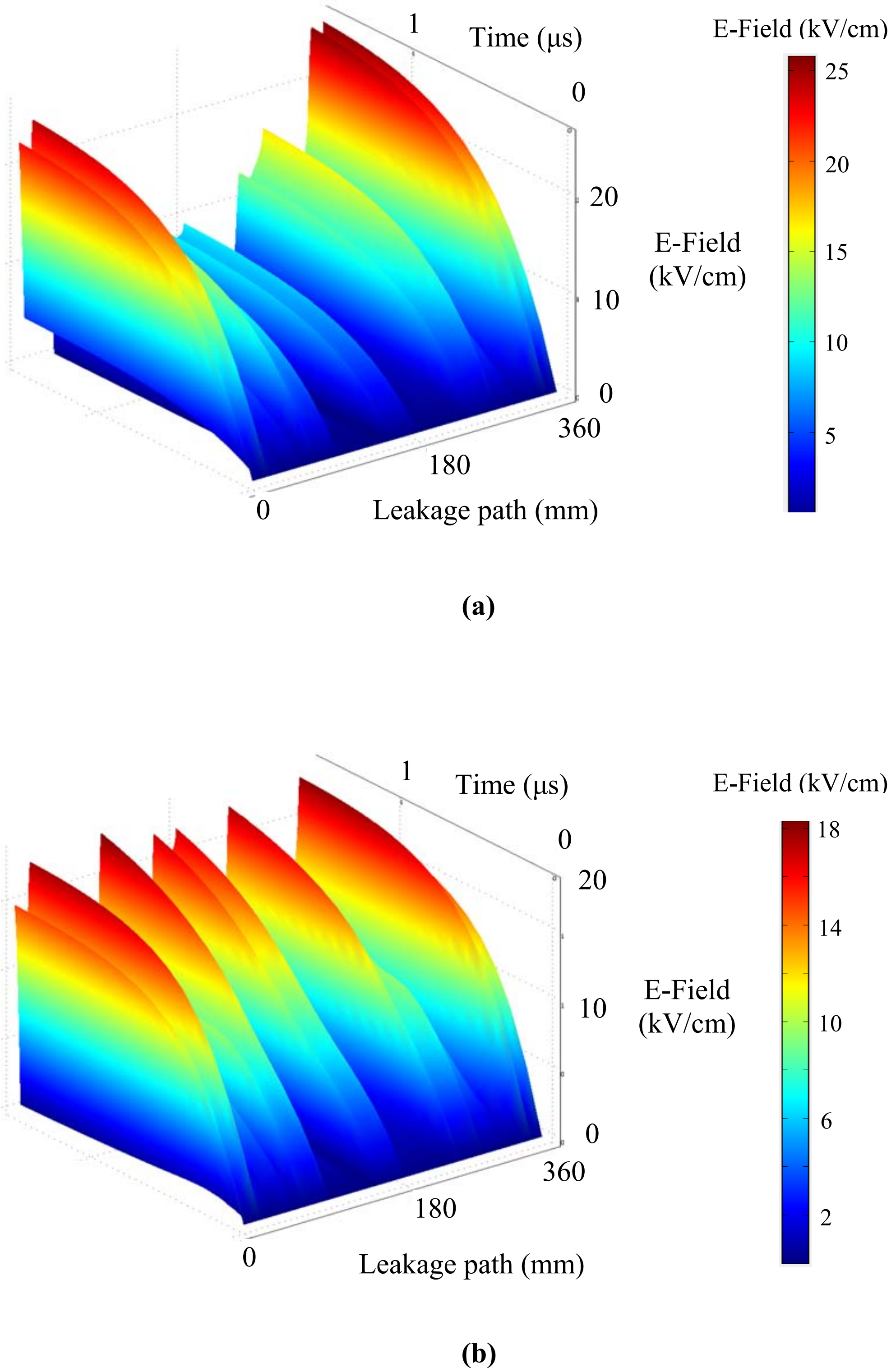

Figure 6.18: Field distribution in time domain plot during impulse rising time, from 0 μs to 1.2 μs

6.8. CONCLUSION

Experimental investigations to determine the electrical characteristics of the microvaristor composite layer have been carried out. The grading compound showed a highly non-linear behaviour with the switching threshold field at approximately 14.0 kV/cm.

A prototype of 11 kV polymeric insulator equipped with the proposed microvaristor coating has been successfully fabricated in-house. Complete building procedures, starting from the application of grading material onto the core and up to the final curing stage, have been described.

The lightning impulse flashover test, U_{50}, has been conducted for both graded and non-graded insulators to evaluate the effect of stress grading coating on the breakdown performance. The presence of microvaristors resulted in a considerable increase in the flashover voltage under the dry-clean surface, from 160 kV up to 199 kV, representing an improvement of approximately 21%. Wet-polluted insulator, however, indicates only a 6% improvement, due to ineffective grading action at lower energisation levels.

Modelling and simulation of polymeric insulator has been presented to evaluate the field response of graded insulators under lightning transient conditions. Substantial field enhancements were demonstrated by the graded insulator. The excessive peaks at the terminals were successfully suppressed, and the distributions were made more uniform over the insulator surface. Excellent field control with the self-recovery approach contributed to the improvement in flashover performance.

CHAPTER 7:

GENERAL CONCLUSIONS AND FUTURE WORKS

The main objectives of the work reported in this thesis were a better understanding of field phenomena on outdoor insulators, and the development of an effective approach for controlling electric field stress on polymeric outdoor insulators. The latter has been successfully achieved using a non-linear grading material, ZnO microvaristor compound, that features a highly field-dependent conductivity. The new proposed field control technique was demonstrated through extensive computational modelling alongside experimental investigations. An overview of the research work findings and major conclusions drawn from the studies undertaken, and recommendations for future research work are presented in this chapter.

7.1. GENERAL CONCLUSIONS

An extensive review of polymeric outdoor insulator focusing on electrical stress and field performance has been presented. The review highlights the need for a good understanding of field distribution and optimisation techniques in minimising stress on the insulation surface. The topics covered include stress-induced degradation, field determination, modelling considerations and field optimisation techniques.

A symmetrical 2D model of an 11 kV polymeric insulator has been developed for computational modelling. Simulation under dry-clean and wet-polluted surfaces with idealised configurations revealed the high field regions along the creepage path.

Artificial pollution tests in accordance with the BS EN 60507 standard were carried out on the practical insulator. Observation of discharge activity and elongation over the polymeric surface has good correlation with the results from simulation studies. Unpredicted negligible electric discharges near the high voltage terminal during laboratory experiments could be explained by wetting imbalances in the fog chamber, and the field grading effect due to the corona ring attachment.

A new pollution model having a non-linear electrical property has been developed for improved and more realistic insulator modelling. Measurements of layer conductance in a non-standard low voltage test were used to derive field-dependent conductivity for the pollution layer to be used in the proposed model and implemented in the simulation studies.

Two wet weather conditions, fog and light rain, have been considered for implementing the benefits of the proposed non-linear pollution model. These wet conditions represent uniform (fog) and non-uniform (light rain) wetting which were classified based on their natural wetting action in practice. It has been demonstrated that the non-linear pollution layer results in a more detailed and realistic field profile compared with that obtained from the linear pollution model. This is particularly useful for an improved dry band prediction.

A novel approach for controlling field stress on polymeric insulators, using microvaristor compounds that exhibit non-linear electrical properties, has been proposed. The proposed insulator design consists of a cone-shaped microvaristor grading layer at the interface between the core and silicone rubber near both insulator terminals. The new design was aimed at addressing the shortfall in other known grading arrangements.

The effect of microvaristor characteristics has been investigated to determine the optimal switching threshold for the studied 11 kV insulator. It was demonstrated that use of grading material with an appropriate electrical property can lead to an improved field distribution on the insulator surface. High field intensity at the high voltage and ground terminals were reduced significantly, and peaks along the creepage path were made more uniform at comparable magnitudes. This improvement is predicted to reduce dry banding and surface discharges on outdoor polymeric insulators.

Dissipated energy along the leakage profile of the polluted insulator has been computed to assess the heating performance. It was identified that the greatest dissipated power occurs around the high field regions near the insulator's electrodes, increasing the risk of dry band formation. With the integration of microvaristor material, the thermal 'hot' spots as seen on the standard non-graded insulator were successfully eliminated, and this could be considered as a significant way forward for outdoor insulation.

A simple A.C. test has been conducted to characterise the electrical properties of a commercial microvaristor grading material. The measured voltage and leakage current indicated a strong non-linear behaviour, with field switching threshold at around 14 kV/cm.

A prototype microvaristor-graded insulator has been designed and fabricated using in-house vacuum casting facilities. The proposed cone-shaped grading structure was created using stacked layers of microvaristor grading sheet, which were tightly wrapped onto the core at different lengths: 2 cm, 4 cm and 6 cm.

Lightning impulse (1.2/50 μs) flashover tests have been carried out to examine the breakdown performance of the prototype polymeric insulators thus constructed. The tests were accomplished using the ‘up and down’ method and the flashover voltage was estimated by the U_{50} approach. The performance of the microvaristor-graded insulator prototype was shown to be superior to non-graded standard insulators of similar shape. The flashover voltage for dry-clean insulator was increased from 164 kV up to 199 kV, which represents an improvement of 21%.

The prototype insulator with the proposed grading with ZnO microvaristor compound has been simulated under high voltage impulse energisation to compute its response when subjected to transient conditions. The results from simulation enhance understanding of the grading mechanism that leads to the considerable increase in flashover voltage for graded-insulator prototype under dry-clean conditions. The computed results correlate well with the laboratory measurements.

7.2. FUTURE WORKS

Based on the work carried out in this study, the following areas for future investigation have been identified:

Development of 3D FEM modelling is necessary to take into account the effect of practical configurations and attachments for a better and more realistic electric field computation and analysis.

Investigation of field grading performance for insulators with different profiles and microvaristor designs could yield useful results for the development of improved electric field and insulation performance.

Experimental investigation to evaluate microvaristor grading performance warrants further work. This could include the evaluation of dry band formation and discharge activity on the insulator surface in artificial pollution tests.

Measurements of surface conductance of polluted insulator require repetitions and further experimental works to validate the results presented in this thesis. This is important in establishing a reliable non-linear pollution model for computational modelling and simulation.

Study of degradation and ageing of microvaristor-filled silicone rubber is a potential research area which could help to assess short and long-term grading performance.

APPENDIX A

LIQUID SILICONE RUBBER

PRELIMINARY PRODUCT INFORMATION

DOW CORNING ® HV 1540/10P

FEATURES
- **mixing ratio 9:1**
- **low temperature cure**
- **low viscosity**
- **castable**
- **good tracking resistance**

APPLICATIONS
- **hollowcore insulators**
- **cable terminations**

TYPICAL PROPERTIES

Please note that these physical properties are to be taken as typical. Specification writers please contact your local Dow Corning office before writing specifications on this product.

Test method	Property	Units	Typical Results
	As supplied		
	Viscosity		
	Base		
	at 0,9 s^{-1}	Pa s	11
	at 10 s^{-1}	Pa s	7
	Curing agent		
	at 0,9 s^{-1}	Pa s	17
	at 10 s^{-1}	Pa s	9
	Color		transparent/grey

Test method	Property	Units	Typical Results
DIN 53479	Specific Gravity	g/cm^3	1.1
DIN 53505	Hardness	Shore A	35
DIN 53504	Tensile Strength	MPa	4,6
DIN 53504	Elongation at Break	%	350
ASTM D 624 B	Tear Strength	kN/m	17
IEC 60093	Volume Resistivity	ohm cm	$> 5x10^{14}$
IEC 60250	Dielectric Constant (100Hz)		2.8
IEC 60250	Dissipation Factor		< 0.001
IEC 60587	Tracking Resistance		1A3.5
IEC 60243	Dielectric Strength	kV/mm	24

Measured on test sheets vulcanised 60 minutes at 60°C and also post cured for 1 hour at 120°C.
Viscosity measured on the Carimed Viscometer.

REFERENCES

[1] Looms J. S. T., *Insulators For High Voltages*. London: The Institution of Electrical Engineers, 1988.

[2] Liptrot F. J., "An examination of the service performance of ceramic insulators," in *IEE Colloquium on Review of Outdoor Insulation Materials*, 1996, pp. 4/1-4/7.

[3] Mishra A. P., Gorur R. S., and Venkataraman S., "Evaluation of Porcelain and Toughened Glass Suspension Insulators Removed from Service," *IEEE Transactions on Dielectrics and Electrical Insulation,* vol. 15, pp. 467-475, 2008.

[4] Lambeth P. J., "Effect of pollution on high-voltage outdoor insulators," *Proceedings of the Institution of Electrical Engineers,* vol. 118, pp. 1107-1130, 1971.

[5] Liang X., Wang S., Fan J., and Zhicheng G., "Development of composite insulators in China," *IEEE Transactions on Dielectrics and Electrical Insulation,* vol. 6, pp. 586-594, 1999.

[6] Kikuchi T., Nishimura S., Nagao M., Izumi K., Kubota Y., and Sakata M., "Survey on the use of non-ceramic composite insulators," *IEEE Transactions on Dielectrics and Electrical Insulation,* vol. 6, pp. 548-556, 1999.

[7] Mackevich J. and Shah M., "Polymer outdoor insulating materials. Part I: Comparison of porcelain and polymer electrical insulation," *IEEE Magazine on Electrical Insulation,* vol. 13, pp. 5-12, 1997.

[8] Bauer E. and Dietz H., "Porcelain and Composite Longrod Insulators - A Solution for Future Line Requirements," *IEEE Transactions on Electrical Insulation,* vol. EI-16, pp. 209-219, 1981.

[9] Salthouse E. C., "Initiation of dry bands on polluted insulation," *Proceedings of the Institution of Electrical Engineers,* vol. 115, pp. 1707-1712, 1968.

[10] Hampton B. F., "Flashover mechanism of polluted insulation," *Journal of Electronics and Power,* vol. 10, p. 113, 1964.

[11] V. M. Moreno and R. S. Gorur, "Accelerated corona discharge performance of polymer compounds used in high voltage outdoor insulators," in *Electrical Insulation and Dielectric Phenomena, 1999 Annual Report Conference on*, 1999, pp. 731-734 vol.732.

[12] Montesinos J., Gorur R. S., Mobasher B., and Kingsbury D., "Mechanism of brittle fracture in nonceramic insulators," *IEEE Transactions on Dielectrics and Electrical Insulation,* vol. 9, pp. 236-243, 2002.

[13] R. S. Gorur, E. A. Cherney, R. Hackam, and T. Orbeck, "The electrical performance of polymeric insulating materials under accelerated aging in a fog chamber," *Power Delivery, IEEE Transactions on,* vol. 3, pp. 1157-1164, 1988.

[14] Ilhan S. and Ozdemir A., "Corona ring optimization for V-insulator string on the point of RIV and AC flashover performance," in *Proceedings of International Conference on High Voltage Engineering and Application (ICHVE)*, 2010, pp. 268-271.

[15] Wenxia S., Kun W., Qing Y., and Caixin S., "Corona Ring Design of 800kV DC Composite Insulator Based on Computer Analysis," in *Proceedings of IEEE Conference on Electrical Insulation and Dielectric Phenomena*, 2006, pp. 457-460.

[16] Weida D., Nevoigt J., Hanyu Y., Clemens M., Stefanini D., and Seifert J., "Effects of microvaristor material on the occurrence of partial discharges upon insulators in rain test," in *2010 IEEE International Power Modulator and High Voltage Conference (IPMHVC)*, 2010, pp. 497-500.

[17] Debus J., Hinrichsen V., Seifert J. M., and Hagemeister M., "Investigation of composite insulators with microvaristor filled silicone rubber components," in *Proceedings of the Tenth IEEE International Conference on Solid Dielectrics (ICSD)*, 2010, pp. 1-4.

[18] Hall J. F., "History and bibliography of polymeric insulators for outdoor applications," *IEEE Transactions on Power Delivery,* vol. 8, pp. 376-385, 1993.

[19] Schneider H. M., Hall J. F., Karady G., and Renowden J., "Nonceramic insulators for transmission lines," *IEEE Transactions on Power Delivery,* vol. 4, pp. 2214-2221, 1989.

[20] Mackevich J. and Simmons S., "Polymer outdoor insulating materials. II. Material considerations," *IEEE Magazine on Electrical Insulation,* vol. 13, pp. 10-16, 1997.

[21] Simmons S., Shah M., Mackevich J., and Chang R. J., "Polymer outdoor insulating materials. Part III-Silicone elastomer considerations," *IEEE Magazine on Electrical Insulation,* vol. 13, pp. 25-32, 1997.

[22] Hackam R., "Outdoor HV composite polymeric insulators," *IEEE Transactions on Dielectrics and Electrical Insulation,,* vol. 6, pp. 557-585, 1999.

[23] Gorur R. S., De La O. A., El-Kishky H., Chowdhary M., Mukherjee H., Sundaram R., and Burnham J. T., "Sudden flashover of nonceramic insulators in artificial contamination tests," *IEEE Transactions on Dielectrics and Electrical Insulation,* vol. 4, pp. 79-87, 1997.

[24] Chang J. W. and Gorur R. S., "Hydrophobicity of silicone rubber used for outdoor insulation," in *Proceedings of the 4th International Conference on Properties and Applications of Dielectric Materials*, 1994, pp. 266-269 vol.261.

[25] Swift D. A., Spellman C., and Haddad A., "Hydrophobicity transfer from silicone rubber to adhering pollutants and its effect on insulator performance," *IEEE Transactions on Dielectrics and Electrical Insulation,* vol. 13, pp. 820-829, 2006.

[26] J. W. Chang and R. S. Gorur, "Surface recovery of silicone rubber used for HV outdoor insulation," *Dielectrics and Electrical Insulation, IEEE Transactions on,* vol. 1, pp. 1039-1046, 1994.

[27] De la O A., Gorur R. S., and Burnham J. T., "Electrical performance of non-ceramic insulators in artificial contamination tests. Role of resting time," *IEEE Transactions on Dielectrics and Electrical Insulation,* vol. 3, pp. 827-835, 1996.

[28] Da Silva E., "Reliability of composite insulators," in *Technical meeting on Optimisation of Overhead Line Infrastructure, Supergen - AMPerES*, Manchester, UK, 2008.

[29] Burnham J. T., Givens P. S., and Grisham T. M., "High strength polymer post insulators enable economical transmission lines with low environmental impact," in *Proceedings of IEEE Power Engineering Conference on Transmission and Distribution*, 1994, pp. 494-503.

[30] Composite insulator-product specifications, Phoenix Technology Group Co. Ltd., [Online WWW] http://www.alibaba.com/product-gs/206311888/Composite_suspension_insulator_porcelain_insulator_composite.html, retrieved on 20th Sep 2012.

[31] *DD IEC/TS 60815 - 3: 2008 - Selection and dimensioning of high-voltage insulators intended for use in polluted conditions - Part 3: Polymer insulators for a.c. systems*: British Standard Institution Std., 2008.

[32] Young H. M., Haddad A., Rowlands A. R., and Waters R. T., "Effect of shape factors on the performance of polluted polymeric insulators," in *Proceedings of the Eleventh International Symposium on High Voltage Engineering, Conf. Publ. No. 467*, 1999, pp. 92-95.

[33] *CIGRE Working Group 33.13 - Polluted Insulators: A review of current knowledge*: Task Force - 33.04.01, CIGRE Brochure:158, 2000.

[34] Moreno V. M. and Gorur R. S., "Effect of long-term corona on non-ceramic outdoor insulator housing materials," *IEEE Transactions on Dielectrics and Electrical Insulation,* vol. 8, pp. 117-128, 2001.

[35] Gubanski S. M. and Vlastos A. E., "Wettability of naturally aged silicon and EPDM composite insulators," *IEEE Transactions on Power Delivery,* vol. 5, pp. 1527-1535, 1990.

[36] Raja Prabu R., Usa S., Udayakumar K., Abdullah Khan M., and Abdul Majeed S. S. M., "Electrical Insulation Characteristics of Silicone and EPDM Polymeric Blends. I," *IEEE Transactions on Dielectrics and Electrical Insulation,* vol. 14, pp. 1207-1214, 2007.

[37] Meyer L. H., Cherney E. A., and Jayaram S. H., "The role of inorganic fillers in silicone rubber for outdoor insulation alumina tri-hydrate or silica," *IEEE Magazine on Electrical Insulation,* vol. 20, pp. 13-21, 2004.

[38] Soo-Boo L., J. Won-Yeong, P. Yong-Hee, and L. June-Ho, "Influence of filler properties on the tracking characteristics of silicone rubbers," in *Proceedings of the 6th International Conference on Properties and Applications of Dielectric Materials*, 2000, pp. 220-222 vol.221.

[39] Cherney E. A., "Silicone rubber dielectrics modified by inorganic fillers for outdoor high voltage insulation applications," *IEEE Transactions on Dielectrics and Electrical Insulation,* vol. 12, pp. 1108-1115, 2005.

[40] Fang S., Jia Z., Gao H., and Guan Z., "Influence of fillers on silicone rubber for outdoor insulation," in *Annual Report of Conference on Electrical Insulation and Dielectric Phenomena (CEIDP)*, 2007, pp. 300-303.

[41] Cheol H. L., Sang W. K., Jin H. N., Woo J. O., Ho K. Y., and Suh K. S., "Effects of particle size of alumina trihydrate on electrical properties of EPDM," in *Annual Report. Conference on Electrical Insulation and Dielectric Phenomena*, 1998, pp. 112-115 vol. 111.

[42] June-Ho L. and Ji W. Y., "Electrical and mechanical properties of silicone rubber for high voltage insulation," in *Proceedings of the 7th International Conference on Properties and Applications of Dielectric Materials*, 2003, pp. 591-594 vol.592.

[43] Spellman C. A., Young H. M., Haddad A., Rowlands A. R., and Waters R. T., "Survey of polymeric insulator ageing factors," in *Proceedings of the Eleventh International Symposium on High Voltage Engineering, Conf. Publ. No. 467*, 1999, pp. 160-163 vol.164.

[44] Amin S. and Amin M., "Natural aging of SiR insulators in Pakistan," in *International Conference on Emerging Technologies (ICET)* 2009, pp. 114-117.

[45] Sima W., Espino-Cortes F. P., Cherney E. A., and Jayaram S. H., "Optimization of corona ring design for long-rod insulators using FEM based computational analysis," in *Conference Record of IEEE International Symposium on Electrical Insulation*, 2004, pp. 480-483.

[46] Doshi T., Gorur R. S., and Hunt J., "Electric field computation of composite line insulators up to 1200 kV AC," *IEEE Transactions on Dielectrics and Electrical Insulation,* vol. 18, pp. 861-867, 2011.

[47] Hartings R., "Electric fields along a post insulator: AC-measurements and calculations," *IEEE Transactions on Power Delivery,* vol. 9, pp. 912-918, 1994.

[48] Hernandez-Corona R., Ramirez-Vazquez I., and Montoya-Tena G., "Evaluation in Laboratory of the Visual Corona and Electric Field Measurement Techniques to Inspect Polymeric Insulators," in *Transmission and Distribution Conference and Exhibition, 2005/2006 IEEE PES*, 2006, pp. 601-604.

[49] Venkatesulu B. and Thomas M. J., "Corona aging studies on silicone rubber nanocomposites," *IEEE Transactions on Dielectrics and Electrical Insulation,* vol. 17, pp. 625-634, 2010.

[50] Moreno V. M. and Gorur R. S., "Corona-induced degradation of nonceramic insulator housing materials," in *Annual Report of Conference on Electrical Insulation and Dielectric Phenomena*, 2001, pp. 640-643.

[51] El-Kishky H. and Gorur R. S., "Electric field computation on an insulating surface with discrete water droplets," *IEEE Transactions on Dielectrics and Electrical Insulation,* vol. 3, pp. 450-456, 1996.

[52] Lopes I. J. S., Jayaram S. H., and Cherney E. A., "A study of partial discharges from water droplets on a silicone rubber insulating surface," *IEEE Transactions on Dielectrics and Electrical Insulation,* vol. 8, pp. 262-268, 2001.

[53] Phillips A. J., Childs D. J., and Schneider H. M., "Aging of nonceramic insulators due to corona from water drops," *IEEE Transactions on Power Delivery,* vol. 14, pp. 1081-1089, 1999.

[54] Krivda A., Greuter F., Rocks J., Kornmann X., and Meier P., "Chemical analysis of outdoor silicone materials after electrical and environmental testing," in *Proceedings of IEEE Conference on Electrical Insulation and Dielectric Phenomena*, 2006, pp. 389-392.

[55] Karady G. G., "Flashover mechanism of non-ceramic insulators," *IEEE Transactions on Dielectrics and Electrical Insulation,* vol. 6, pp. 718-723, 1999.

[56] Krivda A. and Birtwhistle D., "Breakdown between water drops on wet polymer surfaces," in *Conference on Electrical Insulation and Dielectric Phenomena, 2001 Annual Report,*, 2001, pp. 572-580.

[57] Katada K., Takada Y., Takano M., Nakanishi T., Hayashi Y., and Matsuoka R., "Corona discharge characteristics of water droplets on hydrophobic polymer insulator surface," in *Proceedings of the Sixth International Conference on Properties and Applications of Dielectric Materials*, 2000, pp. 781-784 vol.782.

[58] Haddad A., Griffiths H., and Waters R. T., "Principles of anti-fog design for polymeric insulators," Piscataway, NJ 08855-1331, United States, 2007, pp. 302-305.

[59] De la O A. and Gorur R. S., "Flashover of contaminated nonceramic outdoor insulators in a wet atmosphere," *IEEE Transactions on Dielectrics and Electrical Insulation,* vol. 5, pp. 814-823, 1998.

[60] Mukherjee P. K., Ahmed A., and Singer H., "Electric field distortion caused by asymmetric pollution on insulator surfaces," *Dielectrics and Electrical Insulation, IEEE Transactions on,* vol. 6, pp. 175-180, 1999.

[61] *DD IEC/TS 60815 - 1: 2008 - Selection and dimensioning of high-voltage insulators intended for use in polluted conditions - Part 1: Definitions, information and general principles*: British Standard Institution Std., 2008.

[62] Yoshimura N., Kumagai S., and Nishimura S., "Electrical and environmental aging of silicone rubber used in outdoor insulation," *Dielectrics and Electrical Insulation, IEEE Transactions on,* vol. 6, pp. 632-650, 1999.

[63] Chang S. H., Bok H. Y., and Sang Y. L., "Degradation in silicone rubber used for outdoor insulator by UV radiation," in *Proceedings of the 6th International Conference on Properties and Applications of Dielectric Materials*, 2000, pp. 367-370 vol.361.

[64] Kumagai S. and Yoshimura N., "Influence of single and multiple environmental stresses on tracking and erosion of RTV silicone rubber," *IEEE Transactions on Dielectrics and Electrical Insulation,* vol. 6, pp. 211-225, 1999.

[65] Da Silva E. and Rowland S. M., "Natural, rotationally asymmetric ageing of composite insulators," Piscataway, NJ 08855-1331, United States, 2008, pp. 530-534.

[66] Sundararajan R., Mohammed A., Chaipanit N., Karcher T., and Liu Z., "In-service aging and degradation of 345 kV EPDM transmission line insulators in a coastal environment," *IEEE Transactions on Dielectrics and Electrical Insulation,* vol. 11, pp. 348-361, 2004.

[67] Rowland S. M., Xiong Y., Robertson J., and Hoffmann S., "Aging of silicone rubber composite insulators on 400 kV transmission lines," *Dielectrics and Electrical Insulation, IEEE Transactions on,* vol. 14, pp. 130-136, 2007.

[68] Ying S., Cherney E. A., and Jayaram S. H., "Electric stress grading of composite bushings using high dielectric constant silicone compositions," in *Proceedings of IEEE International Symposium on Electrical Insulation*, 2004, pp. 320-323.

[69] Ravi K. N., Ramamoorty M., and Naidu M. S., "Voltage distribution of a string insulator under DC voltages," in *Annual Report of Conference on Electrical Insulation and Dielectric Phenomena*, 1992, pp. 805-810.

[70] Train D. and Dube R., "Measurements of Voltage Distribution on Suspension Insulators for HVDC Transmission Lines," *IEEE Power Engineering Review,* vol. PER-3, pp. 28-28, 1983.

[71] Hidaka K., "Electric field and voltage measurement by using electro-optic sensor," in *Eleventh International Symposium on High Voltage Engineering, (Conf. Publ. No. 467)*, 1999, pp. 1-14 vol.12.

[72] Huang S. J. and Erickson D. C., "The potential use of optical sensors for the measurement of electric field distribution," *IEEE Transactions on Power Delivery,* vol. 4, pp. 1579-1585, 1989.

[73] Hidaka K., "Progress in Japan of space charge field measurement in gaseous dielectrics using a Pockels sensor," *IEEE Magazine on Electrical Insulation,* vol. 12, pp. 17-28, 1996.

[74] Rong Z., Yun Z., Wei-Yuan C., and Bo Zhang, "Measurement of electric field distribution along composite insulators by integrated optical electric field sensor," *IEEE Transactions on Dielectrics and Electrical Insulation,* vol. 15, pp. 302-310, 2008.

[75] Daochun H., Jiangjun R., Yong C., Feng H., Shifeng Y., and Shoubao L., "Calculation and measurement of potential and electric field distribution along 1000 kV AC transmission line composite insulator," in *Proceedings of International Conference on Electrical Machines and Systems (ICEMS)* 2008, pp. 428-433.

[76] Schümann U., Barcikowski F., Schreiber M., Kärner H. C., and Seifert J. M., "FEM Calculation and Measurement of the Electrical Field Distribution of HV Composite Insulator Arrangements," in *CIGRE Proceedings, Session 33, No. 404*, Paris, 2002.

[77] Abdel-Salam M. and Stanek E. K., "Optimizing Field Stress on High-Voltage Insulators," *IEEE Transactions on Electrical Insulation,* vol. EI-22, pp. 47-56, 1987.

[78] Gerdin G., Lakdawala V., and Basappa P., "Computation of ac and dc electric field around a wet polluted insulator," in *Annual Report of Conference on Electrical Insulation and Dielectric Phenomena*, 2002, pp. 176-179.

[79] Chakravorti S. and Mukherjee P. K., "Power frequency and impulse field calculation around a HV insulator with uniform or nonuniform surface pollution," *IEEE Transactions on Electrical Insulation,* vol. 28, pp. 43-53, 1993.

[80] Dhalaan S. M. A. and Elhirbawy M. A., "Simulation of voltage distribution calculation methods over a string of suspension insulators," in *IEEE Proceedings of Conference on Transmission and Distribution*, 2003, pp. 909-914 vol.903.

[81] Li Tianwei, Ruan Jiangjun, Xiao Yanling, and Wu Tian, "Parallel computation the potential distribution and electric field along the 500kV line composite insulators," in *International Conference on Electrical Machines and Systems (ICEMS)* 2008, pp. 501-505.

[82] Yunn-Shiuan L., Shiang-Woei C., and Jeng-Tzong C., "FEM versus BEM," *Circuits and Devices Magazine, IEEE,* vol. 20, pp. 25-34, 2004.

[83] Sebestyn I., "Electric-field calculation for HV insulators using domain-decomposition method," *IEEE Transactions on Magnetics,* vol. 38, pp. 1213-1216, 2002.

[84] Zhao T. and Comber M. G., "Calculation of electric field and potential distribution along nonceramic insulators considering the effects of conductors and transmission towers," *Power Delivery, IEEE Transactions on,* vol. 15, pp. 313-318, 2000.

[85] Stefanini D., Seifert J. M., Clemens M., and Weida D., "Three dimensional FEM electrical field calculations for EHV composite insulator strings," in *IEEE International Power Modulator and High Voltage Conference (IPMHVC)*, 2010, pp. 238-242.

[86] Volat C. and Farzaneh M., "Three-dimensional modeling of potential and electric-field distributions along an EHV ceramic post insulator covered with ice - Part I: Simulations of a melting period," *IEEE Transactions on Power Delivery,* vol. 20, pp. 2006-2013, 2005.

[87] Weiguo Q., Sebo S. A., and Hill R. J., "Practical Cases of Electric Field Distribution Along Dry and Clean Nonceramic Insulators of High-Voltage Power Lines," *IEEE Transactions on Power Delivery,* vol. 22, pp. 1070-1078, 2007.

[88] Jin Hong and Chen Hong, "Electric field analysis of 220kV composite rod insulator," in *Proceedings of IEEE Conference on Power Engineering and Automation (PEAM)*, 2011, pp. 73-77.

[89] Yildiz C., Ozdemir A., and Ilhan S., "Electric field distributions around composite insulators under AC and impulse voltages," in *Proceedings of the International Symposium Modern Electric Power Systems (MEPS)*, 2010, pp. 1-6.

[90] Chakravorti S. and Steinbigler H., "Boundary element studies on insulator shape and electric field around HV insulators with or without pollution," *IEEE Transactions on Dielectrics and Electrical Insulation,* vol. 7, pp. 169-176, 2000.

[91] Eleperuma K., Saha T. K., and Gillespie T., "Electric Field Modelling of Non-Ceramic High Voltage Insulators," *Australian Journal of Electrical & Electronics Engineering,* vol. 4, pp. 239-248, 2008.

[92] Jian-bo Z., Bo G., and Qiao-Gen Z., "Dry Band Formation and Its Influence on Electric Field Distribution along Polluted Insulator," in *Proceeding of Asia-Pacific Conference on Power and Energy Engineering (APPEEC)*, 2010, pp. 1-5.

[93] Gutman I., Lundquist J., Dubickas V., Carlshem L., and Kleveborn R., "Design of corona/arcing rings when replacing cap-and-pin insulators by composite insulators," in *Proceeding of the Seventeenth International Symposium on High Voltage Engineering*, Hannover, Germany, 2011.

[94] Jing L., Zongren P., Yong F., Xiaoyong F., and Tianxi X., "Electric field calculation and grading ring optimization of composite insulator for 500kV AC transmission lines," in *Solid Dielectrics (ICSD), 2010 10th IEEE International Conference on*, 2010, pp. 1-4.

[95] Karady G. G., Shah M., and Brown R. L., "Flashover mechanism of silicone rubber insulators used for outdoor insulation-I," *IEEE Transactions on Power Delivery,* vol. 10, pp. 1965-1971, 1995.

[96] Gorur R. S., Sundhara R. S., and Amburgey O. G., "Contamination performance of polymeric insulating materials used for outdoor insulation applications," *IEEE Transactions on Electrical Insulation,* vol. 24, pp. 713-716, 1989.

[97] Xu J., Su W., Teng Y., and Lin X., "Finite element analysis of electric field of outdoor insulators under pollution un-uniform distribution," in *Proceedings of the First International Conference on Electric Power Equipment - Switching Technology (ICEPE-ST)*, 2011, pp. 462-465.

[98] El-Hag A. H., Jayaram S. H., and Cherney E. A., "Effect of insulator profile on aging performance of silicone rubber insulators in salt-fog," *IEEE Transactions on Dielectrics and Electrical Insulation,* vol. 14, pp. 352-359, 2007.

[99] Chen Y., Huo F., Ding Y., Gao B., and Zhang Q. G., "Study on Withstand Voltage Characteristics and Surface Electrical Field Distribution along Polluted Insulators," in *Proceeding of the International Conference on High Voltage Engineering and Application (ICHVE)*, 2008, pp. 60-62.

[100] Souza A. L. and Lopes I. J. S., "Electric field distribution along the surface of high voltage polymer insulators and its changes under service conditions," in *Conference Record of the 2006 IEEE International Symposium on Electrical Insulation*, 2006, pp. 56-59.

[101] Weiguo Q. and Sebo S. A., "Electric field and potential distributions along non-ceramic insulators with water droplets," in *Proceedings of 2001 Conference on Electrical Insulation and Electrical Manufacturing & Coil Winding* 2001, pp. 441-444.

[102] Weiguo Q. and Sebo S. A., "Typical cases of electric field and voltage distribution calculations along polymer insulators under various wet surface conditions," in *Annual Report Conference on Electrical Insulation and Dielectric Phenomena*, 2002, pp. 840-843.

[103] *STRI Guide 92/1 - Hydrophobicity Classification Guide*: Swedish Transmission Research Institute (STRI), 1992.

[104] Xin Q. W., Zongren P., Peng L., and Zhong Y., "Calculation of Electric-field Distribution and Research on Characteristics of Shielding Ring along the Long-rod Post Porcelain Insulators Used in 1000kv System," in *Proceedings of the Eighth International Conference on Properties and applications of Dielectric Materials*, 2006, pp. 603-606.

[105] Ilhan S. and Ozdemir A., "Effects of corona ring design upon impulse voltage withstand level of 380 kV V-strings," *IEEE Transactions on Dielectrics and Electrical Insulation,* vol. 18, pp. 1638-1646, 2011.

[106] Yang Q., Wenxia S., Deng J., Yuan T., and Chen L., "New optimization method on electric field distribution of composite insulator," in *Annual Report of Conference on Electrical Insulation and Dielectric Phenomena (CEIDP)*, 2010, pp. 1-4.

[107] Zongren P., Peng L., and Peng Y., "Structural Optimization of a New-style Insulator Used in High-Voltage Transmission Lines," in *Proceedings of the Eighth International Conference on Properties and applications of Dielectric Materials*, 2006, pp. 832-835.

[108] Mei H., Peng G., Dai H., Wang L., Guan Z., and Cao L., "Installing insulation jacket to improve outdoor insulation performance of composite insulator," *IEEE Transactions on Dielectrics and Electrical Insulation,* vol. 18, pp. 2004-2012, 2011.

[109] Roberts A., "Stress grading for high voltage motor and generator coils," *IEEE Magazine on Electrical Insulation,* vol. 11, pp. 26-31, 1995.

[110] Wei H. J., Jayaram S., and Cherney E. A., "A study of electrical stress grading of composite bushings by means of a resistive silicone rubber coating," *Journal of Electrostatics,* vol. 63, pp. 273-283, 2005.

[111] Greuter F., Siegrist M., Kluge-Weiss P., Kessler R., Donzel L., Loitzl R., and Gramespacher H. J., "Microvaristors: Functional fillers for novel electroceramic composites," *Journal of Electroceramics,* vol. 13, pp. 739-744, 2004.

[112] Onneby C., Martensson E., Gafvert U., Gustafsson A., and Palmqvist L., "Electrical properties of field grading materials influenced by the silicon carbide grain size," in *Proceedings of IEEE International Conference on Conduction and Breakdown in Solid Dielectrics*, Eindhoven, Netherlands, 2001, pp. 43-45.

[113] Donzel L., Christen T., Kessler R., Greuter F., and Gramespacher H., "Silicone composites for HV applications based on microvaristors," in *Solid Dielectrics, 2004. ICSD 2004. Proceedings of the 2004 IEEE International Conference on*, 2004, pp. 403-406 Vol.401.

[114] Haddad A., "Chapter 5: ZnO surge arresters," in *Advances in High Voltage Engineering*. vol. 40, Haddad A. and Warne D. F., Eds., ed London: The Institution of Electrical Engineers, 2004.

[115] Donzel L. W., Greuter F., and Christen T., "Nonlinear resistive electric field grading Part 2: Materials and applications," *IEEE Magazine on Electrical Insulation,* vol. 27, pp. 18-29, 2011.

[116] Strumpler R. and Kluge-Weiss P., "Smart varistor composites," in *Proceeding of Eighth CIMTEC-World Ceramic Congress & Forum on New Materials*, 1995, pp. 15-22.

[117] H. M. Donzel L. W., *Microvaristor-Based Overvoltage Protection*: U.S. Patent US2009/0200521A1, 13 Aug 2009.

[118] Strobl R., Haverkamp W., and Malin G., "A novel heat-shrinkable medium voltage termination system based on ceramic stress-grading technology," *Journal of Electroceramics, Vol. 99, Issue 26, 11 Dec 2000,* pp. page(s) 68-73, 2000.

[119] Boettcher B., Lietzke R., Malin G., Glembocki R. P., and Spalding M. H., *Electrical insulators, materials and equipment*: U.S. Patent 6864432, 8 Mar 2005.

[120] Espino-Cortes F. P., Cherney E. A., and Jayaram S., "Effectiveness of stress grading coatings on form wound stator coil groundwall insulation under fast rise time pulse voltages," *IEEE Transactions on Energy Conversion,* vol. 20, pp. 844-851, 2005.

[121] Weida D., Bo X., Hmelt S., and Clemens M., "Design of ZnO microvaristor end corona protection for electrical machines," in *Conference Record of the 2010 IEEE International Symposium on Electrical Insulation (ISEI)*, 2010, pp. 1-4.

[122] G. R. Donzel L. W., Gramespacher N. , *High Voltage Bushing with Field Control Material*: U.S. Patent US7262367 B2, 28 Aug 2007.

[123] K. X. L. Donzel L. W., Greuter F., , *Varistor-based Field Control Tape*: U.S. Patent US2008/0152898A1, 26 Jun 2008.

[124] Kemp C., Bachmaier G., and Gramespacher H., *Electrical Stress Control*: U.S. Patent 6124549, 26 Sep 2000.

[125] Weida D., Steinmetz T., and Clemens M., "Electro-Quasistatic High Voltage Field Simulations of Large Scale Insulator Structures Including 2-D Models for Nonlinear Field-Grading Material Layers," *IEEE Transactions on Magnetics,* vol. 45, pp. 980-983, 2009.

[126] Weida D., Steinmetz T., and Clemens M., "Electro-Quasistatic High-Voltage Field Simulations of Insulator Structures Covered with Thin Resistive Pollution or Nonlinear Grading Material," in *Proceedings of IEEE Conference on International Power Modulators and High Voltage* 2008, pp. 580-583.

[127] Zhou P. B., *Numerical Analysis of Electromagnetic Fields*. Berlin: Spinger-Verlag, 1993.

[128] Klaus-Jurgen Bathe., *Finite Element Procedures*. New Jersey: Prentice Hall, 1996.

[129] Williams D. L., Haddad A., Rowlands A. R., Young H. M., and Waters R. T., "Formation and characterization of dry bands in clean fog on polluted insulators," *IEEE Transactions on Dielectrics and Electrical Insulation,* vol. 6, pp. 724-731, 1999.

[130] *COMSOL Multiphysics 3.5a User's Guide*: COMSOL AB., 2008.

[131] Williams D. L., "Insulation failure mechanism in artificial pollution tests," PhD Thesis, Cardiff University, 1997.

[132] *BS EN 60507: 1993 - Artificial pollution tests on high voltage insulators to be used on a.c. systems*: British Standard Institution Std., 1993.

[133] Lambrecht J., "V-I characteristics and Permittivity," Personal email (26 Apr 2010), 2010.

[134] Utkarsh P., "The Impact of Harmonics on the Power Cable Stress Grading System," PhD Thesis, University of Waterloo, Canada, 2012.

[135] Kim J. and Chaudhury M. K., "Corona-discharge-induced hydrophobicity loss and recovery of silicones," in *Annual Report of Conference on Electrical Insulation and Dielectric Phenomena*, 1999, pp. 703-706 vol.702.

[136] *BS EN 60060 - 1: 2010 - High-voltage test techniques. Part 1: General definitions and test requirements*: British Standard Institution Std., 2010.

[137] Dieter K. and Kurt F., *High-Voltage Test Techniques*. India: Reed Educational and Professional Publishing Ltd., 2001.